

Controlled long-range interactions between Rydberg atoms and ions

von

Thomas Secker

Diplomarbeit in Physik
vorgelegt dem Fachbereich Physik, Mathematik und Informatik (FB 08)
der Johannes Gutenberg-Universität Mainz
am 31. März 2016

1. Gutachter: Dr. René Gerritsma
2. Gutachter: Univ.-Prof. Dr. Peter van Loock

Abstract

This thesis is devoted to the study of a novel approach to generate long-range atom-ion interactions. These long-range interactions are suitable to overcome the limitations set by the short-range character of the atom-ion potential in ultracold atom-ion systems putting individual trapping of atoms and ions for interacting systems into experimental reach. An increase in interaction strength over several orders of magnitude can be reached by weakly coupling the atomic ground state to a low lying Rydberg level, since the polarizability and thus the sensitivity of the atom to the ionic field scales with $\propto n^7$, where n is the principal quantum number. The increased sensitivity along with the increased spacial extent of the wave functions make a detailed analysis including higher order terms in the expansion of the potential fields the atom experiences necessary. In this thesis the simplest possible example is studied in detail, namely an atom trapped in an optical dipole field and an ion trapped in the potential of a quadrupole Paul trap in the atoms close vicinity $d \approx 1 \mu\text{m}$, here d denotes the distance of the trap minima. This thesis provides a detailed examination of effects on the Rydberg states, which are then used to derive the interaction potential between the weakly Rydberg admixed atom and the ion. In a final project it is demonstrated how entanglement of the internal states of the atom with the motional and also the internal states of the ion could be obtained. This system comes with attractive features since the form of the derived quantum gate Hamiltonian closely resembles the one of phase gates in trapped ion systems. Therefore no ground state cooling is required. The setup provides full dynamical control and is to large extent immune to micromotion. The results obtained in this thesis are of interest for developing hybrid quantum information platforms and for implementing quantum simulations of solid state physics. Some of the work presented here has been submitted for publication [65].

Zusammenfassung

Die vorliegende Diplomarbeit widmet sich der Analyse eines neuen Ansatzes zur Erzeugung langreichweitiger Atom-Ion Wechselwirkungen. Diese sind geeignet, Einschränkungen zu überwinden, die durch den kurzreichweitigen Charakter des Atom-Ion Potentials entstehen. Es werden somit wechselwirkende Systeme in experimentell zugänglich gemacht, bei denen Atome und Ionen örtlich getrennt voneinander gefangen werden. Eine Verstärkung der Wechselwirkung um mehrere Größenordnungen kann durch schwache Kopplung des atomaren Grundzustands an einen niedrig liegenden Rydberg-Zustand erreicht werden, da die Polarisierbarkeit und damit auch die Sensitivität des Atoms auf das Feld des Ions proportional zur siebten Potenz der atomaren Hauptquantenzahl (n^7) skaliert. Die gesteigerte Sensitivität in Kombination mit der vergrößerten räumlichen Ausdehnung des Rydbergzustand machen eine Detailanalyse, die auch höhere Ordnungen des auf das Atom wirkenden Potentialfeldes mit einbezieht, erforderlich. In dieser Arbeit wird eine solche Detailanalyse für ein einfaches Beispielsystem vollzogen, einem einzelnen Atom, das in einer optischen Dipolfalle im Abstand von einem Mikrometer zu einem Ion im Quadrupolfeld einer Paulfalle gefangen ist. Wir werden eine genaue Analyse der Effekte auf die Rydberg-Zustände durchführen und die Resultate verwenden, um das Wechselwirkungspotential zwischen einem Atom, mit schwach beigemischtem Rydberg-Zustand und einem Ion zu ermitteln. Abschließend werden wir demonstrieren, wie Verschränkung zwischen den internen Zuständen des Atoms und den bewegungs- sowie den inneren Zuständen des Ions erzeugt werden könnten. Das untersuchte System hat diverse Vorzüge, da das verwendete Quantengatter dem von Phasengattern rein ionenbasierter Systeme ähnelt. Aufgrund dessen ist kein Grundzustandskühlen erforderlich, das System erlaubt volle dynamische Kontrolle und ist zu einem großen Ausmaß robust gegenüber der Mikrobewegung des Ions. Die Resultate, die in dieser Arbeit gewonnen wurden, sind für die Entwicklung von hybriden Quanteninformationsplattformen und für die Implementierung der Quantensimulation von Festkörperphysik von Bedeutung. Teile dieser Arbeit wurden zur Publikation eingereicht [65].

Contents

1. Introduction	1
2. Alkali Rydberg atoms	7
2.1. The Rydberg electron in a central core potential	8
2.2. The relativistic Hamiltonian	11
2.3. Radial Rydberg wave functions	14
2.4. Projection method	18
2.5. Stark shifts of Rydberg alkali atoms	20
2.5.1. Projection	20
2.5.2. Stark shifts of lithium	23
3. Rydberg atom-ion interaction	27
3.1. Simple model: Rydberg atom on a line	27
3.2. The Born Oppenheimer method	30
3.3. Free Rydberg atom-ion interactions	36
3.4. Atom-Paul trap interactions	44
4. Alkali atoms in laser fields	49
4.1. Optical dipole trap	49
4.2. Rotating wave approximation inside the BO framework	51
4.3. Dressed Rydberg atom-ion interaction	53
5. Atom-ion spin-spin interactions	57
5.1. Ion motion mediated spin-spin interactions	57
5.1.1. Simulation	63
5.1.2. Spin-spin interactions for particles in thermal states of motion	64
5.1.3. The role of micromotion	65
6. Outlook	69
A. Level scheme of ${}^6\text{Li}$	71
Bibliography	75

1. Introduction

Hybrid atom ion systems

The combination of atoms and ions in the ultracold regime is a fascinating new research field. Schemes for quantum information processing, the study of quantum many body phenomena, quantum simulation and polaronic physics have been proposed [5, 15, 21, 27, 33] and experimental results on topics as quantum chemistry, ultracold quantum collisions, sympathetic cooling and ion-assisted detection of atoms have already been obtained [24, 27, 28, 56, 57, 61, 73, 74]. The strength of these hybrid systems stems from the combination of the complementary properties of the particular ionic and atomic subsystems. The ions on the one hand, can be tightly trapped, which results in long lifetimes, and their repelling force leads to far separated strongly localized wave functions, allowing for single ion addressing and readout. In contrast, due to the much shorter ranged forces between the atoms, huge ensembles can be generated and techniques like evaporative cooling allow for temperatures in the nK range.

Until now the main experimental focus lies on immersing the ion crystal into the atom cloud. It may be possible to control the interaction of the combined systems via the tunability of the scattering length between atoms and ions, e.g. with the help of Feshbach resonances [32, 69]. This typically demands for collisions in the s-wave scattering regime, which requires temperatures of 100 nK- 1 μ K. On the other hand, schemes where one ion interacts with one or only a few atoms have not been studied experimentally so far. Here, it is of interest to couple the systems at the quantum level. In this way the benefits of the trapped ions system may be combined with the inherent scalability of the atomic system to break new ground in quantum simulation and quantum information processing applications or the system may serve as a building block for studying quantum many-body physics.

Micromotion

In radio frequency (rf) traps the achievable temperatures for hybrid systems are bound from below [7, 8, 41, 53, 61, 71, 74]. This effect stems from the fast micromotion the trapped ions undergo at the trap drive frequency [7]. To get a first understanding of the effects that can occur, one can analyze a simple one dimensional model considering elastic hard-core collisions. During a collision the velocities change $v_i \rightarrow v'_i$ and $v_a \rightarrow v'_a$, where v_i (v'_i) and v_a (v'_a) denote the velocities before (and after) the collision of ion and atom, respectively. For the atom initially at rest $v_a = 0$ the ion

1. Introduction

velocity after the collision is given by

$$v'_i = \frac{v_i(m_i - m_a)}{(m_i + m_a)} = v_i \frac{1 - \frac{m_a}{m_i}}{1 + \frac{m_a}{m_i}}, \quad (1.1)$$

which is a simple expression of the atom ion mass ratio m_a/m_i . Since the solutions $x_i(t)$ of the ion's equation of motion can be approximated by

$$x_i(t) \propto \cos(\omega_i t) \left(1 - \frac{q}{2} \cos(\Omega_{\text{rf}} t)\right), \quad (1.2)$$

with ω_i the low secular frequency of ion motion and the micromotion part oscillating with the fast trap drive frequency Ω_{rf} , where q is the stability parameter $q^2 \ll 1$ [16, 42], we can now infer how its trajectory will change due to such a collision. It becomes apparent that the resulting trajectory is sensitive to the phase of the trap drive frequency the collision takes place in, therefore the secular velocity could be even increased and energy may be drawn from the time-dependent trapping field during an atom-ion collision leading to heating. More elaborate classical simulations show that there is a lower bound for achievable temperatures and suggest that high mass ratios between ions and atoms lead to lowest temperatures [7]. The combination of Li and Yb^+ , used in our experiment, has the highest attainable mass ratio of species that allow for straightforward laser cooling. On top the s-wave regime is reached at the comparatively high temperature of 6 μK - owing to the small mass of Li - which makes this species combination the most promising candidate for bringing the quantum regime into experimental reach for ions trapped in a Paul trap.

There are a number of other approaches under consideration to overcome the limitations set by micromotion. For instance, optical trapping of ions may be employed [31, 63]. Another possibility is to use traps of higher order, such as octupole traps, that have large near field-free regions [14]. However, each of these approaches seriously reduces the merits of the trapped ion platform such as long lifetimes and localization of individual ions. Another way is to add optical potentials for the atoms, which prevent atom-ion collisions, but still allow for significant interactions, but for ground state atoms the experimental implementation of such potentials is a demanding task. The reason behind this is due to the short range character of the atom ion potential, which has a steep $1/R^4$ shape, where R denotes the atom ion distance, with an interaction length in the 100 nm range [33]. These short distances are below available laser wavelengths, which makes engineering of such potentials a challenging task. This issue puts severe restraints on proposed schemes to couple the atoms and ions on the quantum level, such as by employing controlled collisions with state-dependent scattering lengths [15], to generate entanglement between atoms and ions [35, 53], or coupling ions to bosonic Josephson junctions [20, 35].

Rydberg atom-ion interactions

To resolve the limitations set by the short range character of the atom-ion interaction, we aim to increase the interaction strength between atom and ion such

that the interaction becomes relevant over distances in the μm range. Therefore we propose to laser-couple the atomic ground state to a low-lying Rydberg state [3, 10, 11, 29, 30, 44, 46, 47, 49, 55]. Since the interaction of ion and Rydberg atom is orders of magnitude stronger than the ground state interaction, even weak admixing will have a sufficient effect. On top the interaction strength can be tuned, because the amount of Rydberg admixture can be controlled e.g. by amplitude modulation of the laser.

The reason for the strong interaction of Rydberg atoms and ions is rooted in the sensitivity of Rydberg atoms to external electric fields. To get a first impression where those properties originate, we perform a short calculation. For simplicity we assume hydrogen for the atom but the calculation can readily be generalized. We start with the ground state case. For a ground state atom far enough separated from the ion, we can assume the ions coulomb potential to be linear over the extent of the electronic wave function. This leads to a dipole term proportional to the electric field \mathbf{E}_{ion} generated by the ion at the atom's position

$$e \mathbf{r} \cdot \mathbf{E}_{\text{ion}}(\mathbf{R}) = -\frac{e^2}{4\pi\epsilon_0} \frac{\mathbf{r} \cdot \mathbf{R}}{|\mathbf{R}|^3}. \quad (1.3)$$

Here we denote with e the elementary charge, with ϵ_0 the permittivity of free space, \mathbf{r} is the relative electron nucleus position and \mathbf{R} the relative position of ion and the atom's center of mass. Without loss of generality, we choose $\mathbf{R} = (0, 0, R)$ and use perturbation theory to obtain the corrected energy levels of the atom. Up to second order, the shifted energy of the k -th level reads [18]

$$\epsilon_k = \epsilon_k^0 - \frac{e^2}{4\pi\epsilon_0} \frac{R}{|\mathbf{R}|^3} \langle \psi_k | z | \psi_k \rangle - \left(\frac{e^2}{4\pi\epsilon_0} \frac{1}{R^2} \right)^2 \sum_{m \neq k} \frac{|\langle \psi_k | z | \psi_m \rangle|^2}{\epsilon_k^0 - \epsilon_m^0}, \quad (1.4)$$

where ϵ_k^0 and $|\psi_k\rangle$ denote the k -th energy level and corresponding eigenstate of the free atom, respectively and z is the last component of \mathbf{r} . For non-degenerate states the first order correction term, which is the second term on the right hand side of Eq. (1.4), vanishes. Let us define the polarizability [18]

$$\alpha_d = -2e^2 \sum_{m \neq k} \frac{|\langle \psi_k | z | \psi_m \rangle|^2}{\epsilon_k^0 - \epsilon_m^0} \quad (1.5)$$

of the k -th energy level. The dominant terms of α_d in this sum are the ones for m , such that ϵ_m^0 is close to ϵ_k^0 . Given this we can approximate $\epsilon_n^0 - \epsilon_m^0 \propto \frac{1}{n^3}$, where n denotes the principle quantum number of the k -th energy eigenstate, further the expectation value $|\langle \psi_k | r | \psi_m \rangle| \propto n^2$ [19]. Therefore we arrive at a scaling law for the polarizability $\alpha_d \propto n^7$. With the knowledge of second order perturbation theory, we can readily solve for the effective potential

$$V_{\text{a-i}}(R) = - \left(\frac{e}{4\pi\epsilon_0} \right)^2 \frac{\alpha_d}{2R^4}, \quad (1.6)$$

1. Introduction

which we define as the difference between the shifted energy ϵ_k due to the presence of the ion and the energy ϵ_k^0 of the free atom case. That this difference can in fact be seen as an approximation for the potential between atom and ion will be derived in chapter 3. Thus we obtain, that the atom-ion interaction scales with $\alpha_d \propto n^7$, and we can conclude that even weak dressing will boost the interaction into the relevant regime. But since we now have a system so sensitive to electric fields, the Paul trapping fields have to be taken into account. In addition, as already mentioned, the radii of the Rydberg wave functions scale proportional to n^2 , thus that we may have to consider also higher order terms, i. e. quadrupole terms, in the expansion of the ion potential. All this makes a careful analysis necessary.

This thesis

In this thesis we will pass through such a detailed examination for the simplest possible example, namely a single alkali Rydberg atom coupled to an ion. In the final project we demonstrate the feasibility of realizing atom-ion spin-spin interactions in a realistic system. Here, let us give an intuitive explanation of how the spin-spin interaction comes about. We imagine the following setup illustrated in Fig. 1.1: left is an ion trapped in the potential of a quadrupole Paul trap (red-left), in its close vicinity $d \approx 1 \mu\text{m}$ there is an atom (blue-right) trapped in an optical dipole field. For the atom in a ground state the interaction between atom and ion is too weak to have an effect, but if we couple the atom's ground state weakly to a Rydberg state $|R\rangle$, this pushes the atom-ion interaction into the regime relevant over μm distances. We can make the interaction dependent on the hyperfine structure state the atom is in, which we denote with $|\uparrow\rangle_a$ and $|\downarrow\rangle_a$, e.g. by choosing appropriate laser polarization. Thus the interaction is now only present, if the atom is say in the state $|\uparrow\rangle_a$. If the amount of Rydberg admixture is varied in time, by amplitude modulating the laser, the atom ion interaction becomes time-dependent. If we now modulate the laser close to the ionic trap frequency, we will induce motion in the ion when the atom is in state $|\uparrow\rangle_a$. As long as $\omega_a \neq \omega_i$, the atomic motion will not be affected. We will show that the effective interaction (to lowest order in the ion position and within the rotating wave approximation) can be described by:

$$\hat{H}_I \propto \left(\hat{a}^\dagger e^{i\delta t} + \hat{a} e^{-i\delta t} \right) |\uparrow\rangle_a \langle \uparrow|, \quad (1.7)$$

with a^\dagger and a the creation and annihilation operators of the ionic motion. An additional laser field that generates an ion spin-motion interaction of the form

$$\hat{H}_{S-M} \propto \left(\hat{a}^\dagger e^{i\delta t} + \hat{a} e^{-i\delta t} \right) |\uparrow\rangle_i \langle \uparrow|, \quad (1.8)$$

can be used to map the ion motion onto internal states of the ion. This generates effective (pseudo) spin-spin interactions between atoms and ions [54]. Note that this work has already been submitted for publication [65].

To attack the system theoretically, we do a step by step analysis of systems with

increasing complexity. The solution at each stage will build the basis for the next more complicated system. We start with the study of a single free alkali Rydberg atom, add static external fields and the ion and finally include the time-dependent dressing and dipole laser fields. We arrive at a two particle description for atom and ion both harmonically trapped with an additional effective interaction force between the two particles. In the fifth chapter, as a final project, we will demonstrate an application of the proposed scheme by discussing the spin-spin interactions announced above, including a study of effects due to micromotion.

1. Introduction

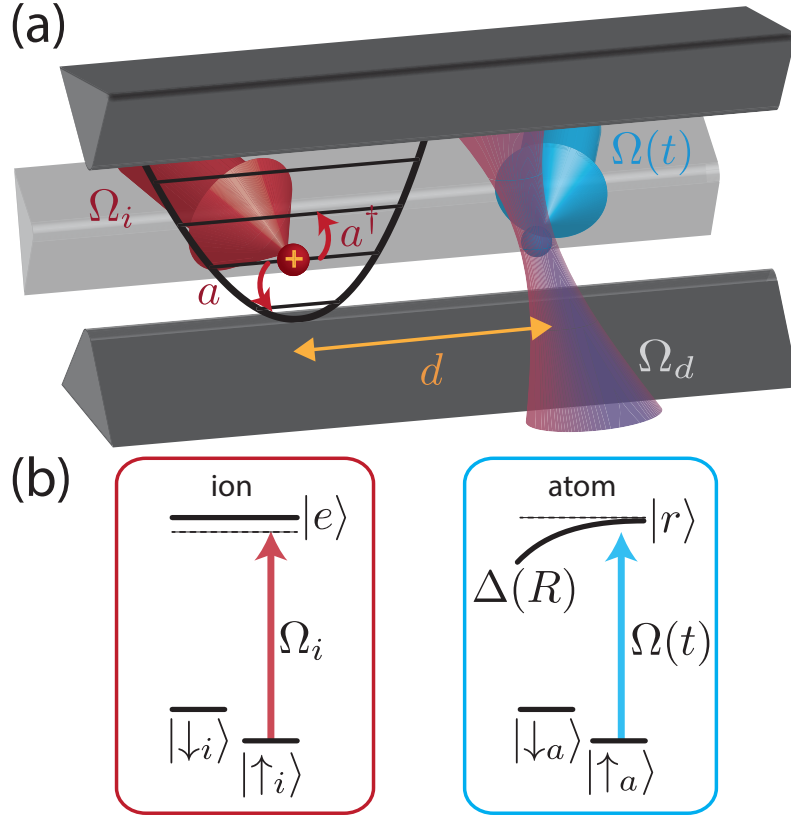


Figure 1.1.: (a) We consider an ion (red ball) trapped in a Paul trap (grey electrodes) experiencing a harmonic confinement with trapping frequency ω_i and lowering (raising) operators a (a^\dagger). A distance d away, an atom (blue ball) is optically trapped with Rabi frequency Ω_d and coupled to a Rydberg state with a time-dependent laser (blue arrow) of Rabi frequency $\Omega(t)$. (b) Internal atomic (right) and ionic (left) level scheme. The Rydberg state experiences a position dependent Stark shift $\Delta(R)$, with R the distance between the atom and the ion, due to the electric field of the ion. The resulting force may be used to entangle the atom and the ion when coupling to the Rydberg state depending on the internal state of the atom as described in the text.

2. Alkali Rydberg atoms

In this chapter we give an overview of single channel quantum defect theory (QDT) and how we apply it to obtain an effective theoretical description of alkali Rydberg atoms. We will derive a formalism to calculate effective eigenvalues and states. In this work we will always stay in a regime, where we can treat all additional fields acting on the atom perturbatively. Thus the single channel QDT framework we introduce here, forms the basis for most of the simulations and considerations in this thesis.

QDT is based on the physical idea that in a highly excited state of the electron shell all electrons of the atom except one are strongly bound to the nucleus [9, 19, 64]. This leads to a charge distribution that is well localized in a small region close to the nucleus position. We call the total object comprised of the nucleus and the inner electrons the core, the remaining electron is called the Rydberg electron. In many situations it is sufficient to describe the total Rydberg atom as an effective two particle system composed of the positively charged core and the single Rydberg electron. Particularly for alkali atoms, where the core is in a stable noble gas configuration, this description is highly suitable. The core and the Rydberg electron interact in the easiest case of single channel QDT via an effective potential $V_{\text{Ryd}}(\mathbf{r})$ [45], where \mathbf{r} is the relative core-Rydberg electron coordinate. For distances much larger than the core extent, the Rydberg potential resembles the potential of a single pointcharge $-V_C(\mathbf{r}) = -e^2/(4\pi\epsilon_0|\mathbf{r}|)$, with e the elementary charge and ϵ_0 the permittivity of free space. Analytical solutions to the pointcharge problem are known [9, 64]. If also solutions for the core region are at hand, one is able to obtain solutions for the complete single channel problem by selecting the specific pointcharge solution for the out-of-core region that matches the core region solution at the core boundary. For the bound case the boundary conditions together with the normalization condition for the solution then yield the Rydberg formula [9]

$$\epsilon = -\frac{R_M}{(n - \delta_l(\epsilon))^2}, \quad (2.1)$$

which accurately describes the experimentally observed energy spectrum of alkali atoms close to the ionization threshold. Here, $R_M = R_\infty(1 - m_e/m_c)$, with R_∞ the Rydberg constant, m_e the electron mass and m_c the core mass is the modified center of mass Rydberg constant, $n \in \mathbb{N}$ is the principle quantum number and $\delta_l(\epsilon)$ is the quantum defect at a given energy ϵ and fixed azimuthal quantum number $l \in \{0, \dots, n - 1\}$. The quantum defect decreases with increasing l , since for higher Angular momentum at fixed energy the classical orbits become more circular, thus the probability of finding the Rydberg electron in the core region decreases. The dependence of the quantum defects $\delta_l(\epsilon)$ on energy is in the alkali case extremely

2. Alkali Rydberg atoms

weak, such that a mild linear energy dependence $\delta_l = \delta_l^0 + \delta_l^1(n - \delta_l^0)^{-2}$ suffices to fit even most accurate experimental measurements [23].

2.1. The Rydberg electron in a central core potential

Here we analyze the interaction of an electron with a charged core. We begin in reducing the total Hamiltonian to a family of radial Hamiltonians. Afterwards we discuss the general solutions to this problem and discuss as a first example the familiar hydrogen case and generalize to the general single channel QDT problem to obtain the Rydberg formula.

We assume that after changing to relative and center-of-mass (COM) coordinates and reduction of the COM motion the effective core-electron Hamiltonian is given by

$$\hat{H} = \frac{\hat{\mathbf{p}}^2}{2\mu} + V_{\text{Ryd}}(|\mathbf{r}|). \quad (2.2)$$

Here \mathbf{r} , $\hat{\mathbf{p}}$ and μ denote the relative electron core position, the corresponding momentum operator and the reduced mass of the system. The operator does not act on the spin component of the wave function, so the problem reduces to a spatial one. Since the problem is spherically symmetric we pass to spherical coordinates

$$\begin{aligned} x &= r \sin(\theta) \cos(\phi), \\ y &= r \sin(\theta) \sin(\phi), \\ z &= r \cos(\theta). \end{aligned} \quad (2.3)$$

In spherical coordinates the Hamiltonian, which now acts on $L^2(\mathbb{R}, r^2 dr) \otimes L^2(S^2)$, reads

$$\hat{H} = -\frac{\hbar^2}{2\mu} \left(\frac{1}{r^2} \partial_r r^2 \partial_r \otimes \mathbf{1}_{L^2(S^2)} - \frac{1}{\hbar^2 r^2} \otimes \hat{\mathbf{L}}^2 \right) + V_{\text{Ryd}}(r) \otimes \mathbf{1}_{L^2(S^2)}, \quad (2.4)$$

where \hbar denotes the reduced Planck constant and

$$\hat{\mathbf{L}}^2 = \hbar^2 \left(-\frac{1}{\sin(\theta)} \partial_\theta \sin(\theta) \partial_\theta - \frac{1}{\sin(\theta)^2} \partial_\phi^2 \right) \quad (2.5)$$

is the operator of the square of the absolute value of angular momentum. $\hat{\mathbf{L}}^2$ as an operator acting on the space of square integrable functions on the sphere in 3 dimensions $L^2(S^2)$, has a purely discrete spectrum, with eigenvalues equal to $\hbar^2 l(l+1)$, $l \in \mathbb{N}_0$. Each eigenvalue is $(2l+1)$ -times degenerate. One base of eigenvectors that span the eigenspaces is given by $|l, m\rangle$ where $m \in \{-l, \dots, l\}$ is the index taking account for degeneracy, in coordinate representation the $|l, m\rangle$ are given by means of spherical harmonics $\langle \theta, \phi | l, m \rangle = Y_{l,m}(\theta, \phi)$ [60, 68]. Rigorous proofs for those results via the theory of Sturm Liouville operators with careful treatment of the various

2.1. The Rydberg electron in a central core potential

domains the operators are defined on, can be found in [67]. Since the projectors $P_{l,m} = \mathbb{1} \otimes |l, m\rangle\langle l, m|$ commute with \hat{H} , we can reduce \hat{H}

$$\begin{aligned}
\hat{H} &= \sum_{l,m,l',m'} P_{l',m'} \hat{H} P_{l,m} \\
&= \sum_{l,m} P_{l,m} \hat{H} P_{l,m} \\
&= \bigoplus_{l,m} \hat{H}_r(l, m) \otimes |l, m\rangle\langle l, m| \\
&= \bigoplus_{l,m} \hat{H}_r(l) \otimes |l, m\rangle\langle l, m|
\end{aligned} \tag{2.6}$$

This yields a radial problem $\hat{H}_r(l)$ for each value of l

$$\hat{H}_r(l) = -\frac{\hbar^2}{2\mu} \left(\frac{1}{r^2} \partial_r r^2 \partial_r - \frac{l(l+1)}{r^2} \right) + V_{\text{Ryd}}(r). \tag{2.7}$$

Thus we have now reached our first goal, the total Hamiltonian is transformed to an orthogonal sum of operators acting on the r coordinate only, depending on the angular momentum state $|l, m\rangle$ the atom is in.

We make use of a unitary transformation to simplify the radial operator

$$\begin{aligned}
L^2((0, \infty), r^2 dr) &\rightarrow L^2((0, \infty)). \\
R(r) &\mapsto u(r) = rR(r)
\end{aligned} \tag{2.8}$$

The transformed operator reads

$$\hat{H}_r(l) = -\frac{\hbar^2}{2\mu} \left(\partial_r^2 - \frac{l(l+1)}{r^2} \right) + V_{\text{Ryd}}(r). \tag{2.9}$$

We restrict the problem now to the non core region, where the potential V_{Ryd} is known to be well approximated by $-V_C(\mathbf{r})$. To arrive at a rescaled version independent on physical constants, we transform coordinates and rescale the Hamiltonian such that the prefactors of the kinetic and potential parts $-\hbar^2/\mu$ and $e^2/(4\pi\epsilon_0)$ are simply given by 1/2 and 1, respectively. Therefore we transform $\mathbf{r} \rightarrow \tilde{\mathbf{r}} = \gamma^{-1}\mathbf{r}$, then $\hat{\mathbf{p}} \rightarrow \tilde{\hat{\mathbf{p}}} = \gamma\hat{\mathbf{p}}$ and rescale with κ^{-1} . Thus

$$\frac{1}{\kappa} \tilde{\hat{H}}_r(l) = -\frac{1}{\kappa\gamma^2} \frac{\hbar^2}{2\mu} \left(\partial_{\tilde{r}}^2 - \frac{l(l+1)}{\tilde{r}^2} \right) - \frac{1}{\kappa\gamma} \frac{e^2}{4\pi\epsilon_0 \tilde{r}}, \tag{2.10}$$

so we have to choose

$$\gamma = \frac{e^2}{\kappa 4\pi\epsilon_0}, \quad \kappa = \left(\frac{e^2}{4\pi\epsilon_0} \right)^2 \frac{\mu}{\hbar^2} \tag{2.11}$$

to get

$$\hat{H}_r(l) = -\frac{1}{2} \left(\partial_r^2 - \frac{l(l+1)}{r^2} \right) - \frac{1}{r}, \tag{2.12}$$

2. Alkali Rydberg atoms

where we replaced \tilde{r} by r again. Since we search for the Eigenfunctions $u(r)$ and Eigenvalues ϵ of this Operator, we have to solve the problems

$$\left[\partial_r^2 - \frac{l(l+1)}{r^2} + \frac{2}{r} + 2\epsilon \right] u(r) = 0. \quad (2.13)$$

Now we want to discuss the solutions to the above problems Eq. (2.13) and remind, that among all solutions we have to figure out the particular ones that yield the approximative description of the radial Rydberg wave functions and the corresponding eigenvalues. The differential equation to be solved is of second order, so the solutions space will be spanned by two linear independent solutions. We discuss two solution pairs that individually span the solution space [9]. These solutions are of special interest in the derivation of the Rydberg and hydrogen energy spectra, due to their properties at $r \rightarrow 0$ and $r \rightarrow \infty$. So we start in defining regular solutions, i.e. a solution is called regular at 0 or ∞ , if it does not diverge for $r \rightarrow 0$ or $r \rightarrow \infty$, respectively. For each value of ϵ there exists exactly one solution not diverging at 0 or ∞ . We start now in defining the first pair of solutions. With $f_l(\epsilon, r)$ we denote the solution that vanishes as $r \rightarrow 0$. $f_l(\epsilon, r)$ together with the solution $g_l(\epsilon, r)$ diverging as $r \rightarrow 0$ and taken to be out of phase with $f_l(\epsilon, r)$, makes the first pair of solutions we want to consider. There is another base of solutions for which the asymptotic behaviour at $r \rightarrow \infty$ is known spanned by $F^{(+)}(\epsilon, l, r) \propto \left(\frac{2r}{\nu}\right)^{-\nu} e^{\frac{r}{\nu}}$ for $r \rightarrow \infty$ and $F^{(-)}(\epsilon, l, r) \propto \left(\frac{2r}{\nu}\right)^{\nu} e^{-\frac{r}{\nu}}$ for $r \rightarrow \infty$. $F^{(-)}$ corresponds to the solution regular at ∞ and $\nu = \sqrt{-1/(2\epsilon)}$. In Fig. 2.1 we show examples of the functions $F^- \propto \tilde{F}^-$ and $f \propto \tilde{f}$ up to proper rescaling and in Fig 2.1 (a) we also constructed an approximate version of g approximately proportional to \tilde{g} , with the help of Eq. (2.14).

As a first example we want to consider the hydrogen case to demonstrate the underlying reasoning at a common example. We have to investigate solutions on the complete positive r -axis. A solution is square integrable on this domain exactly when it is regular at 0 and infinity. This leads to the matching condition, that there is a square integrable solution if and only if $f_l(\epsilon, r) = cF^{(-)}(\epsilon, l, r)$. Therefore we express f_l and g_l in the $F^{(+)}$, $F^{(-)}$ base, which can be done in the following way for properly rescaled solutions

$$\begin{aligned} f_l(\epsilon, r) &= \sin(\beta_l(\epsilon))F^{(+)} - \cos(\beta_l(\epsilon))F^{(-)}, \\ g_l(\epsilon, r) &= -\cos(\beta_l(\epsilon))F^{(+)} - \sin(\beta_l(\epsilon))F^{(-)}, \end{aligned} \quad (2.14)$$

where

$$\beta_l(\epsilon) = [\sqrt{-1/(2\epsilon)} - l]\pi. \quad (2.15)$$

The matching condition demands now that $\sin(\beta_l(\epsilon)) = 0$, which is equivalent to

$$[\sqrt{-1/(2\epsilon)} - l] = m \in \mathbb{Z}. \quad (2.16)$$

Redefining $n = m + l$ leads to the known hydrogen energy spectrum

$$\epsilon = -\frac{1}{2n^2}. \quad (2.17)$$

After this first example we go on and discuss the single channel QDT case. Now equation (2.12) has to be solved just for the non core region. So the matching condition changes to one at the boundary of the core region, which could be specified by ab initio methods from solutions of the full problem inside the core region [9].

We follow another line and expect that the Rydberg potential V_{Ryd} is in the core region steeper than the coulomb potential, since the nucleus gets less and less screened by the inner electron cloud as one moves in nucleus direction. This results in a heavier oscillation of the wave function in the core region causing a slight phase shift at the core boundary compared to the hydrogen case. One can take account for this by a mixture of f_l and g_l

$$\psi_l(\epsilon, r) \propto \cos(\pi\delta_l)f_l(\epsilon, r) - \sin(\pi\delta_l)g_l(\epsilon, r), \quad (2.18)$$

from which follows that

$$\psi_l(\epsilon, r) \propto \sin[\beta_l(\epsilon) + \pi\delta_l(\epsilon)]F^{(+)} - \cos[\beta_l(\epsilon) + \pi\delta_l(\epsilon)]F^{(-)}. \quad (2.19)$$

Demanding regularity at infinity we thus get the condition

$$\sqrt{-1/(2\epsilon)} - l + \delta_l(\epsilon) = m, \quad (2.20)$$

which yields the Rydberg formula

$$\epsilon = -\frac{1}{2(n - \delta_l(\epsilon))^2}. \quad (2.21)$$

With single channel QDT we have now a description at hand which connects the observed quantum defects δ_l with a phase shift in the oscillating part of the wave function, that occurs due to the influence of the non coulomb part in the core region of the Rydberg potential $V_{\text{Ryd}}(\mathbf{r})$.

In the following we will use experimentally determined defect functions [23] to obtain the Rydberg wave functions and assume that a corresponding core potential $V_{\text{Ryd}}(\mathbf{r})$ exists. This guarantees that the wave functions are eigenstates of a self adjoint operator and thus orthogonal. Therefore we first modify the case discussed to include also relativistic corrections and solve the resulting problem by the numerical Numerov method [70].

2.2. The relativistic Hamiltonian

We amend single channel QDT to incorporate fine structure correction terms into the Hamiltonian of the Rydberg electron. We need this, since the experimental defect values we use, are given in fine structure base. Here we derive the fine structure correction terms for a electron core system in the limiting case for an infinitely heavy core from Dirac's equation in an external electric field. Doing this has two reasons, the first is of course to see how the correction terms arise. The second is that to obtain the radial wave functions numerically, we do not want to use the final form in the

2. Alkali Rydberg atoms

derivation, but one step before, where the equations still fit the numerical methods we use.

Let us now start with the derivation of the fine structure correction terms. As announced we approximate by an infinitely heavy core [18]. This yields to the equations of a relativistic electron coupled to an external electrostatic potential V

$$\begin{aligned}\hat{\boldsymbol{\sigma}} \cdot \hat{\mathbf{p}}_e \psi_B &= \frac{1}{c} (E - V(\mathbf{r}_e) - m_e c^2) \psi_A \\ \hat{\boldsymbol{\sigma}} \cdot \hat{\mathbf{p}}_e \psi_A &= \frac{1}{c} (E - V(\mathbf{r}_e) + m_e c^2) \psi_B,\end{aligned}\tag{2.22}$$

with $\hat{\boldsymbol{\sigma}} = (\sigma_x, \sigma_y, \sigma_z)$ and σ_i the Pauli matrices, $\hat{\mathbf{p}}_e$, \mathbf{r}_e and m_e the electron momentum, position and mass, E the relativistic energy, c the speed of light and ψ_A and ψ_B the small and big component of the Dirac wave function, respectively. Instead of solving this set of coupled equations for a spherically symmetric core potential by analytical methods as in [36], we substitute the second into the first of Eqs. (2.22), which yields a one particle problem equivalent to the coupled one if $E - V + m_e c^2 \neq 0$ almost everywhere (*a.e.*)

$$\hat{\boldsymbol{\sigma}} \cdot \hat{\mathbf{p}}_e \frac{c^2}{(E - V(\mathbf{r}_e) + m_e c^2)} \hat{\boldsymbol{\sigma}} \cdot \hat{\mathbf{p}}_e \psi_A = (E - V(\mathbf{r}_e) - m_e c^2) \psi_A\tag{2.23}$$

and approximate the resulting equation by neglecting terms of order higher than α^2 . We note here that in atomic units $1/c = \alpha$, this will become clear when we rescale coordinates, but for now when we state a term is of order α one could as well say it is of order $1/c$. The approximation is done by replacing the non relativistic energy $E - m_e c^2$ with ϵ and expanding $((\epsilon - V(\mathbf{r}_e))/(2m_e c^2) + 1)^{-1}$ for $(\epsilon - V(\mathbf{r}_e))/(2m_e c^2) \ll 1$ (this approximation holds for $r \gg 1/\alpha^2$) up to order $\mathcal{O}(\alpha^4)$, so

$$\hat{\boldsymbol{\sigma}} \cdot \hat{\mathbf{p}}_e \frac{1}{2m_e} \left(1 - \frac{\epsilon - V(\mathbf{r}_e)}{2m_e c^2} \right) \hat{\boldsymbol{\sigma}} \cdot \hat{\mathbf{p}}_e \psi_A = (\epsilon - V(\mathbf{r}_e)) \psi_A.\tag{2.24}$$

We observe that the term $(\epsilon - V(\mathbf{r}_e))$ is present on both sides, but is suppressed by order α^2 on the left hand side. We now commute it on the left hand side to the right, such that we have the expression $(\epsilon - V(\mathbf{r}_e))\psi_A$ on both sides. This yields

$$\left(\frac{\hat{\mathbf{p}}_e^2}{2m_e} + \frac{1}{4m_e^2 c^2} \hat{\boldsymbol{\sigma}} \cdot \hat{\mathbf{p}}_e \hat{\boldsymbol{\sigma}} \cdot [V(\mathbf{r}_e), \hat{\mathbf{p}}_e] - \frac{\hat{\mathbf{p}}_e^2}{4m_e^2 c^2} (\epsilon - V(\mathbf{r}_e)) \right) \psi_A = (\epsilon - V(\mathbf{r}_e)) \psi_A.\tag{2.25}$$

We calculate the commutator

$$[V(\mathbf{r}_e), \hat{\mathbf{p}}_e] = i\hbar \nabla V\tag{2.26}$$

2.2. The relativistic Hamiltonian

and evaluate the second term

$$\begin{aligned}
& \frac{i\hbar}{4m_e^2c^2} \hat{\boldsymbol{\sigma}} \cdot \hat{\mathbf{p}}_e \hat{\boldsymbol{\sigma}} \cdot \nabla V \\
&= \frac{i\hbar}{4m_e^2c^2} \sum_{j,k=1}^3 \hat{\sigma}_j \hat{\sigma}_k \otimes p_{ej} \nabla V_k \\
&= \frac{i\hbar}{4m_e^2c^2} (\hat{\mathbf{p}}_e \cdot \nabla V - i\hat{\boldsymbol{\sigma}} \cdot (\nabla V \times \hat{\mathbf{p}}_e)).
\end{aligned} \tag{2.27}$$

We recursively substitute the left hand side for $(\epsilon - V(\mathbf{r}_e))\psi_A$ in Eq. (2.25) and keep just terms up to order α^2

$$\left(\frac{\hat{\mathbf{p}}_e^2}{2m_e} + \frac{i\hbar}{4m_e^2c^2} \hat{\mathbf{p}}_e \cdot \nabla V + \frac{\hbar}{4m_e^2c^2} \hat{\boldsymbol{\sigma}} \cdot (\nabla V \times \hat{\mathbf{p}}_e) - \frac{\hat{\mathbf{p}}_e^2 \hat{\mathbf{p}}_e^2}{8m_e^3c^2} \right) \psi_A = (\epsilon - V(\mathbf{r}_e)) \psi_A. \tag{2.28}$$

where the second term on the left hand side known as Darwin term has to be modified since it is not self adjoint. We correct this by adding the adjoint and dividing by 2

$$\frac{i\hbar}{4m_e^2c^2} \hat{\mathbf{p}}_e \cdot \nabla V \rightarrow \frac{i\hbar}{8m_e^2c^2} (\hat{\mathbf{p}}_e \cdot \nabla V - \nabla V \cdot \hat{\mathbf{p}}_e) = \frac{\hbar^2}{8m_e^2c^2} \Delta V. \tag{2.29}$$

This yields the order α^2 approximation of the Dirac equation for an electron moving in an external electrostatic potential

$$\left(\frac{\hat{\mathbf{p}}_e^2}{2m_e} + \frac{\hbar^2}{8m_e^2c^2} \Delta V + \frac{\hbar}{4m_e^2c^2} \hat{\boldsymbol{\sigma}} \cdot (\nabla V \times \hat{\mathbf{p}}_e) - \frac{\hat{\mathbf{p}}_e^2 \hat{\mathbf{p}}_e^2}{8m_e^3c^2} \right) \psi_A = (\epsilon - V(\mathbf{r}_e)) \psi_A. \tag{2.30}$$

To arrive at this equation was our first goal for this section.

To continue, let us give a small prospect on the terms we consider in the next sections. There we have to deal with the atom Hamiltonian H_a similar to the above one

$$H_a = \frac{\hat{\mathbf{p}}^2}{2\mu} + V_{\text{Ryd}}(\mathbf{r}) - \frac{\hat{\mathbf{p}}^2 \hat{\mathbf{p}}^2}{8m_e^3c^2} + \frac{\hbar}{4m_e^2c^2} \hat{\boldsymbol{\sigma}} \cdot (\nabla V_{\text{Ryd}} \times \hat{\mathbf{p}}), \tag{2.31}$$

where $\hat{\mathbf{p}}$ and \mathbf{r} denote the momentum and center of mass of the relative Rydberg electron core coordinate, μ is the reduced mass and V_{Ryd} denotes as before the Rydberg potential. We note that we think of the Darwin term to be already absorbed in the Rydberg potential. We search for approximate eigenstates of this Hamiltonian, while the eigenenergies will be given. To find those approximate eigenstates, we resubstitute $(\epsilon - V(\mathbf{r}_e))$ in the kinetic energy correction, which is correct up to order α^4 and also restrict the problem to the non-core region, thus

$$V_{\text{Ryd}} = -\frac{e^2}{4\pi\epsilon_0} \frac{1}{|\mathbf{r}|} \tag{2.32}$$

and we are left with the eigenvalue problem

$$\left[\frac{\hat{\mathbf{p}}^2}{2\mu} \left(1 - \frac{\epsilon - V_{\text{Ryd}}}{2m_e c^2} \right) - \frac{e^2 \hbar}{16\pi\epsilon_0 m_e^2 c^2} \frac{1}{|\mathbf{r}|^3} \boldsymbol{\sigma} \cdot (\mathbf{r} \times \hat{\mathbf{p}}) \right] \psi = (\epsilon - V_{\text{Ryd}}) \psi. \tag{2.33}$$

2. Alkali Rydberg atoms

We substitute $\hbar\boldsymbol{\sigma} \cdot (\mathbf{r} \times \hat{\mathbf{p}}) \rightarrow 2\hat{\mathbf{L}} \cdot \hat{\mathbf{S}} = \hat{\mathbf{J}}^2 - \hat{\mathbf{L}}^2 - \hat{\mathbf{S}}^2$ for $\mathbf{J} = \mathbf{L} \otimes \mathbb{1} + \mathbb{1} \otimes \mathbf{S}$:

$$\left[\frac{\hat{\mathbf{p}}^2}{2\mu} \left(1 - \frac{\epsilon - V_{\text{Ryd}}}{2m_e c^2} \right) - \frac{e^2}{16\pi\epsilon_0 m_e^2 c^2} \frac{1}{|\mathbf{r}|^3} (\hat{\mathbf{J}}^2 - \hat{\mathbf{L}}^2 - \hat{\mathbf{S}}^2) \right] \psi_{=(\epsilon - V_{\text{Ryd}})} \psi. \quad (2.34)$$

and change to the fine structure base $R(r) \otimes |l, j, m_j\rangle$, in which $(\hat{\mathbf{J}}^2 - \hat{\mathbf{L}}^2 - \hat{\mathbf{S}}^2)$ is diagonal. As in the hydrogen case we can reduce the operator now to a family of radial problems:

$$\left[\frac{\hbar^2}{2\mu} \left(-\frac{1}{r^2} \partial_r r^2 \partial_r + \frac{l(l+1)}{r^2} \right) \left(1 - \frac{\epsilon - V}{2m_e c^2} \right) - \frac{e^2 \hbar^2}{16\pi\epsilon_0 m_e^2 c^2} \frac{1}{r^3} \left(j(j+1) - l(l+1) - \frac{3}{4} \right) \right] R(r) = (\epsilon - V) R(r). \quad (2.35)$$

We change coordinates as in the foregoing section $\mathbf{r} \rightarrow \tilde{\mathbf{r}} = \gamma^{-1} \mathbf{r}$, then $\hat{\mathbf{p}} \rightarrow \tilde{\hat{\mathbf{p}}} = \gamma \hat{\mathbf{p}}$ and also rescale with κ^{-1} . This yields

$$\left[\frac{1}{2} \left(-\frac{1}{r^2} \partial_r r^2 \partial_r + \frac{l(l+1)}{r^2} \right) \left(1 - \frac{\alpha^2 \mu (\epsilon + \frac{1}{r})}{2m_e} \right) - \frac{\alpha^2 \mu^2}{4m_e^2} \frac{1}{r^3} \left(j(j+1) - l(l+1) - \frac{3}{4} \right) \right] R(r) = (\epsilon + \frac{1}{r}) R(r). \quad (2.36)$$

After an additional transformation this problem can be solved by the numerical method discussed in the following section.

2.3. Radial Rydberg wave functions

We want to obtain the radial wave functions numerically via the Numerov method [70], which enables us to find numerical solutions to differential equations of the type

$$\chi''(x) = -a(x)\chi(x) \quad (2.37)$$

on a grid of spacing h . With the help of Taylor expansion methods, one can derive the following relation for values of the solution χ at neighbouring grid points

$$\chi_{n-1} = \frac{2\chi_n \left(1 - \frac{5h^2}{12} a_n \right) - \chi_{n+1} \left(1 + \frac{h^2}{12} a_{n+1} \right)}{1 + \frac{h^2}{12} a_{n-1}} + \mathcal{O}(h^6), \quad (2.38)$$

where $x_n := x_0 + hn$, $\chi_n := \chi(x_0 + hn)$ and $a_n := a(x_0 + hn)$.

Before we address the relativistic problem Eq. (2.36), we test the Numerov method in the coulomb case Eq. (2.13) and compare the solutions obtained to the analytic ones. For better accuracy of the Numerov algorithm in the close to core region, we first transform Eq. (2.13) to logarithmic coordinates via the unitary transformation

$$\begin{aligned} L^2((0, \infty), r^2 dr) &\rightarrow L^2((0, \infty), e^{2x} dx) \\ R(r) &\mapsto \chi(x) = e^{\frac{x}{2}} R(e^x). \end{aligned} \quad (2.39)$$

2.3. Radial Rydberg wave functions

After rearrangement of terms this yields

$$\chi''(x) = \left[l(l+1) + \frac{1}{4} - \epsilon e^{2x} - e^x \right] \chi(x), \quad (2.40)$$

such that the Numerov algorithm can be applied.

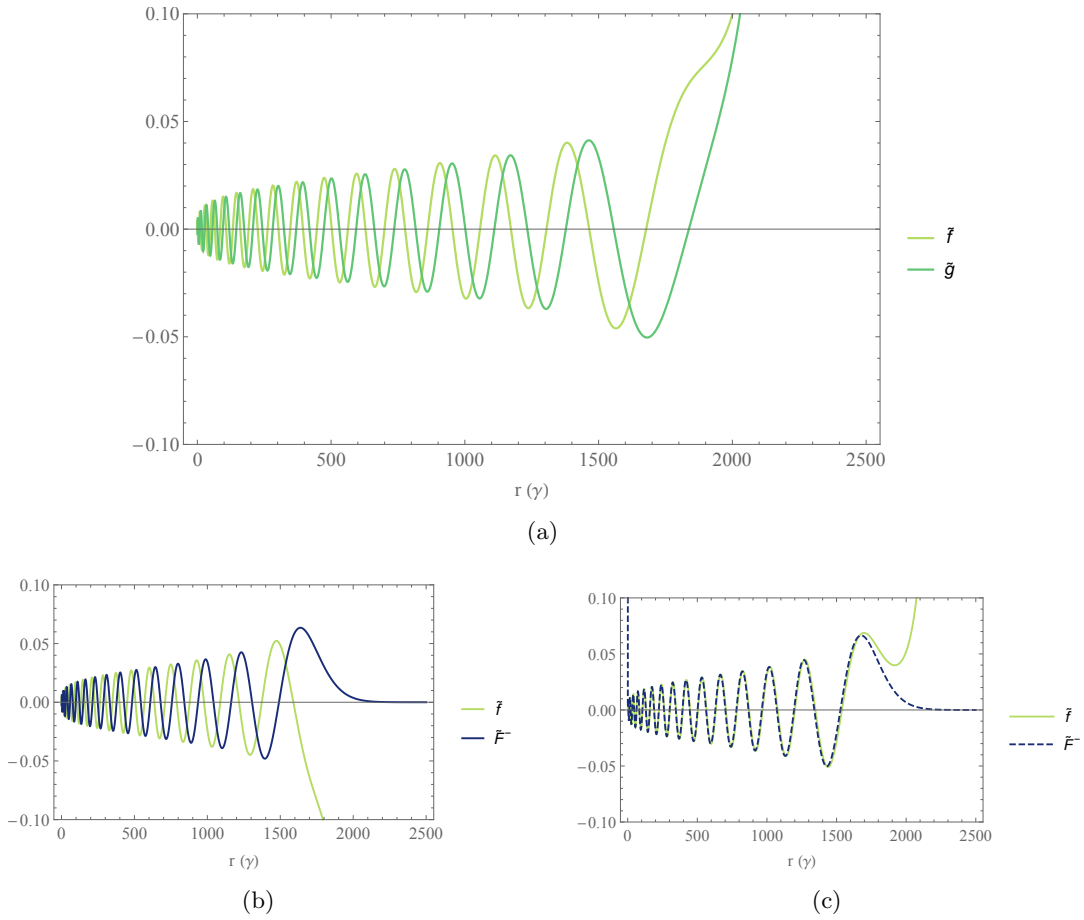


Figure 2.1.: Coulomb wave functions \tilde{F}^- , \tilde{f} and \tilde{g} as defined in the main text for: (a) $n = 30.75$ and $l = 0$, the functions are normed on the interval $(50, 1800)$, (b) $n = 30 - \delta_{30,0,1/2} = 29.6005$ and $l = 0$, (c) $n = 30 - \delta_{30,1,1/2} = 29.9528$ and $l = 1$. The functions in (b) and (c) are all normed on $(50, 1600)$ with $\delta_{n,l,j}$ the quantum defect values for ${}^6\text{Li}$ taken from [23]. We note that the functions \tilde{g} and \tilde{F}^- we plotted here are all diverging for $r \rightarrow 0$.

Since the analytical solutions discussed in section 2.1 are not available in Wolfram Mathematica, we transform the differential equation to one, for which the solutions are included. Therefore we introduce new variables in Eq. (2.13) $v(x) =$

2. Alkali Rydberg atoms

$e^{x/2}/x^{l+1}u(x/(2\sqrt{-2\epsilon}))$, this transforms Eq. (2.13) into Kummer's equation [67]

$$xv''(x) + (b-x)v'(x) - av(x) = 0, \quad (2.41)$$

with $b = 2l + 1$ and $a = (l + 1) - 1/\sqrt{-2\epsilon}$. Two independent solutions, namely Kummer's function $M(a, b, x) = {}_1F_1(a, b, x)$, which is a generalized hypergeometric series and the Tricomi confluent hypergeometric function $U(a, b, x)$. Thus the analytic solutions to the coulomb problem read

$$\begin{aligned} \tilde{f} &\propto (2\sqrt{-2\epsilon r})^{l+1} e^{-\sqrt{-2\epsilon r}} M((l+1) - 1/\sqrt{-2\epsilon}, 2l+1, 2\sqrt{-2\epsilon r}) \\ &\text{and} \\ \tilde{F}^- &\propto (2\sqrt{-2\epsilon r})^{l+1} e^{-\sqrt{-2\epsilon r}} U((l+1) - 1/\sqrt{-2\epsilon}, 2l+1, 2\sqrt{-2\epsilon r}). \end{aligned} \quad (2.42)$$

$U(a, b, x)$ is known to converge to a polynomial in $1/x$ with exponents bigger than a for $x \rightarrow \infty$ so \tilde{F}^- decays exponentially. M is regular at $r = 0$ and so is \tilde{f} [1]. We mention that despite a constant factor the so obtained solutions are equal to f and F^- and we know that the solutions will be linearly independent except in the hydrogen case. In figure 2.1 (b) and (c) we show \tilde{f} and \tilde{F}^- for the for the 30S and P state of ${}^6\text{Li}$ rescaled such that the integral of the absolute value squared of the solution over a reasonable region of the oscillating part, i.e. where the divergence has not started, is equal to one. With this rescaling one can construct another solution $\tilde{g} = -(\tilde{F}^- - \tilde{f} \cos(\beta_l(\epsilon))) \sin(\beta_l(\epsilon))^{-1}$ according to Eq. (2.14), to also get an approximate version up to a prefactor for the functions g , discussed in section 2.1. For the rescaling described above we observe that \tilde{f} and \tilde{g} are indeed approximately out of phase as announced in section 2.1.

We now have the analytic solutions at hand, thus we now search for the decaying solution with the Numerov method. We start the Numerov iteration at a point far separated from the core at $x_{\max} = \ln(2n(n+15))$, where the solution we search for is of the decaying form. We iterate into core direction and stop at the classical inner turning point $x_{\min} = \ln\left(n^* - \sqrt{n^{*2} - (l+1/2)^2}\right)$, before the solution starts diverging. The values x_{\max} and x_{\min} are chosen in accordance with [70]. Before starting the iteration, we have to choose two starting conditions, but since we are only interested in rescaled solutions, such that they are normed on the interval (x_{\min}, x_{\max}) , there remains only one free parameter, which can be determined by the relative slope at the starting point $\chi'(x_{\max})/\chi(x_{\max}) = (\chi(x_{\max}) - \chi(x_{\max} - h))/(h\chi(x_{\max}))$. For a starting value we take the relative slope of the decaying solution of the coulomb problem in the logarithmic coordinate frame see Eq. (2.39) at x_{\max} . We compared the numerical results with \tilde{F}^- . The numerical solutions are in good agreement with the analytical ones, as can be seen in figure 2.2, where we exemplarily give the results for the 30S state of ${}^6\text{Li}$ for different step sizes h .

Since we have now assured for the quality of the Numerov method, we now apply it to solve the relativistically corrected radial problem Eq. (2.36). We again perform

2.3. Radial Rydberg wave functions

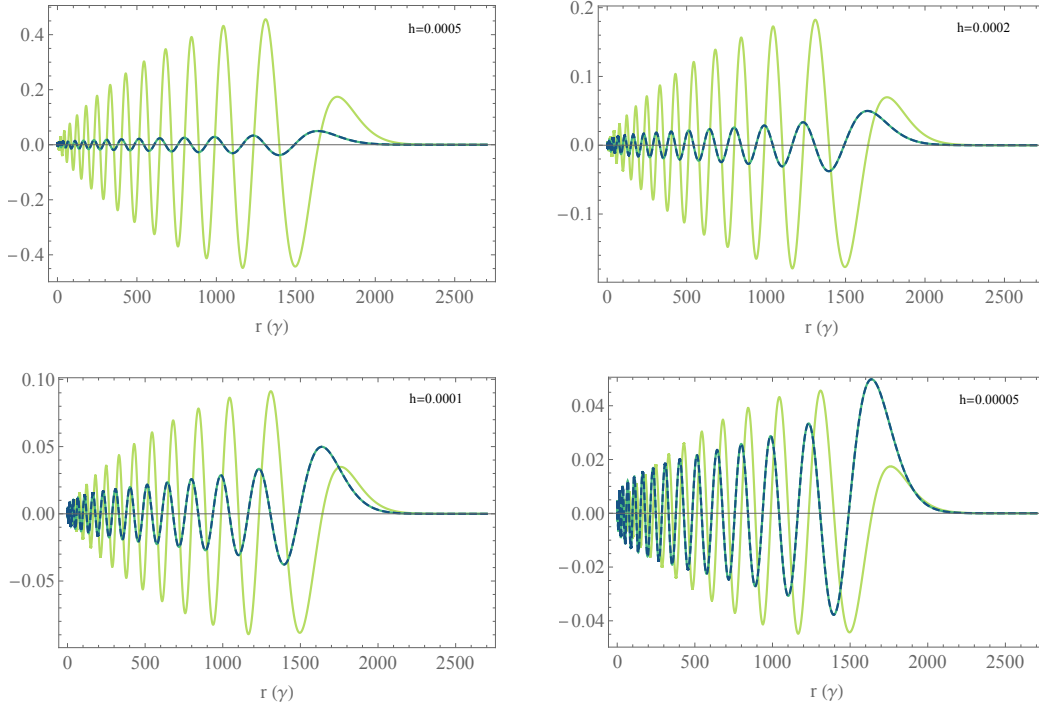


Figure 2.2.: Comparison of the numerically obtained solutions (dark green) with the analytical solution \tilde{F}^- (blue dashed) with $n = 29.6005$, $l = 0$ for different step sizes h . We also give the difference numerical minus analytical solution (light green), which we scaled up by a factor of 1000. We note that h is the step size in the logarithmic coordinate frame.

the transformation to logarithmic coordinates Eq. (2.39). This yields

$$\left[\frac{1}{2} e^{-2x} \left(-\partial_x^2 + l(l+1) + \frac{1}{4} \right) \left(1 - \frac{\alpha^2 \mu (\epsilon + e^{-x})}{2m_e} \right) - \frac{\alpha^2 \mu^2}{4m_e^2} e^{-3x} \left(j(j+1) - l(l+1) - \frac{3}{4} \right) \right] \chi(x) = (\epsilon + e^{-x}) \chi(x). \quad (2.43)$$

We transform

$$\chi \mapsto \tilde{\chi} = \left(1 - \frac{\alpha^2 \mu (\epsilon + e^{-x})}{2m_e} \right) \chi \quad (2.44)$$

and solve for $\tilde{\chi}''(x)$

$$\tilde{\chi}''(x) = \left[l(l+1) + \frac{1}{4} - \frac{\epsilon e^{2x} + e^x + \frac{\alpha^2 \mu^2}{4m_e^2} e^{-x} (j(j+1) - l(l+1) - \frac{3}{4})}{\frac{1}{2} \left(1 - \frac{\alpha^2 \mu (\epsilon + e^{-x})}{2m_e} \right)} \right] \tilde{\chi}(x). \quad (2.45)$$

This equation is now of the desired form and can be solved by the Numerov method. Since Eq. (2.36) is equivalent to the coulomb case Eq. (2.12) up to order $\mathcal{O}(\alpha^2)$,

2. Alkali Rydberg atoms

we expect the solutions of the relativistically corrected and the coulomb problem to be similar, therefore we choose the same parameters for the Numerov algorithm as in the coulomb case. In figure 2.3 we compare a relativistically corrected solution we obtained with the non relativistic analytic solution \tilde{F}^- and it can be seen that they are indeed very similar, but we have to state that for the step sizes used the relativistic corrections are presumably smaller than the numerical precession obtained. We conclude that for future work we have to either decrease the step size, or use the analytical solutions for the relativistic problem [36] for a more precise treatment. This completes the discussion of the radial solutions of the alkali Rydberg states we will use in the simulations done in this work.

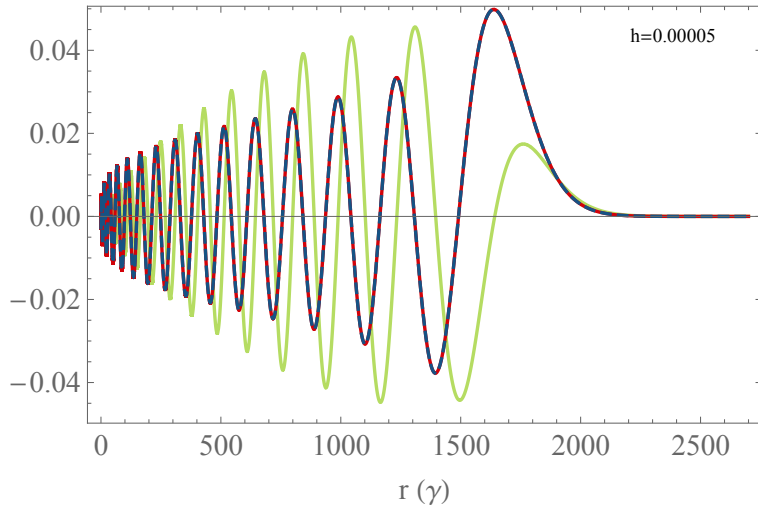


Figure 2.3.: Comparison of the numerically obtained relativistically corrected solutions (red) with the analytical solution \tilde{F}^- (blue dashed) with $n = 29.6005$, $l = 0$. We also give the difference numerical minus analytical solution (light green), which we scaled up by a factor of 1000. We note that h is the step size in the logarithmic coordinate frame.

2.4. Projection method

We aim to analyze the spectrum and eigenstates of operators of the type

$$\hat{H} = \hat{H}_0 + \hat{H}'. \quad (2.46)$$

To obtain approximate eigenvalues and states we first project the total operator \hat{H} on a finite dimensional subspace \mathcal{V} spanned by a orthonormal set of eigenstates $\{|j\rangle\}$ of \hat{H}_0 [70]. The resulting operator

$$\hat{H}_{\mathcal{V}} = \hat{P}_{\mathcal{V}} \hat{H} \hat{P}_{\mathcal{V}}|_{\mathcal{V}}, \quad (2.47)$$

with $P_{\mathcal{V}} = \sum_j |j\rangle\langle j|$, can be represented in the $\{|j\rangle\}$ base as a finite dimensional square matrix with matrix elements

$$\begin{aligned}\langle j'|\hat{H}_{\mathcal{V}}|j\rangle &= \langle j'|H_0|j\rangle + \langle j'|\hat{H}'|j\rangle \\ &= \epsilon_j^0 \delta_{j'j} + h'_{j'j},\end{aligned}\tag{2.48}$$

where ϵ_j^0 denotes the eigenvalue corresponding to $|j\rangle$. The eigenvalues as well as the eigenstates of this finite matrix can be obtained by standard numerical algorithms and serve us as an approximation of the eigenvalues and states of the full operator. We note that, in all cases we discuss \hat{H}_0 is the free Hamiltonian of an alkali Rydberg atom with fixed core or center of mass position, thus we want to use the single channel QDT approach for the unperturbed Hamiltonian and project on a set of states constructed in the last section.

To clarify how to choose a proper subspace \mathcal{V} to project on for a given problem and to see where the advantages and differences in comparison to standard perturbation theory lie, we give a short comparison of perturbation theory [34] and the projection method here. In the easiest perturbation theoretic setting, one considers a Hamiltonian of the type

$$\hat{H}(\kappa) = H_0 + \kappa H'.\tag{2.49}$$

For proper operators H_0 and H' , there exists $\delta > 0$, such that for all $\kappa < \delta$, the eigenvalues and states of $H(\kappa)$ are given as analytic functions of κ [38, 58]. If one expands those functions in the spectral representation of the unperturbed operator H_0 (assuming for now pure singular spectrum for H_0) up to second respectively first order in κ the eigenvalues ϵ_j and states $|j\rangle$ are given as the following series

$$\begin{aligned}\epsilon_j &= \epsilon_j^0 + \kappa \langle j^0|H'|j^0\rangle + \kappa^2 \sum_{k \neq j} \frac{|\langle j^0|H'|k^0\rangle|^2}{\epsilon_j^0 - \epsilon_k^0} + \mathcal{O}(\kappa^3) \\ |j\rangle &= |j^0\rangle + \kappa \sum_{j \neq k} \frac{\langle k^0|H'|j^0\rangle}{\epsilon_j^0 - \epsilon_k^0} + \mathcal{O}(\kappa^2)\end{aligned}\tag{2.50}$$

with ϵ_j^0 and $|j^0\rangle$ the eigenvalues and states of the unperturbed operator. Here we assumed ϵ_j^0 to be non degenerate. We can as well use perturbation theory after the projection for $H_{\text{proj}}(\kappa)$. In the finite and self adjoint case the above power series always exist, and converges on an open set around zero [38, 58]. On this set we can now compare the projection method with perturbation theory and obtain that the projection method takes all orders in κ into account, but is limited in the range of unperturbed states to the ones projected on. This also guides us which states to project on, when we are interested in a specific energy level, i.e. those that lie close to the original one in energy or have big couplings to the specific eigenstate. So we can sum up that, in the region of convergence of the perturbation series the projection method is equivalent to perturbation theory limited to the range of states we project on. The main advantage of the projection method is that it is valid even beyond this

2. Alkali Rydberg atoms

region of convergence, if the projected subspace yields still a good approximation of the total operator. Perturbation theory typically breaks down, when the energy lines cross. As we will see in the following examples, the projection approach gives then rise to avoided crossings. So let us now come to a first application of the theory discussed until now.

2.5. Stark shifts of Rydberg alkali atoms

As a first example we consider a Rydberg alkali atom in a static and uniform electric field. In the single channel QDT framework after changing to relative and COM coordinates and reduction of the center of mass motion the Hamiltonian is given by

$$\hat{H}_{\text{Stark}} = \hat{H}_0 + e \mathbf{E} \cdot \mathbf{r}, \quad (2.51)$$

where \hat{H}_0 is the Hamiltonian of a single Rydberg atom, \mathbf{r} the relative core-electron coordinate and \mathbf{E} a static and uniform electric field. We note that, although the eigenstates of H_0 will be given in fine structure basis, we neglected all relativistic correction terms that arise due to the external electric field. Without loss of generality we can choose coordinates such that the electric field points into z -direction

$$\hat{H}_{\text{Stark}} = \hat{H}_0 + e E_0 z, \quad (2.52)$$

with E_0 the electric field strength of \mathbf{E} . If experimentally obtained quantum defect values are at hand, we can construct the eigenstates of H_0 according to section 2.3, such that we can apply the projection method to obtain approximate expressions for the eigenvalues of a Rydberg atom in an external static and uniform electric field.

2.5.1. Projection

We now discuss how to obtain the finite dimensional matrices announced in section 2.4. We want to project on the eigenstates of the unperturbed Hamiltonian H_0 , which we assume to be given in the fine structure base $|R_n\rangle \otimes |l, j, m_j\rangle$ with $|R_n\rangle$ the radial part obtained by the relativistic Numerov method.

We need to determine the matrix elements

$$\langle n', l', j', m'_j | e E_0 z | n, l, j, m_j \rangle. \quad (2.53)$$

Since the perturbing operator in spherical coordinate representation

$$e E_0 z = e E_0 r \cos(\theta) \quad (2.54)$$

is a product of an angular and a radial part and the eigenstates are given as products of spin-angular and radial wave functions $|R_n\rangle \otimes |l, j, m_j\rangle$, we can also rewrite the matrix elements as a product of a radial and a spin-angular part

$$\begin{aligned} & \langle R_{n'} | \otimes \langle l', m', m'_j | e E_0 r \cos(\theta) | R_n \rangle \otimes | l, m, m_j \rangle \\ & = e E_0 \langle R_{n'} | r | R_n \rangle \langle l', m', m'_j | \cos(\theta) | l, m, m_j \rangle. \end{aligned} \quad (2.55)$$

2.5. Stark shifts of Rydberg alkali atoms

Since the radial and spin-angular terms are now just two independent factors we can split the discussion into a spin-angular and a radial part.

Spin-angular part

Here we present one way to compute the expressions

$$\langle l', j', m_{j'} | \cos(\theta) | l, j, m_j \rangle. \quad (2.56)$$

We want to use the following identity [60] to rewrite the expression as a sum of products in Clebsch Gordon (CG) coefficients CG

$$\langle l', m_{l'} | Y_{l_1, m_{l_1}} | l, m_l \rangle = \sqrt{\frac{(2l_1 + 1)(2l + 1)}{4\pi(2l' + 1)}} \text{CG} \begin{pmatrix} l_1 & l & l' \\ 0 & 0 & 0 \end{pmatrix} \text{CG} \begin{pmatrix} l_1 & l & l' \\ m_{l_1} & m_l & m_{l'} \end{pmatrix}, \quad (2.57)$$

where $Y_{l_1, m_{l_1}}$ denotes a spherical harmonic function as defined in section 2.1. Therefore we first expand the multiplication operator $\cos(\theta)$ in spherical harmonics. We note that this is possible for all L^2 functions defined on the sphere, since the spherical harmonic functions form a orthonormal base. The expansion yields

$$\cos(\theta) = 2\sqrt{\frac{\pi}{3}} Y_{1,0}. \quad (2.58)$$

For the fine structure base states we know that we can expand them into a sum of tensor products of angular and spin states $|l, m_l\rangle \otimes |1/2, m_s\rangle$ using the CG coefficients [60]

$$|l, j, m_j\rangle = \sum_{m_l, m_s} \text{CG} \begin{pmatrix} l & 1/2 & j \\ m_l & m_s & m_j \end{pmatrix} |l, m_l\rangle \otimes |1/2, m_s\rangle. \quad (2.59)$$

We state the following properties of the CG coefficients [60], which will be used in the following calculations

$$\text{CG} \begin{pmatrix} l_1 & l_2 & l_3 \\ m_{l_1} & m_{l_2} & m_{l_3} \end{pmatrix} = 0, \text{ for } m_{l_1} + m_{l_2} \neq m_{l_3} \text{ or } l_3 \notin \{|l_1 - l_2|, \dots, |l_1 + l_2|\}. \quad (2.60)$$

2. Alkali Rydberg atoms

With equations 2.58 and 2.59 we can now rewrite Eq. (2.56)

$$\begin{aligned}
& \langle l', j', m'_j | \cos(\theta) | l, j, m_j \rangle \\
&= \sum_{m'_l, m'_s} \sum_{m_l, m_s} \overline{\text{CG}} \begin{pmatrix} l' & 1/2 & j' \\ m'_l & m'_s & m'_j \end{pmatrix} \text{CG} \begin{pmatrix} l & 1/2 & j \\ m_l & m_s & m_j \end{pmatrix} \\
& \qquad \qquad \qquad \langle l', m'_l | 2\sqrt{\frac{\pi}{3}} Y_{1,0} | l, m_l \rangle \langle 1/2, m'_s | 1/2, m_s \rangle \\
&= \sum_{m'_l, m'_s} \sum_{m_l, m_s} \overline{\text{CG}} \begin{pmatrix} l' & 1/2 & j' \\ m'_l & m'_s & m'_j \end{pmatrix} \text{CG} \begin{pmatrix} l & 1/2 & j \\ m_l & m_s & m_j \end{pmatrix} \\
& \qquad \qquad \qquad 2\sqrt{\frac{\pi}{3}} \sqrt{\frac{3(2l+1)}{4\pi(2l'+1)}} \text{CG} \begin{pmatrix} 1 & l & l' \\ 0 & 0 & 0 \end{pmatrix} \text{CG} \begin{pmatrix} 1 & l & l' \\ 0 & m_l & m'_l \end{pmatrix} \delta_{m'_s m_s} \quad (2.61) \\
&= \sum_{m'_l, m_l, m_s} \overline{\text{CG}} \begin{pmatrix} l' & 1/2 & j' \\ m'_l & m_s & m'_j \end{pmatrix} \text{CG} \begin{pmatrix} l & 1/2 & j \\ m_l & m_s & m_j \end{pmatrix} \\
& \qquad \qquad \qquad \sqrt{\frac{(2l+1)}{(2l'+1)}} \text{CG} \begin{pmatrix} 1 & l & l' \\ 0 & 0 & 0 \end{pmatrix} \text{CG} \begin{pmatrix} 1 & l & l' \\ 0 & m_l & m'_l \end{pmatrix} \\
&= \sum_{m_l, m_s} \overline{\text{CG}} \begin{pmatrix} l' & 1/2 & j' \\ m_l & m_s & m'_j \end{pmatrix} \text{CG} \begin{pmatrix} l & 1/2 & j \\ m_l & m_s & m_j \end{pmatrix} \\
& \qquad \qquad \qquad \sqrt{\frac{(2l+1)}{(2l'+1)}} \text{CG} \begin{pmatrix} 1 & l & l' \\ 0 & 0 & 0 \end{pmatrix} \text{CG} \begin{pmatrix} 1 & l & l' \\ 0 & m_l & m_l \end{pmatrix}
\end{aligned}$$

From this we can now also infer that the matrix element is zero for $m_j \neq m'_j$, so m_j is conserved and the total problem reduces to a sum of those with equal m_j . Further it is zero for $l' \neq |l \pm 1|$. Since the CG coefficients are known, the spin-angular matrix elements can now be obtained.

Radial part

For the radial part we have to evaluate

$$\langle R_{n'} | r | R_n \rangle = \sum_i \overline{\chi_{n'}(x_i)} e^{3x_i} \chi_n(x_i), \quad (2.62)$$

which becomes a simple sum on the grid we used for the Numerov algorithm. We note that also the volume element needed to be transformed to the logarithmic coordinates.

We can now obtain the total projected Hamiltonian as the sum of the diagonal free alkali Hamiltonian H_0 and the electric field Hamiltonian for a given electric field strength E_0 and quantum defect values $\delta_{n,l,j}$.

2.5.2. Stark shifts of lithium

As a particular example we consider a ${}^6\text{Li}$ Rydberg atom. The quantum defect values are given by [23]

$$\delta_{n,l,j} = \delta_{l,j}^0 + \delta_{l,j}^1(n - \delta_{l,j}^0)^{-2} \quad (2.63)$$

with $\delta_{0,1/2}^0 = 0.3995101$, $\delta_{1,1/2}^0 = 0.0471835$, $\delta_{1,3/2}^0 = 0.0471720$, $\delta_{0,1/2}^1 = 0.0290$, $\delta_{1,1/2}^1 = \delta_{1,1/2}^1 = -0.024$, all other defect values are zero. We are most interested in the $n = 30$ manifold, thus we project on the states spanned by $\{|n, l, j, m_j\rangle\}$ with $n \in \{23, \dots, 35\}$, $l \in \{0, \dots, n-1\}$, $j = |l \pm 1/2|$ and m_j constant. For the simulations we discuss here $m_j = 1/2$. To assure that we have taken all dominant terms into account, we show one row of the matrix related to the 30 S state in figure 2.4 (a), and notice, that the terms for states further separated in n from the 30 S state decrease due to the radial matrix elements $\langle R_{n'} | r | R_n \rangle$. In a perturbational approach up to second order, these terms would be the only ones that contribute, if one restricts the sums just to the given states. To convey a feeling for the matrices that have to be diagonalized we also visualized the perturbing matrix in Fig. 2.4 (b). We can now diagonalize the stark shift Hamiltonian for different values of the external field. This leads to the result we present in figure 2.5, where one can observe the shifts of the different electron states, which are to leading order linear for the degenerate states $l \geq 2$ and quadratic for the non degenerate S and P states, as expected from the perturbation theoretic approach, for high fields it can be seen that the lines do not cross, as they would in the perturbational approach.

We summarize that we have now the theoretical framework at hand to describe the Rydberg states of free alkali atoms with fixed center of mass position perturbed by external fields. In the next chapter we will generalize this approach to the case of a alkali Rydberg atom interacting with an ion.

2. Alkali Rydberg atoms

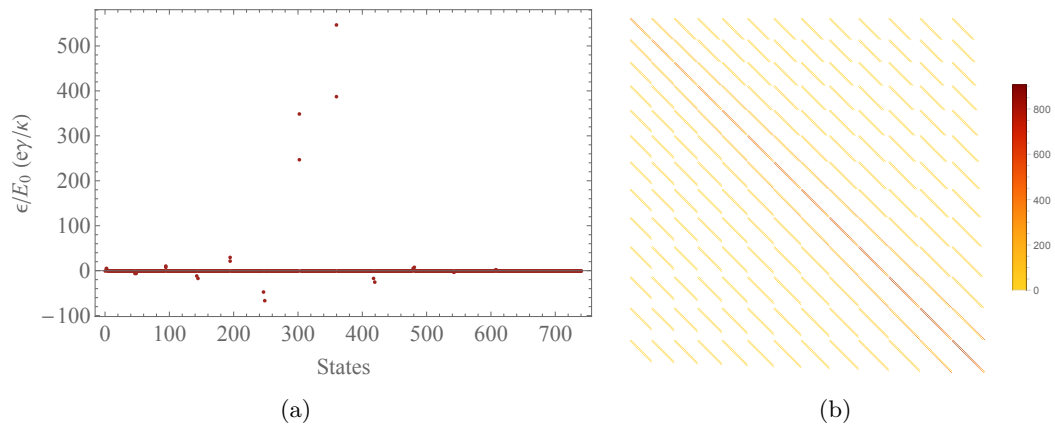


Figure 2.4.: (a) Matrix values of the perturbing matrix $\langle j'|ez|j\rangle$ that couple to the $30S$ state (the states $|n, l, j, m_j\rangle$ are numbered by first running through m_j , then j, \dots , but here m_j is constant), (b) visualization of the absolute value of the entries in the perturbing matrix (values equal to zero are just white).

2.5. Stark shifts of Rydberg alkali atoms

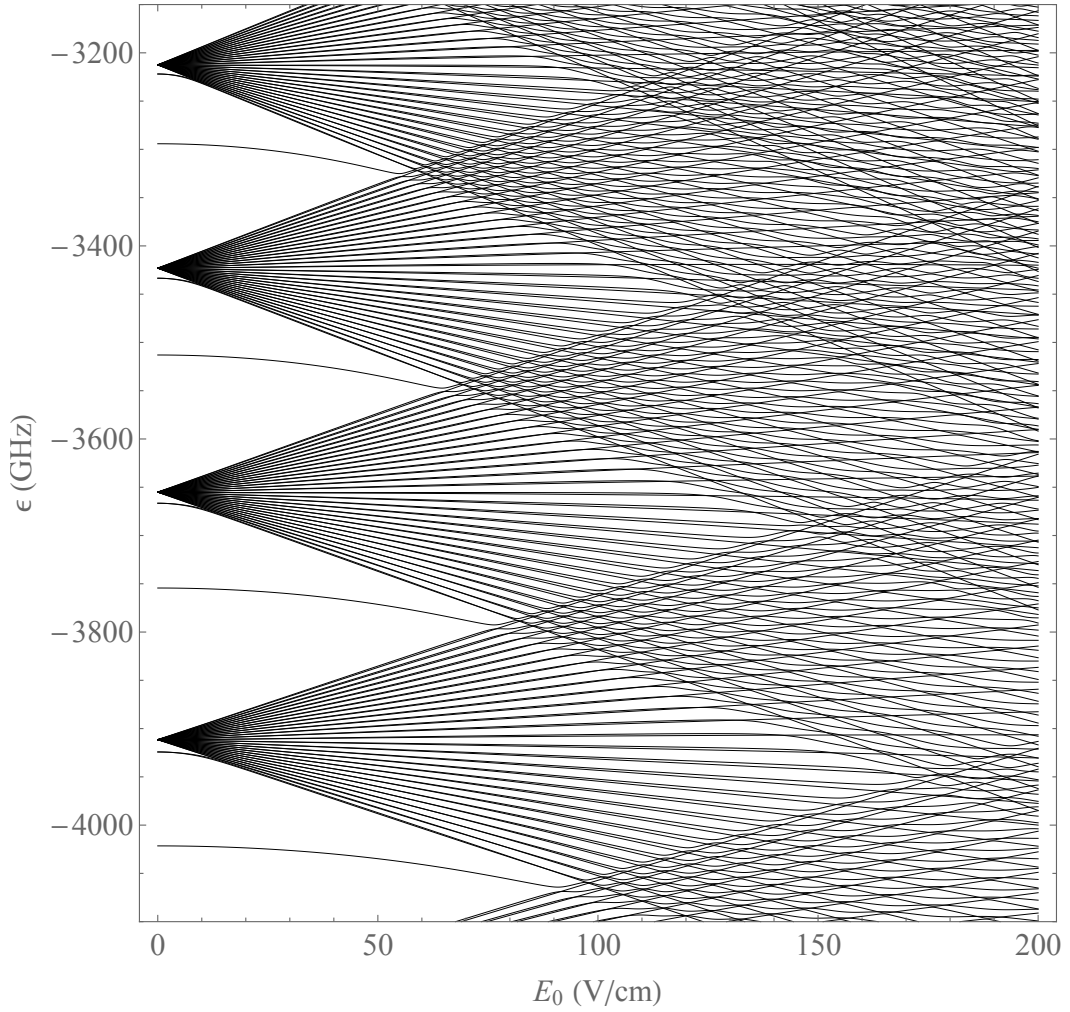


Figure 2.5.: Starkmap for ${}^6\text{Li}$ with $m_j = 1/2$, for external field strengths up to 200 V/cm. We show the eigenenergies, that emanate from the $n \in \{29, \dots, 32\}$ manifolds. One can see the separation of the S and P states from the rest of the n manifolds. For example the $30S$ and $30P$ energies lie separated at -3754.4 GHz and -3666.7 GHz.

3. Rydberg atom-ion interaction

In this chapter we aim to derive the Rydberg atom-ion potential, which in combination with the dressing field we study in the next chapter yields the dressed potential we use for the atom-ion spin-spin interactions in our final project. In contrast to the case of the static uniform field we discussed in the last section, the ion potential is inhomogeneous, which results in a force between atom and ion. To see, how the effective interaction potential related to this force arises and to derive its shape, we start with a simple example: a Rydberg atom confined to a line in an inhomogeneous external field. This will provide us with some first intuition of the effects that occur. In the second section we discuss those effects in a general setting and obtain how the effective interaction potential between the heavy particles, i. e. ion and atom, can be derived by diagonalizing the light particle, i. e. the Rydberg electron, problem. We note that the problems treated here closely resemble the Born-Oppenheimer (BO) formalism [22, 25]. In the last section we apply the obtained results to the Rydberg atom-ion scenario. There we start with atom and ion in the free case without external electric fields, which we then generalize to include also the fields of the ion Paul trap.

3.1. Simple model: Rydberg atom on a line

Let us start with a simple example. A Rydberg alkali atom confined on a straight line in an inhomogeneous electric field pointing in direction of the line. We start already in COM coordinates and assume that the dipole approximation holds for fixed atom position, this means $\mathbf{E}(Z) = e E_0(Z) \hat{\mathbf{e}}_z$ with $\hat{\mathbf{e}}_z$ the unit vector in z -direction, thus the total Hamiltonian reads

$$H = \frac{P_Z^2}{2M} + \frac{\hat{\mathbf{p}}^2}{2\mu} + V_{\text{Ryd}}(\mathbf{r}) + e E_0(Z) \hat{\mathbf{e}}_z \cdot \mathbf{r}, \quad (3.1)$$

here P_Z , Z and $\hat{\mathbf{p}}$, \mathbf{r} denote the momentum and position of the center-of-mass respectively the relative Rydberg electron-core coordinate. M is the total and μ the relative mass. As in the foregoing chapter, we project on a n -dimensional subspace, $n \in \mathbb{N}$, spanned by a set $\{|j\rangle\}$ of bound Rydberg eigenstates, with corresponding eigenenergies ϵ_j^0 , of the free alkali Rydberg Hamiltonian $H_0 = \hat{\mathbf{p}}^2/(2\mu) + V_{\text{Ryd}}(\mathbf{r})$. After the projection we are left with

$$H_{\text{proj}} = \frac{P_Z^2}{2M} + \mathbf{1}_Z \otimes \sum_{j=1}^n \epsilon_j^0 |j\rangle\langle j| + \sum_{j',j=1}^n [E_0(Z) \cdot d_{j'j}^z \otimes |j'\rangle\langle j|], \quad (3.2)$$

3. Rydberg atom-ion interaction

with $d_{j'j}^z = \langle j' | e z | j \rangle$. We want to pass to a representation of this operator where the Born Oppenheimer Hamiltonian defined as

$$H_{\text{BO}} = \mathbb{1}_Z \otimes \sum_{j=1}^n \epsilon_j^0 |j\rangle\langle j| + \sum_{j',j=1}^n [E_0(Z) \cdot d_{j'j}^z \otimes |j'\rangle\langle j|] \quad (3.3)$$

is of diagonal form

$$\mathcal{U}^\dagger H_{\text{BO}} \mathcal{U} = \sum_{j=1}^n \epsilon_j(Z) \otimes |j\rangle\langle j|. \quad (3.4)$$

We note that $\{|j\rangle\}$ corresponds now to an orthonormal base for each Z in the transformed Hilbert space. In the original Hilbert space and for fixed Z position, the $\{|j\rangle\}$ can be viewed as the eigenvectors of the matrix $(\epsilon_k^0 \delta_{k'k} + E_0(Z) d_{k'k}^z)$, with corresponding eigenvalues $\epsilon_j(Z)$. We will show that such a transformation can always be done in the mathematical part following this section.

To see how the total Hamiltonian looks in the new representation, we also need to transform the kinetic energy operator of the center-of-mass coordinate. Since the eigenstates are in general Z dependent, we get additional terms related to their derivatives

$$\mathcal{U}^\dagger \frac{P_Z^2}{2M} \mathcal{U} = \sum_{j=1}^n \frac{P_Z^2}{2M} \otimes |j\rangle\langle j| - \sum_{j,p=1}^n \left[\frac{i\hbar}{M} b_{pj}(Z) P_Z + \frac{\hbar^2}{2M} b_{pj}(Z) \right] \otimes |p\rangle\langle j|. \quad (3.5)$$

In regions in the Z coordinate space, where the last terms can safely be neglected we have now a representation of the total Hamiltonian H_{proj} that is approximately

$$\mathcal{U}^\dagger H_{\text{proj}} \mathcal{U} \approx \sum_{j=1}^n \left[\frac{P_Z^2}{2M} + \epsilon_j(Z) \right] \otimes |j\rangle\langle j|, \quad (3.6)$$

thus the problem reduces to a sum of single particle problems. One for each eigenstate of the BO Hamiltonian. We remark the similarity to the reduction of e.g. the full hydrogen problem to the radial ones Eq. (2.6). The Z dependent eigenenergies now act as effective potentials in the center-of-mass variable. Since we already calculated the eigenenergies of the Stark Hamiltonian Eq. (2.52) the potentials $\epsilon_j(Z)$ can readily be obtained by reading off the eigenenergies at the given field strength $E_0(Z)$. As an example let us consider the case we are most interested in, i.e. a Rydberg atom in the dipole approximated coulomb field of an ion, as discussed in a perturbation theoretic treatment in the introduction. We fix the ion at $Z = 0$, thus the dipole term reads

$$V_{\text{dip}}^{a-i} = -\frac{e^2}{4\pi\epsilon_0} \frac{z Z}{|Z|^3} \quad (3.7)$$

with the help of the methods employed in the stark shift case we can arrive at the Z dependent eigenenergies $\epsilon_j(Z)$. Here we give those energies, for ${}^6\text{Li}$, with quantum defects as in section 2.5.2. In Fig. 3.1 we show the lines that emanate from the $n = 30$

3.1. Simple model: Rydberg atom on a line

manifold, the well separated lines at -3754.4 GHz and -3666.7 GHz are the $30S$ and P states respectively. We observe the expected $\propto -1/Z^4$ character for these states. We announced that also the eigenstates will get Z dependent this can be seen in Fig. 3.2, where we plot the Z -dependence of the coefficients of the $30S$ state vector. This Z -dependence gives rise to the terms b_{ij} and b_{ij} . We show the coupling terms to the $30S$ state in Fig. 3.3, where we assumed the mass of ${}^6\text{Li}$. We observe that they are indeed small for reasonable atom velocities compared to the BO Hamiltonian, which is for distances $Z \approx 1 \mu\text{m}$ in the 1 GHz range. Therefore we can safely neglected them.

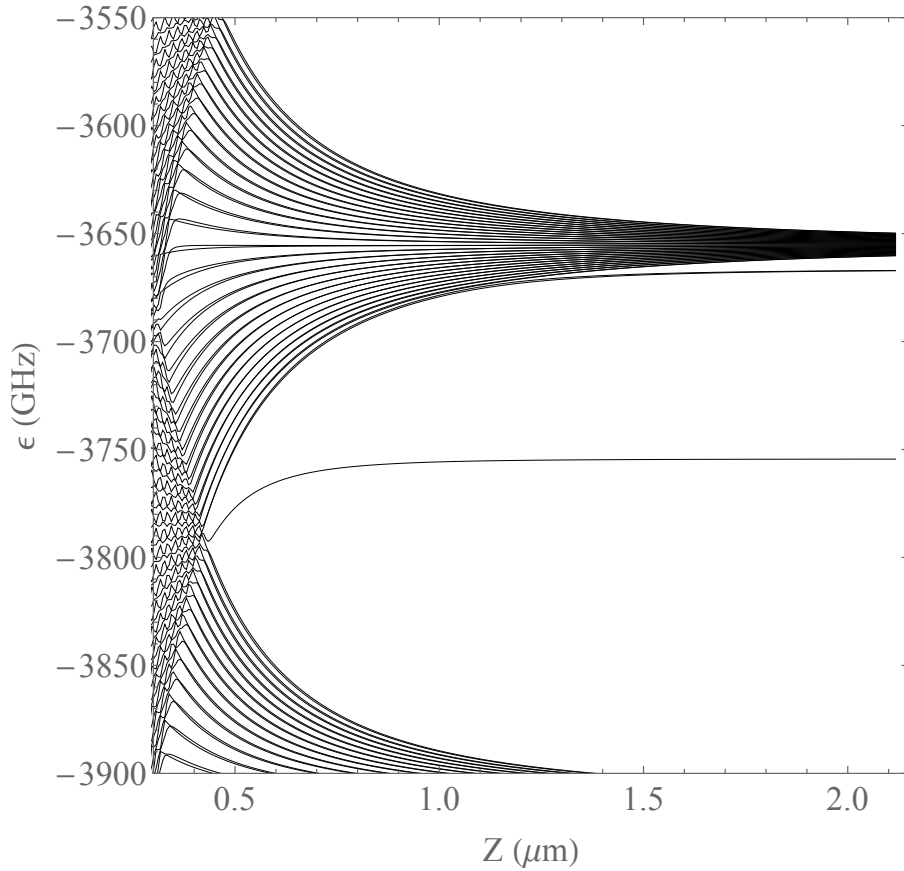


Figure 3.1.: Effective potential lines for the perturbing term $V_{\text{dip}}^{a-i} = -\frac{e^2}{4\pi\epsilon_0} \frac{zZ}{|Z|^3}$, for the states emanating from the $n = 30$ manifold, we again note the well separated $30S$ and $30P$ energies at -3754.4 GHz and -3666.7 GHz

Let us comment on the choice of this class for a first example. We want to discuss the situation of an external electric field in free space, thus $\nabla \cdot \mathbf{E}(\mathbf{x}) = 0$. This makes it impossible to have a field that points just into one direction of space while varying the absolute value. But if the direction of the field changes and we want to choose the atom coordinates such that the field points into z -

3. Rydberg atom-ion interaction

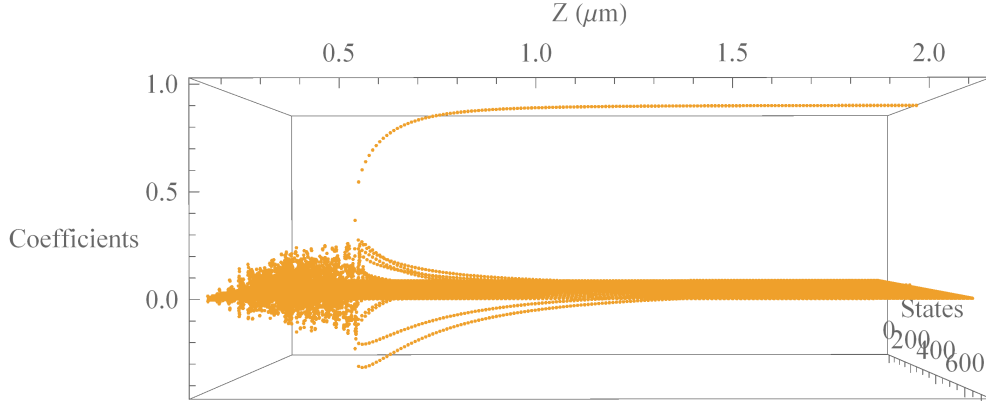


Figure 3.2.: Z dependence of the eigenstate emanating from the $30S$ state.

direction at every point in space, to ease the diagonalization, the atom base gets \mathbf{R} dependent, with \mathbf{R} the atom center-of-mass position. To start step by step and not have both effects at once we have begun with this oversimplified class of examples.

3.2. The Born Oppenheimer method

Before going over to the mathematical discussion let us gain some intuition on the transformation process. Therefore we depict the states $F \in \mathcal{H}$ of the underlying Hilbert space $\mathcal{H} = L^2(\mathbb{R}) \otimes \mathbb{C}^n$ as mappings $Z \mapsto (f_1(Z), \dots, f_n(Z)) \in \mathbb{C}^n$, where we define the functions $f_j(Z)$ as the coefficients in the representation $F = \sum_{j=1}^n f_j(Z) \otimes |j\rangle$ (see figure 3.4). In figure 3.5 we show exemplarily how the operator \mathcal{U} transforms a simple state of the new base, which e.g. corresponds to an eigenstate of H_{BO} to the related eigenstate in the old base. So in the new base H_{BO} acts as a simple multiplication operator on the functions lying in the planes. We also show the direction of the derivative in Z direction for one coordinate function in the old frame, we can see that it transforms to a directional derivative not constant in Z . We mention the close similarity to gauge transformations. Since the kinetic energy operator includes even quadratic derivatives the transformation gets even more complicated and two terms are needed to take account for the transformation, namely the ones written in Eq. (3.5). In Fig. 3.3 we show the resulting terms for the example potential discussed in the last section for a fixed eigenstate.

Now we start and analyze Hamiltonians of a more general type than the above example. Since we may want to choose even the projection dependent on the heavy particle coordinate, we include from the start the correction terms just discussed, so we want

3.2. The Born Oppenheimer method

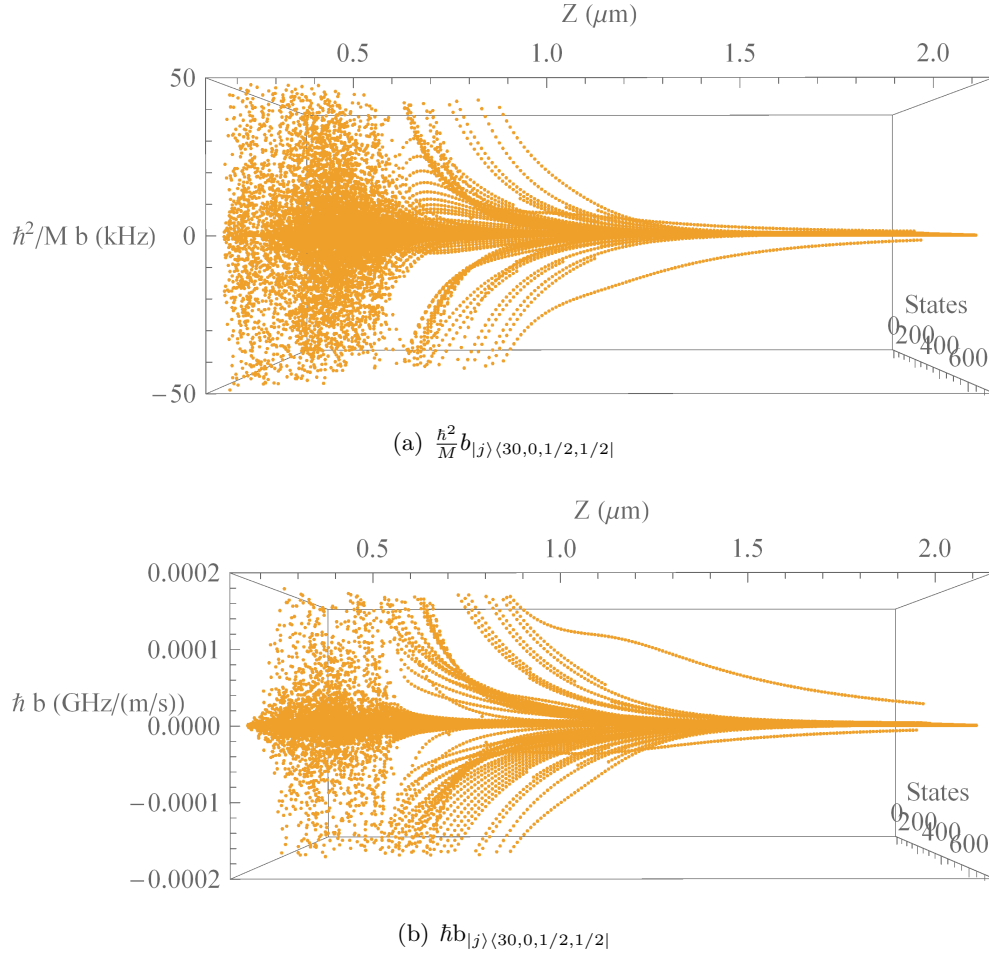


Figure 3.3.: Correction terms that arise in the transformation of the kinetic energy operator, due to the position dependence of the eigenstates. We inserted the mass for ${}^6\text{Li}$. (a) $\frac{\hbar^2}{M} b_{|j\rangle\langle 30,0,1/2,1/2|}$, (b) $\hbar b_{|j\rangle\langle 30,0,1/2,1/2|}$.

to consider a systems of the following type

$$\hat{H} = \sum_{j,i=1}^n \left[\sum_{k=1}^N \left(\frac{\hat{\mathbf{p}}_k^2}{2m_k} \delta_{ji} - \frac{i\hbar}{m_k} \mathbf{b}_{ji}^{(k)}(\mathbf{Y}) \cdot \hat{\mathbf{p}}_k - \frac{\hbar^2}{2m_k} b_{ji}^{(k)}(\mathbf{Y}) \right) + h_{ij}(\mathbf{Y}) \right] \otimes |j\rangle\langle i|. \quad (3.8)$$

\hat{H} is meant to act on the Hilbert space

$$\mathcal{H} = L^2(\mathbb{R}^{3N}) \otimes \mathbb{C}^n, \quad (3.9)$$

where the total position of the heavy particles is $\mathbf{Y} = (\mathbf{y}_1, \dots, \mathbf{y}_N) \in \mathbb{R}^{3N}$ with \mathbf{y}_k , $\hat{\mathbf{p}}_k$ and m_k the position, momentum and mass of the k -th heavy particle. Since the

3. Rydberg atom-ion interaction

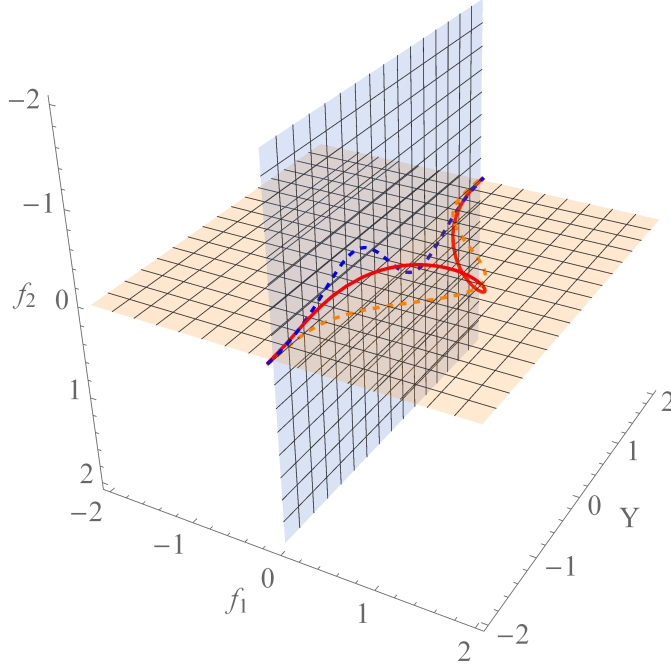


Figure 3.4.: Simplified visualization of a real valued 2-tuple state (f_1, f_2) (red line), with $f_1 = e^{-Y^2} \cos(Y)$ (orange dashed line) and $f_2 = e^{-Y^2} \sin(Y)$ (blue dashed line), where $Y \in \mathbb{R}$.

light particle Hilbert space is finite dimensional after projecting, we represent it with a general complex Hilbert space \mathbb{C}^n , where $n \in \mathbb{N}$ is the finite dimension and $\{|j\rangle\}$ denotes an orthonormal base. The Born Oppenheimer Hamiltonian at fixed Y position is given by the square Matrix $H_{\text{BO}}(Y) = (h_{ij}(Y)) \in \mathcal{M}_{n \times n}(\mathbb{C})$, whereas the total BO Oppenheimer Hamiltonian is defined as

$$H_{\text{BO}} = \int dY |Y\rangle\langle Y| \otimes \hat{H}_{\text{BO}}(Y) = \sum_{i,j=1}^n h_{ij}(Y) \otimes |i\rangle\langle j|. \quad (3.10)$$

As already mentioned the terms $\mathbf{b}_{ji}^{(k)}$ and $b_{ji}^{(k)}$ result from projecting on a base that is Y dependent and vanish, if we project on bases of the light particle Hilbert space, that are fixed for all Y in the original representation of the full Hamiltonian operator. We note that one could as well include parts of $\sum_{k=1}^N \hbar^2 / (2m_k) b_{ij}^k(Y)$ into the Born Oppenheimer Hamiltonian. With some constraints on $\hat{H}_{\text{BO}}(Y)$, which will become obvious in the following calculations, we can construct a unitary transformation \mathcal{U} , such that the transformed Hamilton operator can, at least for some region in the Y space, approximately be reduced to a sum of effective operators acting just on the

3.2. The Born Oppenheimer method

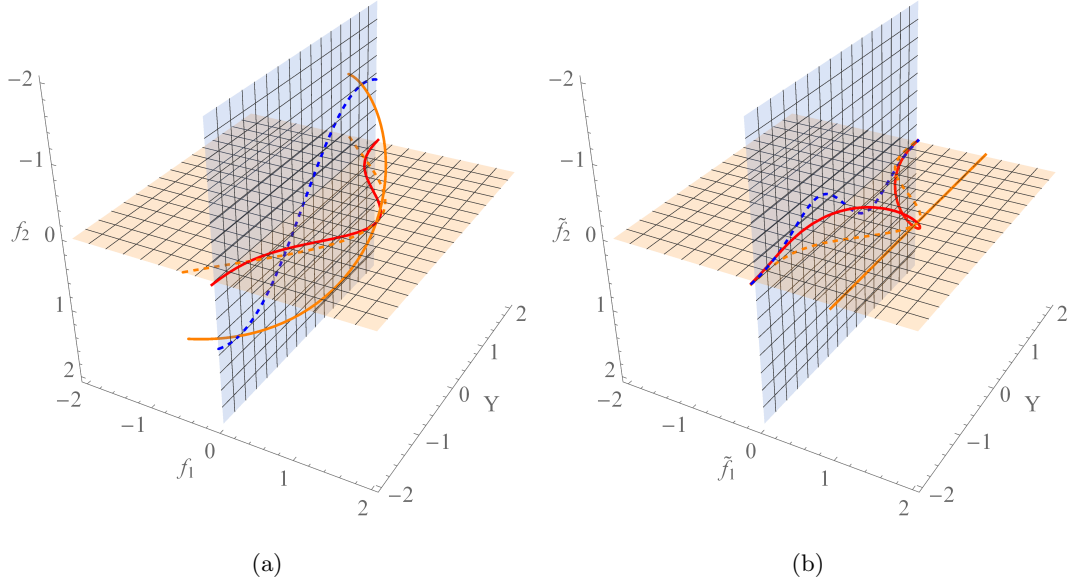


Figure 3.5.: Visualization of \mathcal{U} with $\mathbf{w}_1 = (\cos(Y), \sin(Y))$ and $\mathbf{w}_2 = (-\sin(Y), \cos(Y))$: (a) shows $F = (f_1, f_2)$ (red) with components $f_1 = e^{-Y^2}$, $f_2 = 0$ and $\mathcal{U}^\dagger \tilde{\mathbf{w}}_1 = (\cos(Y), -\sin(Y))$ (orange) (b) shows $\tilde{\mathbf{w}}_1 = (1, 0)$ (orange) and $\mathcal{U}F = (\tilde{f}_1, \tilde{f}_2)$ (red) with components $\tilde{f}_1 = e^{-Y^2} \cos(Y)$ (orange dashed line) and $\tilde{f}_2 = e^{-Y^2} \sin(Y)$ (blue dashed line).

heavy particle coordinates \mathbf{Y}

$$\mathcal{U}^\dagger \hat{H} \mathcal{U} \approx \bigoplus_{j=1}^n \left[\sum_{k=1}^N \frac{\hat{\mathbf{p}}_k^2}{2m_k} + \epsilon_j(\mathbf{Y}) \right], \quad (3.11)$$

where the $\epsilon_j(\mathbf{Y})$ turn out to be the eigenvalues of $\hat{H}_{\text{BO}}(\mathbf{Y})$. Since $\hat{H}_{\text{BO}}(\mathbf{Y})$ is a finite dimensional hermitian matrix for every point \mathbf{Y} , we know that we can find orthonormal eigenstates $\mathbf{w}_j(\mathbf{Y})$ and corresponding eigenvalues $\epsilon_j(\mathbf{Y})$ at each point \mathbf{Y} . We demand the components of $\mathbf{w}_j(\mathbf{Y}) = (w_{1j}(\mathbf{Y}), \dots, w_{nj}(\mathbf{Y}))$ to be in $L^\infty(\mathbb{R}^{3N})$, such that we can define

$$\mathcal{U} : F = \sum_{j=1}^n f_j \otimes |j\rangle \mapsto \tilde{F} = \sum_{j,l=1}^n w_{jl} f_l \otimes |j\rangle. \quad (3.12)$$

Let us proof that $\int d\mathbf{Y} |\mathbf{Y}\rangle \langle \mathbf{Y}| \otimes \hat{H}_{\text{BO}}(\mathbf{Y})$ transforms to diagonal form under \mathcal{U} . Therefore we act with $\mathcal{U}^\dagger \int d\mathbf{Y} |\mathbf{Y}\rangle \langle \mathbf{Y}| \otimes \hat{H}_{\text{BO}}(\mathbf{Y}) \mathcal{U}$ on a general state $F = \sum_{j=1}^n f_j \otimes |j\rangle$ and

3. Rydberg atom-ion interaction

calculate

$$\begin{aligned}
& \mathcal{U}^\dagger \int d\mathbf{Y} |\mathbf{Y}\rangle \langle \mathbf{Y}| \otimes \hat{H}_{\text{BO}}(\mathbf{Y}) \mathcal{U} F \\
&= \mathcal{U}^\dagger \left(\int d\mathbf{Y} |\mathbf{Y}\rangle \langle \mathbf{Y}| \otimes \hat{H}_{\text{BO}}(\mathbf{Y}) \right) \sum_{j,l=1}^n (w_{lj} f_j \otimes |l\rangle) \\
&= \mathcal{U}^\dagger \sum_{j,l,i=1}^n h_{il}(\mathbf{Y}) w_{lj}(\mathbf{Y}) f_j(\mathbf{Y}) \otimes |i\rangle \\
&= \mathcal{U}^\dagger \sum_{j,i=1}^n \left(\sum_{l=1}^n h_{il}(\mathbf{Y}) w_{lj}(\mathbf{Y}) \right) f_j(\mathbf{Y}) \otimes |i\rangle \\
&= \mathcal{U}^\dagger \sum_{j,i=1}^n \epsilon_j(\mathbf{Y}) w_{ij}(\mathbf{Y}) f_j(\mathbf{Y}) \otimes |i\rangle \\
&= \sum_{k=1}^n \sum_{j,i=1}^n \overline{w_{ik}(\mathbf{Y})} \epsilon_j(\mathbf{Y}) w_{ij}(\mathbf{Y}) f_j(\mathbf{Y}) \otimes |k\rangle \\
&= \sum_{j,i,k=1}^n \epsilon_j(\mathbf{Y}) \overline{w_{ik}(\mathbf{Y})} w_{ij}(\mathbf{Y}) f_j(\mathbf{Y}) \otimes |k\rangle \\
&= \sum_{j=1}^n \epsilon_j(\mathbf{Y}) f_j(\mathbf{Y}) \otimes |j\rangle,
\end{aligned} \tag{3.13}$$

where we used the representation $H_{\text{BO}} = \sum_{i,j=1}^n h_{ij}(\mathbf{Y}) \otimes |i\rangle \langle j|$ in the $\{|j\rangle\}$ base and we obtain that in fact H_{BO} is of diagonal form after the transformation. To see how the total Hamiltonian \hat{H} transforms, we have to analyze the transformation of $\sum_{k=1}^N \hat{\mathbf{p}}_k^2 / (2m_k)$

$$\begin{aligned}
& \mathcal{U}^\dagger \sum_{k=1}^N \frac{\hat{\mathbf{p}}_k^2}{2m_k} \mathcal{U} F \\
&= \mathcal{U}^\dagger \sum_{k=1}^N \frac{\hat{\mathbf{p}}_k^2}{2m_k} \tilde{F} \\
&= \mathcal{U}^\dagger \sum_{j,l=1}^n \left(\sum_{k=1}^N \frac{\hat{\mathbf{p}}_k^2}{2m_k} w_{lj}(\mathbf{Y}) f_j(\mathbf{Y}) \right) \otimes |l\rangle \\
&= \sum_{p,j,l=1}^n \left[\left(\sum_{k=1}^N \overline{w_{lp}(\mathbf{Y})} \frac{\hat{\mathbf{p}}_k^2}{2m_k} w_{lj}(\mathbf{Y}) f_j(\mathbf{Y}) \right) \right] \otimes |p\rangle
\end{aligned} \tag{3.14}$$

At this point we want to use the product rule to transform the operator into the desired form of Eq. (3.11). Therefore we demand that the $w_{lj}(\mathbf{Y})$ are two times differentiable. For non-differentiable $w_{lj}(\mathbf{Y})$ the operator $\mathcal{U}^\dagger \sum_{k=1}^N \hat{\mathbf{p}}_k^2 / (2m_k) \mathcal{U}$ is defined just on those states, that after multiplication with w_{lj} are two times differentiable. Assuming the

3.2. The Born Oppenheimer method

differentiability we can apply the product rule and further simplify

$$\begin{aligned}
& \sum_{p,j,l=1}^n \left[\left(\sum_{k=1}^N \overline{w_{lp}(\mathbf{Y})} \frac{\hat{\mathbf{p}}_k^2}{2m_k} w_{lj}(\mathbf{Y}) f_j(\mathbf{Y}) \right) \right] \otimes |p\rangle \\
&= \sum_{p,j,l=1}^n \left[\overline{w_{lp}(\mathbf{Y})} \sum_{k=1}^N \left(w_{lj}(\mathbf{Y}) \left(\frac{\hat{\mathbf{p}}_k^2}{2m_k} f_j(\mathbf{Y}) \right) \right. \right. \\
&\quad \left. \left. + \frac{1}{m_k} (\hat{\mathbf{p}}_k w_{lj}(\mathbf{Y})) \cdot (\hat{\mathbf{p}}_k f_j(\mathbf{Y})) + \left(\frac{\hat{\mathbf{p}}_k^2}{2m_k} w_{lj}(\mathbf{Y}) \right) f_j(\mathbf{Y}) \right) \right] \otimes |p\rangle \\
&= \sum_{p,j,l=1}^n \left[\sum_{k=1}^N \left(\overline{w_{lp}(\mathbf{Y})} w_{lj}(\mathbf{Y}) \left(\frac{\hat{\mathbf{p}}_k^2}{2m_k} f_j(\mathbf{Y}) \right) \right. \right. \\
&\quad \left. \left. + \frac{1}{m_k} \overline{w_{lp}(\mathbf{Y})} (\hat{\mathbf{p}}_k w_{lj}(\mathbf{Y})) \cdot (\hat{\mathbf{p}}_k f_j(\mathbf{Y})) \right. \right. \\
&\quad \left. \left. + \frac{1}{2m_k} \overline{w_{lp}(\mathbf{Y})} (\hat{\mathbf{p}}_k^2 w_{lj}(\mathbf{Y})) f_j(\mathbf{Y}) \right) \right] \otimes |p\rangle. \tag{3.15}
\end{aligned}$$

This expression is equivalent to

$$\begin{aligned}
\mathcal{U}^\dagger \sum_{k=1}^N \frac{\hat{\mathbf{p}}_k^2}{2m_k} \mathcal{U} &= \sum_{j=1}^n \sum_{k=1}^N \frac{\hat{\mathbf{p}}_k^2}{2m_k} \otimes |j\rangle \langle j| \\
&+ \sum_{j,l,p=1}^n \sum_{k=1}^N \left[\frac{1}{m_k} \overline{w_{lp}(\mathbf{Y})} (\hat{\mathbf{p}}_k w_{lj}(\mathbf{Y})) \cdot \hat{\mathbf{p}}_k \right. \\
&\quad \left. + \frac{1}{2m_k} \overline{w_{lp}(\mathbf{Y})} (\hat{\mathbf{p}}_k^2 w_{lj}(\mathbf{Y})) \right] \otimes |p\rangle \langle j|. \tag{3.16}
\end{aligned}$$

The only terms that still need to be transformed are

$$\sum_{k=1}^N \frac{i\hbar}{m_k} \mathbf{b}_{ji}^{(k)}(\mathbf{Y}) \cdot \hat{\mathbf{p}}_k \quad \text{and} \quad \sum_{k=1}^N \frac{\hbar^2}{2m_k} b_{ji}^{(k)}(\mathbf{Y}). \tag{3.17}$$

We just give the results

$$\begin{aligned}
& \mathcal{U}^\dagger \left[\sum_{k=1}^N \frac{i\hbar}{m_k} \mathbf{b}_{ji}^{(k)}(\mathbf{Y}) \cdot \hat{\mathbf{p}}_k \otimes |j\rangle \langle i| \right] \mathcal{U} \\
&= \sum_{k=1}^N \sum_{p,j,i,l=1}^n \left[\frac{\hbar^2}{m_k} \overline{w_{jp}(\mathbf{Y})} \mathbf{b}_{ji}^{(k)}(\mathbf{Y}) \cdot (\nabla_k w_{il}(\mathbf{Y})) \right. \\
&\quad \left. + \frac{i\hbar}{m_k} \overline{w_{jp}(\mathbf{Y})} w_{il}(\mathbf{Y}) \mathbf{b}_{ji}^{(k)}(\mathbf{Y}) \cdot \hat{\mathbf{p}}_k \right] \otimes |p\rangle \langle l| \tag{3.18}
\end{aligned}$$

3. Rydberg atom-ion interaction

and

$$\begin{aligned} \mathcal{U}^\dagger \left[\sum_{k=1}^N \frac{\hbar^2}{2m_k} b_{ji}^{(k)}(\mathbf{Y}) \otimes |j\rangle\langle i| \right] \mathcal{U} \\ = \sum_{k=1}^N \sum_{p,j,i,l=1}^n \left[\frac{\hbar^2}{2m_k} \overline{w_{jp}(\mathbf{Y})} b_{ji}^{(k)}(\mathbf{Y}) w_{il}(\mathbf{Y}) \right] \otimes |p\rangle\langle l| \end{aligned} \quad (3.19)$$

Thus the total Hamiltonian is given by

$$\begin{aligned} \tilde{H} &= \mathcal{U}^\dagger H \mathcal{U} \\ &= \sum_{j=1}^n \left[\sum_{k=1}^N \frac{\hat{\mathbf{p}}_k^2}{2m_k} + \epsilon(\mathbf{Y}) \right] \otimes |j\rangle\langle j| \\ &\quad - \sum_{j,p=1}^n \sum_{k=1}^N \left[\frac{i\hbar}{m_k} \tilde{\mathbf{b}}_{pj}^{(k)}(\mathbf{Y}) \cdot \hat{\mathbf{p}}_k + \frac{\hbar^2}{2m_k} \tilde{b}_{pj}^{(k)}(\mathbf{Y}) \right] \otimes |p\rangle\langle j|, \end{aligned} \quad (3.20)$$

with

$$\tilde{\mathbf{b}}_{pj}^{(k)}(\mathbf{Y}) = \sum_{l=1}^n \left[\overline{w_{lp}(\mathbf{Y})} (\nabla_k w_{lj}(\mathbf{Y})) + \sum_{i=1}^n \overline{w_{lp}(\mathbf{Y})} w_{ij}(\mathbf{Y}) \mathbf{b}_{li}^{(k)}(\mathbf{Y}) \right] \quad (3.21)$$

and

$$\begin{aligned} \tilde{b}_{pj}^{(k)}(\mathbf{Y}) &= \sum_{l=1}^n \left[\overline{w_{lp}(\mathbf{Y})} (\Delta_k w_{lj}(\mathbf{Y})) \right. \\ &\quad \left. + \sum_{i=1}^n \left(\overline{w_{lp}(\mathbf{Y})} b_{li}^{(k)}(\mathbf{Y}) w_{ij}(\mathbf{Y}) + 2\overline{w_{lp}(\mathbf{Y})} \mathbf{b}_{li}^{(k)}(\mathbf{Y}) \cdot (\nabla_k w_{ij}(\mathbf{Y})) \right) \right]. \end{aligned} \quad (3.22)$$

The expression in Eq. (3.20) closely resembles the form of the approximate operator we search for, defined in Eq. (3.11). If the last term of Eq. (3.20) is small compared to the first one, we can neglect it and get the desired approximate expression

$$\tilde{H} \approx H_{\text{eff}} = \bigoplus_{j=1}^n H_{\text{eff}}(j) = \bigoplus_{j=1}^n \left[\sum_{k=1}^N \frac{\hat{\mathbf{p}}_k^2}{2m_k} + \epsilon(\mathbf{Y}) \right]. \quad (3.23)$$

We note that the terms defined in Eq. (3.22) lead to corrections of the operators $\hat{H}_{\text{eff}}^{(k)}$ as well as to couplings between the orthogonal subspaces the $\hat{H}_{\text{eff}}^{(k)}$ act on. Note that the coupling terms $\tilde{\mathbf{b}}_{ij}$ and \tilde{b}_{ij} are known as non adiabatic coupling terms in the BO literature [2]. This completes the mathematical part.

3.3. Free Rydberg atom-ion interactions

In this section we start the theoretical investigation of the Rydberg atom-ion system. We begin with an alkali Rydberg atom and an ion in free space, where we take terms

3.3. Free Rydberg atom-ion interactions

up to quadrupole order in the ion potential, as well as order α^2 corrections due to fine structure into account. Afterwards we include the Paul trap fields, starting with a short discussion of the electric fields that are present, when we fix the ion in the Paul trap minimum. We will use this analysis in later chapters to choose an adequate position for the atom's optical dipole trap that keeps the influence of the Paul trap on the atom minimal, while keeping the atom ion interaction relevant. We complete this chapter with the discussion of our simulations, where we treat the time-dependent Paul trap fields in an adiabatic limit as time-independent. We compare the results with and without Paul trap fields to estimate their effect.

We start with the following approximation for a three particle model system comprised of, a relativistic Rydberg electron, the atomic core and an ion [6]

$$\begin{aligned} \hat{H} &= \frac{\hat{\mathbf{p}}_i^2}{2m_i} + \frac{\hat{\mathbf{p}}_c^2}{2m_c} + \frac{\hat{\mathbf{p}}_e^2}{2m_e} & (1) \\ &+ V_{\text{Ryd}}^{c-e}(\mathbf{r}_c - \mathbf{r}_e) + V_{\text{Ryd}}^{i-e}(\mathbf{r}_i - \mathbf{r}_e) + V_C(\mathbf{r}_i - \mathbf{r}_c) & (2) \\ &+ \frac{1}{2m_e^2 c^2} \hat{\mathbf{S}} \cdot \left[\nabla_e (V_{\text{Ryd}}^{e-c}(\mathbf{r}_e - \mathbf{r}_c) + V_{\text{Ryd}}^{e-i}(\mathbf{r}_e - \mathbf{r}_i)) \times \hat{\mathbf{p}}_e \right] & (3) \\ &- \frac{\hat{\mathbf{p}}_e^2 \hat{\mathbf{p}}_e^2}{8m_e^3 c^2}, & (4) \end{aligned} \tag{3.24}$$

here \mathbf{r}_j , $\hat{\mathbf{p}}_j$ and m_j , $j \in \{i, c, e\}$, correspond to the position, the momentum operator and the mass of the particles, where the indices i , c and e indicate the ion, the atom's core and the electron respectively. In the above equation (3.24) (1) are the kinetic energy terms, (2) the electrostatic interaction potentials between the particles, we later discuss in detail, (3) the electron spin-orbit coupling terms for the atom and the ion potential and (4) is the relativistic kinetic energy correction of the electron. We note that in writing Eq. (3.24), we have neglected terms due to the orbit-orbit coupling of ion and core, as well as the coupling terms arising due to the magnetic field generated by the electron spin and orbit at the ion and core position. All these terms are part of the order α^2 approximation to the relativistic equation, but have additional prefactors proportional to the inverse mass of the involved heavy particles [6]. The above equation is well suited to explain the different relativistic effects that occur in the scenario under consideration, but for further analysis it is more appropriate to regroup the terms.

Since we envision the atom and ion to be trapped separately, it is quite logical to split into terms that just correspond to the atomic or ionic part. For the atom Hamiltonian \hat{H}_a we just take the Hamiltonian of a relativistic alkali Rydberg atom in free space

$$\hat{H}_a = \frac{\hat{\mathbf{p}}_c^2}{2m_c} + \frac{\hat{\mathbf{p}}_e^2}{2m_e} + V_{\text{Ryd}}^{c-e}(\mathbf{r}_e - \mathbf{r}_c) - \frac{\hat{\mathbf{p}}_e^2 \hat{\mathbf{p}}_e^2}{8m_e^3 c^2} + V_{\text{SO}}^{c-e}. \tag{3.25}$$

It consists of the kinetic energy terms of core and electron, also the relativistic correction to kinetic energy of the electron is included. Further there is the electron core Rydberg potential V_{Ryd}^{c-e} which mediates the interaction between core and electron.

3. Rydberg atom-ion interaction

For the spin-orbit terms we introduced the abbreviation $V_{\text{SO}}^{e-\circ}$, where at the \circ position there is a letter indicating to which of the different potentials of the total Hamiltonian the corresponding spin-orbit term is related. Here c is for core, thus V_{SO}^{e-c} stands for the electron-core spin-orbit interaction

$$V_{\text{SO}}^{e-c} = \frac{1}{2m_e^2 c^2} \hat{\mathbf{S}} \cdot [\nabla_e V_{\text{Ryd}}(\mathbf{r}_e - \mathbf{r}_c) \times \hat{\mathbf{p}}_e]. \quad (3.26)$$

We collect the following terms, which concern only the ion

$$\hat{H}_i = \frac{\hat{\mathbf{p}}_i^2}{2m_i} + e\Phi_{PT}(\mathbf{r}_i, t) + \hat{H}_i^{\text{int}}. \quad (3.27)$$

The terms on the right hand side are, the kinetic term of the ion, the influence of the Paul trap and the internal Hamilton operator of the ion \hat{H}_i^{int} , taking account for the ion internal structure, which at this point could be omitted because there is until now no term that couples to it, but as already announced, we will use this term for the gate under consideration in the fifth chapter.

What is still missing is the term taking account for the interaction of the ion with the atom the atom-ion interaction term.

$$\hat{H}_{ia} = V_C(\mathbf{r}_c - \mathbf{r}_i) - V_C(\mathbf{r}_e - \mathbf{r}_i) + V_{\text{SO}}^{e-i}, \quad (3.28)$$

where $V_C(\mathbf{x}) = e^2/(4\pi\epsilon_0|\mathbf{x}|)$ is a simple coulombic charge-charge interaction terms. Here we substituted $-V_C$ for the ion Rydberg potential V_{Ryd}^{i-e} , since we imagine the electron to be bound to the core for the cases we consider in this work, which is far separated from the ion due to the traps. We remind at the notation introduced for the spin orbit like terms

$$V_{\text{SO}}^{e-i} = -\frac{1}{2m_e^2 c^2} \hat{\mathbf{S}} \cdot [\nabla_e V_C(\mathbf{r}_e - \mathbf{r}_i) \times \hat{\mathbf{p}}_e]. \quad (3.29)$$

We sum up in writing the total Hamiltonian as

$$\hat{H} = \hat{H}_a + \hat{H}_i + \hat{H}_{ia}. \quad (3.30)$$

Since we have collected all relevant terms now we can proceed in singling out the terms that go into the Born Oppenheimer Hamiltonian. Having done this, we perform approximations which yield a simpler Hamiltonian suitable for the projection method. The projected Hamiltonian will then be of the form we discussed in the last section, thus that we are able to obtain the effective potential between atom and ion for the electron staying in a fixed energy level. Before we define the BO Hamiltonian, we first change into a COM coordinate frame for atom and ion, which is most convenient for the following discussion. We define the atomic COM coordinate $\mathbf{r}_a = (m_e \mathbf{r}_e + m_c \mathbf{r}_c)/M$ and the relative electron-core coordinate $\mathbf{r} = \mathbf{r}_e - \mathbf{r}_c$ with $M = m_e + m_c$ the total

3.3. Free Rydberg atom-ion interactions

mass and denote the corresponding COM and relative momentum operators with $\hat{\mathbf{p}}_a$ and $\hat{\mathbf{p}}$, respectively. We start with rearranging terms in the full Hamiltonian

$$\begin{aligned}\hat{H} &= \hat{H}_a + \hat{H}_i + \hat{H}_{ia} \\ &= \hat{H}_i + \frac{\hat{\mathbf{p}}_a^2}{2M} + \hat{H}_{\text{BO}} + \bar{V}_{\text{SO}}^{e-c} + \bar{V}_{\text{SO}}^{e-i} + \hat{K}\end{aligned}\quad (3.31)$$

with

$$\begin{aligned}\hat{H}_{\text{BO}} &= \frac{\hat{\mathbf{p}}^2}{2\mu} + V_{\text{Ryd}}(\mathbf{r}) - \frac{\hat{\mathbf{p}}^2 \hat{\mathbf{p}}^2}{8m_e^3 c^2} + \frac{1}{2m_e^2 c^2} \hat{\mathbf{S}} \cdot [\nabla V_{\text{Ryd}}(\mathbf{r}) \times \hat{\mathbf{p}}] \\ &\quad - V_C\left(\mathbf{R} + \frac{m_c}{M}\mathbf{r}\right) + V_C\left(\mathbf{R} - \frac{m_e}{M}\mathbf{r}\right) - \frac{1}{2m_e^2 c^2} \hat{\mathbf{S}} \cdot \left[\nabla V_C\left(\mathbf{R} + \frac{m_c}{M}\mathbf{r}\right) \times \hat{\mathbf{p}}\right],\end{aligned}\quad (3.32)$$

where we use $\mathbf{R} = \mathbf{r}_a - \mathbf{r}_i$ and have split the spin-orbit terms of the electron into two parts as follows

$$V_{\text{SO}}^{e-o} = \frac{1}{2m_e^2 c^2} \hat{\mathbf{S}} \cdot (\circ \times \hat{\mathbf{p}}_e) = V_{\text{SO}}^{\prime e-o} + \bar{V}_{\text{SO}}^{e-o}, \quad (3.33)$$

with

$$V_{\text{SO}}^{\prime e-o} = \frac{1}{2m_e^2 c^2} \hat{\mathbf{S}} \cdot (\circ \times \hat{\mathbf{p}}) \quad \text{and} \quad \bar{V}_{\text{SO}}^{e-o} = \frac{m_e}{M} \frac{1}{2m_e^2 c^2} \hat{\mathbf{S}} \cdot (\circ \times \hat{\mathbf{p}}_a), \quad (3.34)$$

since $\hat{\mathbf{p}}_e = \hat{\mathbf{p}} + \frac{m_e}{M}\hat{\mathbf{p}}_a$ in the COM coordinate frame we just introduced. The operator \hat{K} comprises the terms of the relativistic kinetic energy correction, that also include the momentum operator $\hat{\mathbf{p}}_a$ of the atom

$$\begin{aligned}\hat{K} &= -\frac{m_e}{M} \frac{1}{8m_e^3 c^2} \left[4\hat{\mathbf{p}}^2 \hat{\mathbf{p}} \cdot \hat{\mathbf{p}}_a - 4\frac{m_e}{M} \left((\hat{\mathbf{p}} \cdot \hat{\mathbf{p}}_a)^2 + 2\hat{\mathbf{p}}^2 \hat{\mathbf{p}}_a^2 \right) \right. \\ &\quad \left. - 4\left(\frac{m_e}{M}\right)^2 \hat{\mathbf{p}} \cdot \hat{\mathbf{p}}_a \hat{\mathbf{p}}_a^2 - \left(\frac{m_e}{M}\right)^3 \hat{\mathbf{p}}_a^2 \hat{\mathbf{p}}_a^2 \right].\end{aligned}\quad (3.35)$$

We can neglect the terms $\bar{V}_{\text{SO}}^{e-o}$ and \hat{K} , since they are in addition to a prefactor of α^2 suppressed by m_e/M .

We note, that the so defined Born-Oppenheimer Hamiltonian, \hat{H}_{BO} , commutes with \mathbf{r}_i and \mathbf{r}_a , and therefore we can express \hat{H}_{BO} as $\int \int d\mathbf{r}_i d\mathbf{r}_a |\mathbf{r}_i, \mathbf{r}_a\rangle \langle \mathbf{r}_i, \mathbf{r}_a| \otimes \hat{H}_{\text{BO}}(\mathbf{r}_i, \mathbf{r}_a)$, so after projecting on a finite dimensional set of states at each fixed value of $(\mathbf{r}_i, \mathbf{r}_a)$ we are indeed in the finite dimensional BO case discussed.

Let us now begin to transform the BO Hamiltonian. First we restrict to the particular configuration we are interested in, namely in the case of atom-ion distances R in the μm range with the electron close to the core. In the close to core region, the potential V_{Ryd} dominates the remaining potential terms. Therefore we assume that projecting on a subspace of bound states of a single alkali Rydberg atom

$$\hat{H}_0 = \frac{\hat{\mathbf{p}}^2}{2\mu} + V_{\text{Ryd}}(\mathbf{r}) - \frac{\hat{\mathbf{p}}^2 \hat{\mathbf{p}}^2}{8m_e^3 c^2} + V_{\text{SO}}^{\prime e-c} \quad (3.36)$$

3. Rydberg atom-ion interaction

yields a good approximation. To simplify the situation further we expand the ion part \hat{H}'_{ia} in the BO Hamiltonian in \mathbf{r}/R , since \mathbf{r}/R is small for the considered separations in combination with the states we will project on. Here \hat{H}'_{ia} denotes \hat{H}_{ia} with V_{SO}^{e-i} replaced by V_{SO}^{e-i} . The expansion up to quadrupole order yields

$$\hat{H}'_{ia} \approx \frac{e^2}{4\pi\epsilon_0} \left(\frac{-\mathbf{r} \cdot \mathbf{R} + \frac{m_c - m_e}{2M} \mathbf{r}^2}{|\mathbf{R}|^3} - \frac{3(m_c - m_e)(\mathbf{r} \cdot \mathbf{R})^2}{2M|\mathbf{R}|^5} \right) - \frac{e^2}{8\pi\epsilon_0 m_e^2 c^2} \hat{\mathbf{S}} \cdot \left(\left(\frac{m_e}{M} \mathbf{r} - \mathbf{R} \right) + \frac{3m_c}{M} \frac{\mathbf{r} \cdot \mathbf{R}}{|\mathbf{R}|^5} \mathbf{R} \right) \times \hat{\mathbf{p}}. \quad (3.37)$$

We now use the identity

$$\hat{\mathbf{p}} = i2\frac{\mu}{\hbar} [\hat{H}_0, \mathbf{r}] - \frac{\mu}{\hbar m_e^2 c^2} (\hat{\mathbf{S}} \times (\nabla_e V_{\text{Ryd}})) - i\frac{\mu}{4\hbar m_e^3 c^2} [\hat{\mathbf{p}}^2 \hat{\mathbf{p}}^2, \mathbf{r}] \quad (3.38)$$

to substitute the momentum operator $\hat{\mathbf{p}}$ in Eq. (3.37). We can immediately neglect the last two terms of this equation, observing that they carry prefactors of α^2 and thus will be of order α^4 in the total Hamiltonian. Because $\alpha^2 = (e^2/(4\pi\epsilon_0\hbar c))^2 \lesssim \mathcal{O}(\mathbf{r}/R)$ for the distances we are interested in, we neglect terms of the form $\alpha^2 \mathcal{O}(\mathbf{r}^2/R^2)$ in order to obtain an approximate expression of \hat{H}'_{ia} up to $\mathcal{O}(\mathbf{r}^2/R^2)$:

$$\hat{H}'_{ia} \approx \frac{e^2}{4\pi\epsilon_0 |\mathbf{R}|^3} \left(-\mathbf{r} \cdot \mathbf{R} + \frac{m_c - m_e}{2M} \mathbf{r}^2 \right) - \frac{3e^2(m_c - m_e)}{8\pi\epsilon_0 M |\mathbf{R}|^5} (\mathbf{r} \cdot \mathbf{R})^2 - i\frac{e^2\mu}{4\pi\epsilon_0 \hbar m_e^2 c^2} \frac{1}{|\mathbf{R}|^3} \hat{\mathbf{S}} \cdot (\mathbf{R} \times [\hat{H}_0, \mathbf{r}]). \quad (3.39)$$

With this we have the following approximation of the BO Hamiltonian

$$\hat{H}_{\text{BO}} \approx H_0 + \frac{e^2}{4\pi\epsilon_0 |\mathbf{R}|^3} \left(-\mathbf{r} \cdot \mathbf{R} + \frac{m_c - m_e}{2M} \mathbf{r}^2 \right) - \frac{3e^2(m_c - m_e)}{8\pi\epsilon_0 M |\mathbf{R}|^5} (\mathbf{r} \cdot \mathbf{R})^2 - i\frac{e^2\mu}{4\pi\epsilon_0 \hbar m_e^2 c^2} \frac{1}{|\mathbf{R}|^3} \hat{\mathbf{S}} \cdot (\mathbf{R} \times [\hat{H}_0, \mathbf{r}]). \quad (3.40)$$

Now \hat{H}_{BO} is in the form where we want to apply the projection method to obtain the effective potentials.

To determine the eigenvalues of the BO Hamiltonian for fixed \mathbf{R} and thus the effective potential for atom and ion, we project on a finite set of bound eigenstates of the free Rydberg alkali Hamiltonian H_0 . Since \mathbf{R} is fixed we can transform coordinates such that $\mathbf{R} = (0, 0, R)$, as will become clear this choice of coordinates yields the conservation of m_j . We note that in doing this the base we project on gets \mathbf{R} -dependent, but for now we assume that the terms arising due to this can be neglected and leave a more detailed analysis for a later project. At least the radial correction terms that will arise after the diagonalization should be of the same order as the ones

3.3. Free Rydberg atom-ion interactions

already considered in section 3.1. In these coordinates the BO Hamiltonian reads

$$\hat{H}_{\text{BO}}(\mathbf{r}_i, \mathbf{r}_a) \approx \hat{H}_0 + \frac{e^2}{4\pi\epsilon_0|R|^3} \left(-zR + \frac{m_c - m_e}{2M} r^2 \right) - \frac{3e^2(m_c - m_e)}{8\pi\epsilon_0 M |R|^5} (zR)^2 \quad (3.41)$$

$$- i \frac{e^2 \mu}{8\pi\epsilon_0 m_e^2 c^2} \frac{1}{|R|^3} (\sigma_2 R [\hat{H}_0, x] - \sigma_1 R [\hat{H}_0, y]).$$

Since we rescaled coordinates and the unit of energy for H_0 in section 2.2, we also transform the \mathbf{R} coordinates according to Eq. (2.11) and regroup terms

$$\hat{H}_{\text{BO}}(\mathbf{r}_i, \mathbf{r}_a) \approx \hat{H}_0 - \frac{R}{|R|^3} \left(z + i\alpha^2 \frac{\mu^2}{m_e^2} (\sigma_2 [\hat{H}_0, x] - \sigma_1 [\hat{H}_0, y]) \right) \quad (3.42)$$

$$+ \frac{1}{|R|^3} \frac{m_c - m_e}{2M} (r^2 - 3z^2)$$

From this equation it is clear that we have to evaluate two perturbing matrices, namely

$$h_{|n', l', j', m'_j\rangle\langle n, l, j, m_j|}^1 = \langle n', l', j', m'_j | \left(z + i\alpha^2 \frac{\mu^2}{m_e^2} (\sigma_2 [\hat{H}_0, x] - \sigma_1 [\hat{H}_0, y]) \right) | n, l, j, m_j \rangle \quad (3.43)$$

and

$$h_{|n', l', j', m'_j\rangle\langle n, l, j, m_j|}^2 = \langle n', l', j', m'_j | (r^2 - 3z^2) | n, l, j, m_j \rangle, \quad (3.44)$$

which then result in the following matrix for the projected BO Hamiltonian at each fixed value of R

$$h_{|j'\rangle\langle j|} = \epsilon_j^0 \delta_{|j'\rangle\langle j|} - \frac{R}{|R|^3} h_{|j'\rangle\langle j|}^1 + \frac{1}{|R|^3} \frac{m_c - m_e}{2M} h_{|j'\rangle\langle j|}^2, \quad (3.45)$$

where we abbreviated $|n, l, j, m_j\rangle$ with $|j\rangle$. This matrix can then be diagonalized to yield the eigenvalues and states of the BO Hamiltonian for fixed R position. To obtain the matrix elements of $h_{|j'\rangle\langle j|}^1$ and $h_{|j'\rangle\langle j|}^2$, we have to evaluate the following terms:

$$\langle n', l', j', m'_j | z | n, l, j, m_j \rangle \quad (1)$$

$$\langle n', l', j', m'_j | (\sigma_2 [\hat{H}_0, x] - \sigma_1 [\hat{H}_0, y]) | n, l, j, m_j \rangle \quad (2) \quad (3.46)$$

$$\langle n', l', j', m'_j | (r^2 - 3z^2) | n, l, j, m_j \rangle \quad (3)$$

The first term (1) has already been discussed in the Stark shift scenario in chapter 2 Eq. (2.55) and we remind that it is zero if $m'_j \neq m_j$. The last term (3) can be evaluated in an analogous way, changing to spherical coordinates we obtain

$$\langle n', l', j', m'_j | (r^2 - 3z^2) | n, l, j, m_j \rangle \quad (3.47)$$

$$= \delta_{l'l} \delta_{j'j} \delta_{m'_j m_j} \langle R'_n | r^2 | R_n \rangle - 3 \langle R'_n | r^2 | R_n \rangle \langle l', j', m'_j | \cos(\theta)^2 | l, j, m_j \rangle$$

The terms $\langle R'_n | r^2 | R_n \rangle$ can be obtained as sums over the the grid we used for the Numerov algorithm. We proceed in expanding $\cos(\theta)^2$ in spherical Harmonics

$$\cos(\theta)^2 = \frac{2\sqrt{\pi}}{3} Y_{0,0} + \frac{4\sqrt{\pi/5}}{3} Y_{2,0}. \quad (3.48)$$

3. Rydberg atom-ion interaction

We note that $Y_{0,0} = 1/\sqrt{2\pi}$. We stop the calculation here, since expanding also the states into spin-angular base $|l, ml\rangle \otimes |1/2, m_s\rangle$ and using the identity [60]

$$\langle l', m'_l | Y_{l_1, m_{l_1}} | l, m_l \rangle = \sqrt{\frac{(2l_1 + 1)(2l + 1)}{4\pi(2l' + 1)}} \text{CG} \begin{pmatrix} l_1 & l & l' \\ 0 & 0 & 0 \end{pmatrix} \text{CG} \begin{pmatrix} l_1 & l & l' \\ m_{l_1} & m_l & m'_l \end{pmatrix}, \quad (3.49)$$

yield the desired values in a straightforward way. We note that from Eq. (3.49) we can infer that also this term is zero for $m_j \neq m'_j$, since the m_{l_1} value of the spherical harmonics is for both terms zero, thus the term is zero for $m_l \neq m'_l$ and also for $m_s \neq m'_s$, since there are no Pauli matrices in this part of the operator.

Let us now come to term (2) of Eq. (3.46), which needs to be further approximated since $[\sigma_i, H_0] \neq 0$. Therefore let us have a look at how σ_i acts on an eigenstate of H_0 .

$$\begin{aligned} & |n, l, j, m_j\rangle \\ &= |R_n\rangle \otimes \sum_{m_l, m_s} \text{CG} \begin{pmatrix} l & 1/2 & j \\ m_l & m_s & m_j \end{pmatrix} |l, m_l\rangle \otimes \sigma_i |1/2, m_s\rangle. \end{aligned} \quad (3.50)$$

Thus, just the m_s states get mixed, but n and l are conserved. Therefore we can estimate the commutator applied to a bound state $[\sigma_i, H_0]|n, l, j, m_j\rangle$ to be of order $|\epsilon_{n,l,l-1/2}^0 - \epsilon_{n,l,l+1/2}^0|$, which is of order α^2 in combination with the order α^2 prefactor of term (2) the contribution of $[\sigma_i, H_0]|n, l, j, m_j\rangle$ will in total be of order α^4 and can be neglected. So we can now start in calculating the contribution of term (2) of Eq. (3.46)

$$\begin{aligned} & \langle n', l', j', m'_j | \left(\sigma_2 [\hat{H}_0, x] - \sigma_1 [\hat{H}_0, y] \right) |n, l, j, m_j\rangle \\ & \approx \langle n', l', j', m'_j | \left(\sigma_2 (\epsilon_{n',l',j'} - \epsilon_{n,l,j}) r \sin(\theta) \cos(\phi) \right. \\ & \quad \left. - \sigma_1 (\epsilon_{n',l',j'} - \epsilon_{n,l,j}) r \sin(\theta) \sin(\phi) \right) |n, l, j, m_j\rangle \\ & = (\epsilon_{n',l',j'} - \epsilon_{n,l,j}) \langle R_{n'} | r | R_n \rangle \\ & \quad \langle l', j', m'_j | \left(\sigma_2 \sin(\theta) \cos(\phi) - \sigma_1 \sin(\theta) \sin(\phi) \right) |l, j, m_j\rangle. \end{aligned} \quad (3.51)$$

The radial part $\langle R_{n'} | r | R_n \rangle$ can easily be obtained as a sum, thus it is left to evaluate

$$\langle l', j', m'_j | \left(\sigma_2 \sin(\theta) \cos(\phi) - \sigma_1 \sin(\theta) \sin(\phi) \right) |l, j, m_j\rangle \quad (3.52)$$

We first change to the spin-angular base

$$\begin{aligned} & \langle l', j', m'_j | \left(\sigma_2 \sin(\theta) \cos(\phi) - \sigma_1 \sin(\theta) \sin(\phi) \right) |l, j, m_j\rangle \\ &= \sum_{m'_l, m'_s} \sum_{m_l, m_s} \overline{\text{CG}} \begin{pmatrix} l' & 1/2 & j' \\ m'_l & m'_s & m'_j \end{pmatrix} \text{CG} \begin{pmatrix} l & 1/2 & j \\ m_l & m_s & m_j \end{pmatrix} \\ & \quad (\delta_{m'_s, 1/2} \delta_{m_s, -1/2} \langle l', m'_l | (-i \sin(\theta) \cos(\phi) - \sin(\theta) \sin(\phi)) |l, m_l\rangle \\ & \quad + \delta_{m'_s, -1/2} \delta_{m_s, 1/2} \langle l', m'_l | (i \sin(\theta) \cos(\phi) - \sin(\theta) \sin(\phi)) |l, m_l\rangle) \end{aligned} \quad (3.53)$$

3.3. Free Rydberg atom-ion interactions

and expand in spherical harmonics

$$\begin{aligned} (-i \sin(\theta) \cos(\phi) - \sin(\theta) \sin(\phi)) &= i2\sqrt{\frac{2\pi}{3}} Y_{1,1} \\ (i \sin(\theta) \cos(\phi) - \sin(\theta) \sin(\phi)) &= i2\sqrt{\frac{2\pi}{3}} Y_{1,-1}. \end{aligned} \quad (3.54)$$

We substitute this in Eq. (3.53) and get

$$\begin{aligned} &\langle l', j', m'_j | (\sigma_2 \sin(\theta) \cos(\phi) - \sigma_1 \sin(\theta) \sin(\phi)) | l, j, m_j \rangle \\ &= \sum_{m'_l, m_l} \overline{\text{CG}} \begin{pmatrix} l' & 1/2 & j' \\ m'_l & 1/2 & m'_j \end{pmatrix} \text{CG} \begin{pmatrix} l & 1/2 & j \\ m_l & -1/2 & m_j \end{pmatrix} \\ &\quad i\sqrt{\frac{2+4l}{1+2l'}} \text{CG} \begin{pmatrix} 1 & l & l' \\ 0 & 0 & 0 \end{pmatrix} \text{CG} \begin{pmatrix} 1 & l & l' \\ 1 & m_l & m'_l \end{pmatrix} \\ &+ \sum_{m'_l, m_l} \overline{\text{CG}} \begin{pmatrix} l' & 1/2 & j' \\ m'_l & 1/2 & m'_j \end{pmatrix} \text{CG} \begin{pmatrix} l & 1/2 & j \\ m_l & -1/2 & m_j \end{pmatrix} \\ &\quad i\sqrt{\frac{2+4l}{1+2l'}} \text{CG} \begin{pmatrix} 1 & l & l' \\ 0 & 0 & 0 \end{pmatrix} \text{CG} \begin{pmatrix} 1 & l & l' \\ -1 & m_l & m'_l \end{pmatrix}. \end{aligned} \quad (3.55)$$

Let us stop here, since we can now infer that also this term vanishes for $m_j \neq m'_j$, since the changes in m_l and m_s exactly cancel.

Now we know how to obtain the matrix elements in this case and that we can restrict to states with equal m_j . In Fig. (3.6) we show the obtained adiabatic eigenenergies for the BO Hamiltonian for ${}^6\text{Li}$ projecting on the space of eigenstates $\{|n, l, j, m_j\rangle\}$ with $n \in \{25, \dots, 35\}$ and $m_j = 1/2$. We obtain, that the $30S$ states stay well separated in energy from the other states down to distances of about 500 nm. We compare the results of our simulation to a potential we obtained based on second order perturbation theory within the dipole approximation $-C_4^{(R)}/R^4 = -\alpha_{|R}\mathbf{E}_{ion}^2(\mathbf{R})/2$ with $\mathbf{E}_{ion}(\mathbf{R})$ the electric field of the ion evaluated at the atom position, and $\alpha_{|R}$ the polarizability of the Rydberg state [26]. We observe that for distances in the μm range both potentials are in excellent agreement. For instance, for Lithium in the $|30S_{1/2}\rangle$ state, $\alpha_{|R} = 3.5 \times 10^8 \alpha_{|2S_{1/2}}$ [37, 48]. Note that the electron orbit in a Rydberg-atom is given by $r_n = n^2 a_0$ with a_0 being the Bohr radius. For $n = 30$ we have $r_{30} \simeq 0.05 \mu\text{m}$, which is indeed much smaller than the atom-ion separation ($\sim 1 \mu\text{m}$) we are interested in.

3. Rydberg atom-ion interaction

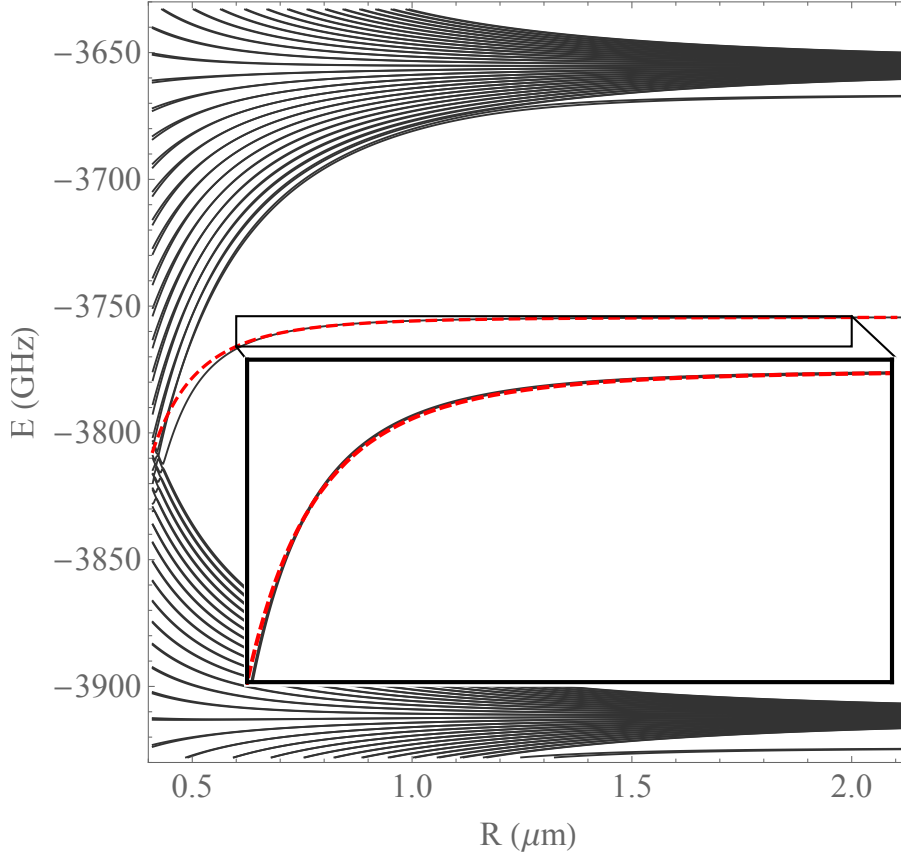


Figure 3.6.: Eigenenergies ϵ_k of \hat{H}_{BO} for ${}^6\text{Li}$ interacting with an ion as a function of the ion-core distance R , that emanate from the $n = 30$ and the $n = 29$ manifolds based on our simulation without trapping fields. The $30S$ and $30P$ energies lie separated at -3754.4 GHz and -3666.7 GHz. The dashed red line shows a $-C_4^{|30S_{1/2}\rangle}/R^4$ potential shifted down by the $30S$ energy that is based on second order perturbation theory within the dipole approximation. Here $C_4^{|30S_{1/2}\rangle}$ was taken from Refs. [48], [37]. We see that the $30S$ state remain well separated from the others down to distances of ~ 500 nm, whereas second order perturbation theory works well for distances $\geq 1\mu\text{m}$.

3.4. Atom-Paul trap interactions

In the foregoing section we discussed the Rydberg atom-ion interaction in free space, now we also want to include the external electric potential $\Phi_{PT}(\mathbf{x}, t)$ due to the Paul trap. We note that to estimate also the influence of the time-dependent part of Φ_{PT} , we will adiabatically approximate the rf part by an infinitely slow changing

3.4. Atom-Paul trap interactions

one and thus take time as a parameter. We start with a short section on the electric fields, that are present, when we fix the ion in the Paul trap minimum. We will use the results obtained in chapter 5 to figure out preferable positions of the atom dipole trap. We continue in adding the Paul trap terms to the full Hamiltonian Eq. (3.30) of the previous sections and explain how the BO Hamiltonian has to be modified.

We begin in discussing the effect of the ionic trapping field from the Paul electrodes on the Rydberg atom. The interaction between the atom and the Paul trapping field is described by

$$\hat{H}_a^t = e\Phi_{PT}(\mathbf{r}_c, t) - e\Phi_{PT}(\mathbf{r}_e, t) + V_{SO}^{e-t}, \quad (3.56)$$

with the spin orbit trap term

$$V_{SO}^{e-t} = \frac{e}{2m_e^2c^2} \hat{\mathbf{S}} \cdot [\mathbf{E}_{PT}(\mathbf{r}_e, t) \times \hat{\mathbf{p}}_e]. \quad (3.57)$$

Where we define the potential of a standard quadrupole Paul trap to be

$$\Phi_{PT}(\mathbf{x}, t) = \frac{m_i\omega_i^2}{4e} (x^2 + y^2 - 2z^2) + \frac{m_i\Omega_{rf}^2q}{4e} \cos \Omega_{rf}t (x^2 - y^2), \quad (3.58)$$

with q the stability parameter for an ion of mass m_i , Ω_{rf} the trap drive frequency and corresponding electric field given by $\mathbf{E}_{PT}(\mathbf{x}, t) = \mathbf{E}_s(\mathbf{x}) + \mathbf{E}_{rf}(\mathbf{x}, t)$, where

$$\mathbf{E}_s(x, y, z) = \frac{m_i\omega_i^2}{e} \left(\frac{x}{2}, \frac{y}{2}, -z \right), \quad (3.59)$$

$$\mathbf{E}_{rf}(x, y, z, t) = \frac{m_i\Omega_{rf}^2q}{2e} \cos \Omega_{rf}t (x, -y, 0). \quad (3.60)$$

We note that the static part of the field \mathbf{E}_s confines positively charged particles in the z -direction, while the confinement in the transverse direction is realized by the time-dependent part \mathbf{E}_{rf} , for appropriate parameters of the trapping field [42].

We know that the ion is going to be confined in a small region around the trap minimum. We want atom and ion to interact, but prevent collisions, while keeping the influence of the trapping field minimal. As a first step we seek to determine the region where the ions field is dominant. In the case considered there is no time varying field in z -direction as is clear from Eq. (3.60), so we can give a distance in z -direction where the ion, which we assume to be fixed in the trap center $\mathbf{r}_i = 0$, and trapping field cancel. This distance is given by $\ell_z = [e^2/(4\pi\epsilon_0 m_i \omega_i^2)]^{1/3}$. For $^{171}\text{Yb}^+$ with $\omega_i = 2\pi \cdot 250$ kHz, we have $\ell_z = 6.9 \mu\text{m}$. So we conclude that for $z \ll \ell_z$, we can neglect the Stark shift of the static trapping field on the Rydberg level, whereas for $z \gg \ell_z$, the Stark shift of the trapping field dominates. For the radial direction both the electric field of the ion and the static Paul trap field add up and no cancellation occurs so we give here the lowest value of the combined field $\ell_{\perp} = 2^{2/3}\ell_z$. The oscillating field, is typically 10 – 100 times stronger than the static field. Thus it is preferable to trap the atoms close to the radio frequency null line $x, y \sim 0$. In Fig. 3.7 we plot the region where the absolute value of the ions field is 10 times larger than

3. Rydberg atom-ion interaction

the trap rf field for maximal amplitude. We also included the atoms and ions spatial probability densities, with the trap frequencies considered for the simulations. For the numbers considered in this work ($\Omega_{\text{rf}} = 2\pi \cdot 2.5$ MHz and $q = 0.28$), the oscillating field at maximal amplitude starts to dominate over the ion field at $2.9 \mu\text{m}$ distance. From Fig. 3.6 we see that this is within the range where second order perturbation theory can be used. Furthermore, since the energy gaps between the Rydberg states lie in the 100 GHz range, the MHz trapping field cannot drive transitions between the Rydberg states allowing us to treat the effect quasi-statically.

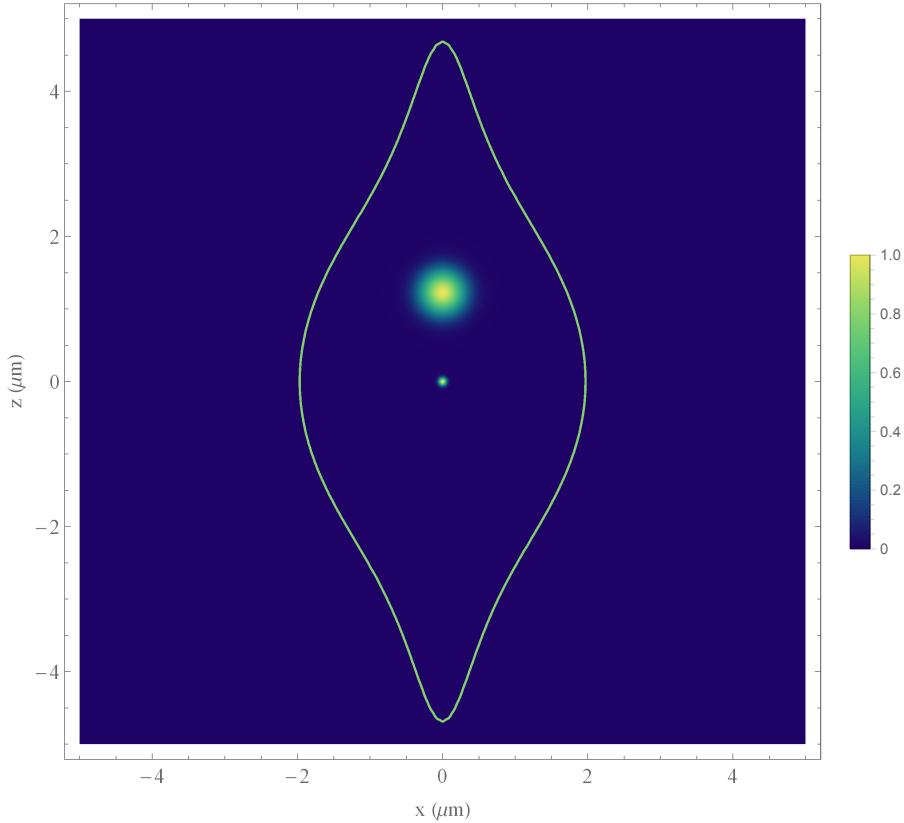


Figure 3.7.: Density plots: atom and ion probability densities with trap frequencies as in the simulations done in chapter 5. The probability densities are normed such that the peak value is one. The contour (green) shows the positions with $\mathbf{E}_{\text{ion}} = 10 \mathbf{E}_{\text{trap}}(t_{\text{max}})$ with t_{max} such that $|\mathbf{E}_{\text{trap}}|$ is maximal.

We adjust the BO Hamiltonian in the following way

$$\begin{aligned}
 \hat{H}_{\text{BO}}(\mathbf{r}_i, \mathbf{r}_a) &\approx \hat{H}_0 \\
 &+ \frac{e^2}{4\pi\epsilon_0|\mathbf{R}|^3} \left(-\mathbf{r} \cdot \mathbf{R} + \frac{m_c - m_e}{2M} \mathbf{r}^2 \right) - \frac{3e^2(m_c - m_e)}{8\pi\epsilon_0 M |\mathbf{R}|^5} (\mathbf{r} \cdot \mathbf{R})^2 \\
 &- i \frac{e^2 \mu}{4\pi\epsilon_0 \hbar m_e^2 c^2} \frac{1}{|\mathbf{R}|^3} \hat{\mathbf{S}} \cdot (\mathbf{R} \times [\hat{H}_0, \mathbf{r}]) \\
 &+ e\phi_{PT}(\mathbf{r}_c, t) - e\phi_{PT}(\mathbf{r}_e, t) + i \frac{e\mu}{\hbar m_e^2 c^2} \hat{\mathbf{S}} \cdot (\mathbf{E}_{PT}(\mathbf{r}_e, t) \times [\hat{H}_0, \mathbf{r}]),
 \end{aligned} \tag{3.61}$$

where we added just the last line. As in the free case we split the term V_{SO}^{e-t} into two parts $V_{\text{SO}}'^{e-t}$ and $\bar{V}_{\text{SO}}^{e-t}$ and neglect the $\bar{V}_{\text{SO}}^{e-t}$ term. In $V_{\text{SO}}'^{e-t}$ we also substituted Eq. (3.38) for the momentum operator $\hat{\mathbf{p}}$ and neglected the terms of order α^4 . Thus we can now as in the free case project on a finite base of bound states of the free Rydberg electron. But now we take a fixed H_0 base. To calculate the matrix elements we automatized the process of splitting into spherical and radial parts, as well as evaluating the angular and radial matrix elements. For completeness we give here the formula for a general spin-angular matrix element that is a product of a spherical Harmonic and a pauli matrix

$$\begin{aligned}
 &\langle l', j', m'_j | \sigma_i Y_{\tilde{l}, \tilde{m}_l} | l, j, m_j \rangle \\
 &= \sum_{m'_l, m'_s} \sum_{m_l, m_s} \overline{\text{CG}} \begin{pmatrix} l' & 1/2 & j' \\ m'_l & m'_s & m'_j \end{pmatrix} \text{CG} \begin{pmatrix} l & 1/2 & j \\ m_l & m_s & m_j \end{pmatrix} \\
 &\quad \langle l, m_l | Y_{\tilde{l}, \tilde{m}_l} | l, m_l \rangle \langle 1/2, m'_s | \sigma_i | 1/2, m_s \rangle \\
 &= \sum_{m'_l, m'_s} \sum_{m_l, m_s} \overline{\text{CG}} \begin{pmatrix} l' & 1/2 & j' \\ m'_l & m'_s & m'_j \end{pmatrix} \text{CG} \begin{pmatrix} l & 1/2 & j \\ m_l & m_s & m_j \end{pmatrix} \\
 &\quad \sqrt{\frac{(2\tilde{l}+1)(2l+1)}{4\pi(2l'+1)}} \text{CG} \begin{pmatrix} \tilde{l} & l & l' \\ 0 & 0 & 0 \end{pmatrix} \text{CG} \begin{pmatrix} \tilde{l} & l & l' \\ \tilde{m}_l & m_l & m'_l \end{pmatrix} \langle 1/2, m'_s | \sigma_i | 1/2, m_s \rangle
 \end{aligned} \tag{3.62}$$

For our simulation we choose to fix the ion in the Paul trap minimum and evaluate the effect of the Paul trap for zero and maximal amplitudes of the rf electric field along the radial direction from the trap center. In Fig. 3.4 we compare the results of our simulations including Paul trapping fields with the results obtained in the free case. We obtain that the effects are in the order of ~ 0.5 GHz. For the simulations we projected on the eigenstates $|n, l, j, m_j\rangle$ of H_0 for $n \in \{26, \dots, 34\}$ and $l \in \{0, \dots, 25\}$. This completes the third chapter and we can now start the analysis of the interaction with laser fields.

3. Rydberg atom-ion interaction

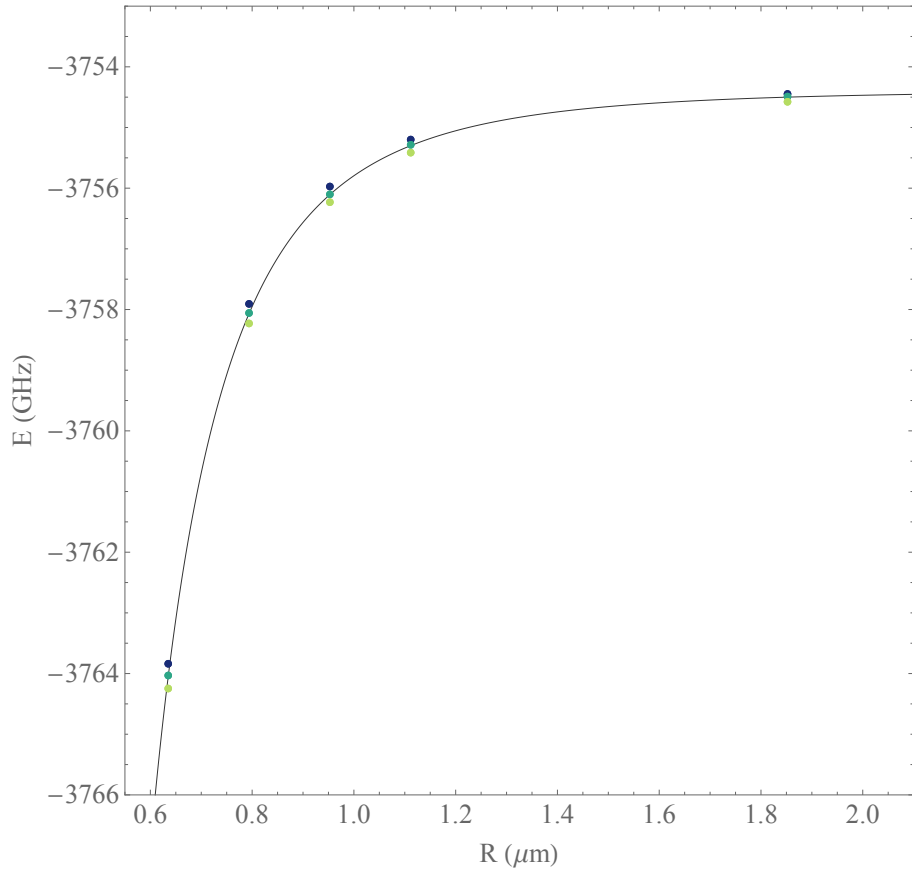


Figure 3.8.: Comparison of the effective potential emanating from the 30S of ${}^6\text{Li}$ state with (dots) and without (gray line) trapping field in the radial direction. The three points correspond to the trapping field at maximal positive and negative and zero amplitude. In this calculation we used the following parameters, $\Omega_{\text{rf}} = 2\pi \cdot 2.5$ MHz, $q = 0.28$, assuming Yb^+ .

4. Alkali atoms in laser fields

Our final goal is to derive atom ion spin-spin interactions, therefore we need a Rydberg dressed atom in an optical dipole trap in the close vicinity of a trapped ion. In the last chapter we already treated the case of a Rydberg atom and an ion, so what is still missing are the dipole and dressing laser fields. We will first study the case of the optical dipole trap, where a laser field off resonantly couples the atomic ground state to an excited state resulting in a weakly dressed state. The whole process leads to an effective potential which depends on the laser intensity. To describe the atom laser interactions we will always change to a rotating frame. Since for the Rydberg atom, we are already in the BO representation before doing such a time-dependent transformation, we will make a careful investigation of this scenario in the second section. In the last section we will treat the case of Rydberg dressing including the dipole trap in the presence of a nearby ion. This will result in a tunable dressed potential between atom and ion, which forms the basis for the study of the announced spin-spin interactions in the next chapter.

4.1. Optical dipole trap

We start general with a free atom \hat{H}_0 in an external light field $\mathbf{E}(\mathbf{x}, t)$ where \mathbf{x} denotes the position in the laboratory frame.

$$\hat{H} = \frac{\hat{\mathbf{p}}_a^2}{2\mu} + \hat{H}_{\text{BO}}(\mathbf{r}_a, t), \quad (4.1)$$

where in dipole approximation $\hat{H}_{\text{BO}}(\mathbf{r}_a, t)$ is given by

$$\hat{H}_{\text{BO}}(\mathbf{r}_a, t) = \hat{H}_0 + e\mathbf{E}(\mathbf{r}_a, t) \cdot \sum_i \mathbf{r}_i, \quad (4.2)$$

with \mathbf{r}_i the relative nucleus electron positions and $\hat{\mathbf{p}}_a$ and \mathbf{r}_a the momentum respectively position operator of the center of mass coordinate, which is here the only heavy particle. For simplicity we assume $\mathbf{E}(\mathbf{x}, t) = \hat{\mathbf{e}}E^0(\mathbf{x})\cos(\omega t)$ to be linearly polarized. If the field is tuned close to a single transition with low coupling strength we can project on the coupled states, which we denote with ground $|g\rangle$ and excited $|e\rangle$ state. Since we consider no additional external fields here, these states will be independent of the atom center-of-mass position \mathbf{r}_a . We define the dipole operator $\mathbf{d}_{j'j} = \langle j'|e\sum_i \mathbf{r}_i|j\rangle$, $j \in \{g, e\}$ and assume $\mathbf{d}_{jj} = 0$. So the projected BO Hamiltonian reads

$$\hat{H}_{\text{BO}}(\mathbf{r}_a, t) = \begin{pmatrix} \epsilon_g & 2\hbar\Omega_d(\mathbf{r}_a)\cos(\omega_d t) \\ 2\hbar\Omega_d^*(\mathbf{r}_a)\cos(\omega_d t) & \epsilon_e \end{pmatrix}, \quad (4.3)$$

4. Alkali atoms in laser fields

with

$$\Omega_d(\mathbf{r}_a) = \frac{1}{\hbar} \mathbf{d}_{ge} \cdot \hat{\mathbf{e}}_{\text{dip}} E_{\text{dip}}^0(\mathbf{r}_a) \quad (4.4)$$

We change to a rotating frame with

$$\mathcal{U}(t) = \begin{pmatrix} e^{i\epsilon_g/\hbar t} & 0 \\ 0 & e^{i(\epsilon_g/\hbar + \omega_d)t} \end{pmatrix} \quad (4.5)$$

this results in

$$\tilde{H}_{\text{BO}}(\mathbf{r}_a, t) = \begin{pmatrix} 0 & \hbar\Omega_d(\mathbf{r}_a)(1 + e^{-2i\omega_d t}) \\ \hbar\Omega_d^*(\mathbf{r}_a)(1 + e^{2i\omega_d t}) & \hbar\Delta \end{pmatrix}, \quad (4.6)$$

with the detuning $\Delta = (\epsilon_e - \epsilon_g)/\hbar - \omega_d$. We neglect the terms rotating with twice the laser frequency and arrive at

$$\tilde{H}_{\text{BO}}(\mathbf{r}_a, t) \approx \begin{pmatrix} 0 & \hbar\Omega_d(\mathbf{r}_a) \\ \hbar\Omega_d^*(\mathbf{r}_a) & \hbar\Delta \end{pmatrix}. \quad (4.7)$$

For adiabatic changes of the laser intensity the electron will stay in an eigenstate of this operator. We are now in the time-independent BO scenario discussed in the last chapter. The eigenvalues, which will serve as effective potentials, read

$$\epsilon_1(\mathbf{r}_a) = \frac{\hbar}{2} \left(\Delta - \sqrt{\Delta^2 + 4|\Omega_d(\mathbf{r}_a)|^2} \right) \quad \text{and} \quad \epsilon_2(\mathbf{r}_a) = \frac{\hbar}{2} \left(\Delta + \sqrt{\Delta^2 + 4|\Omega_d(\mathbf{r}_a)|^2} \right). \quad (4.8)$$

Since $\Omega(\mathbf{r}_a) \propto E_d^0(\mathbf{r}_a)$ the eigenvalues depend on the dipole laser intensity I , $\sqrt{I(\mathbf{r}_a)} \propto E_d^0(\mathbf{r}_a)$. In figure 4.1 we plot ϵ_1 for a gaussian beam shape. For simplicity, we give the eigenstates up to first order in Ω , assuming $|\Omega| \ll \Delta$ and $\Delta > 0$. This yields

$$\mathbf{w}_1 = \begin{pmatrix} 1 \\ -\frac{\Omega}{\Delta} \end{pmatrix} \quad \text{and} \quad \mathbf{w}_2 = \begin{pmatrix} \frac{\Omega^*}{\Delta} \\ 1 \end{pmatrix}, \quad (4.9)$$

thus the eigenvectors are just weakly dependent on \mathbf{r}_a , therefore we assume the correction terms arising due to the \mathbf{r}_a dependence of the eigenstates to be neglectable and arrive at

$$\hat{H} \approx \sum_{j \in \{1,2\}} \left[\frac{\hat{\mathbf{p}}_a^2}{2\mu} + \epsilon_j(\mathbf{r}_a) \right] \otimes |j\rangle\langle j|. \quad (4.10)$$

For a treatment taking also the decay of the excited state into account we refer to [12]. This was a simple first example of a rotating wave approximation in the BO framework, but in the above example initially no shifts due to external fields were present. To analyze which terms arise in that case is the subject of the next section.

4.2. Rotating wave approximation inside the BO framework

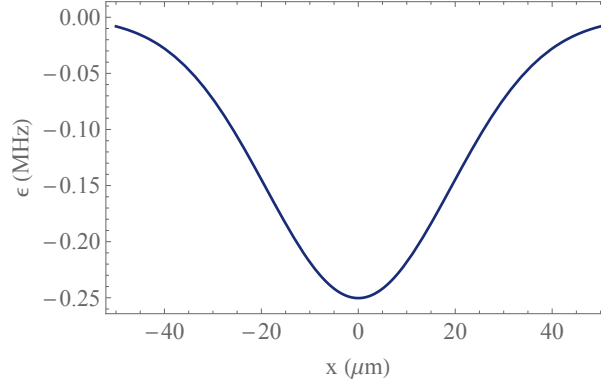


Figure 4.1.: Effective potential $\epsilon_1(x)$ for $\Omega(x) = \Omega_0 \sqrt{e^{-(x/\sigma)^2}}$ with $\Omega_0 = 6.128$ MHz, $\sigma = 27$ μm and $\Delta = 2\pi 0.15$ GHz.

4.2. Rotating wave approximation inside the BO framework

We now want to consider the case where the BO Hamiltonian consists of a time-dependent and a time-independent part. To transform into the rotating frame we need the time-independent part to be diagonal, thus we start with the total Hamiltonian in the diagonal representation of the time-independent part

$$\begin{aligned} \hat{H}(t) = & \sum_{j,p=1}^n \left[\delta_{pj} \sum_{k=1}^N \frac{\hat{\mathbf{p}}_k^2}{2m_k} + (\delta_{pj}\epsilon_j(\mathbf{Y}) + h_{pj}(\mathbf{Y}, t)) \right] \otimes |p\rangle\langle j| \\ & - \sum_{j,p=1}^n \sum_{k=1}^N \left[\frac{i\hbar}{m_k} \tilde{\mathbf{b}}_{pj}^{(k)}(\mathbf{Y}) \cdot \hat{\mathbf{p}}_k + \frac{\hbar^2}{2m_k} \tilde{b}_{pj}^{(k)}(\mathbf{Y}) \right] \otimes |p\rangle\langle j|, \end{aligned} \quad (4.11)$$

We can transform into a rotating frame in the light particle Hilbert space with the time-dependent unitary transformation

$$\mathcal{U}(t) = \mathbf{1} \otimes \sum_j u_j(t) |j\rangle\langle j| = \mathbf{1} \otimes \mathbf{u}(t), \quad (4.12)$$

as in the non BO case we have to consider the time-dependent Schrödinger equation

$$i\hbar \partial_t \psi(t) = \hat{H}(t) \psi(t), \quad (4.13)$$

which transforms under $\mathcal{U}(t)$ to

$$i\hbar \partial_t \mathcal{U} \psi(t) = \mathcal{U}(t) \hat{H}(t) \mathcal{U}^\dagger(t) \mathcal{U}(t) \psi(t) + i\hbar \dot{\mathcal{U}}(t) \mathcal{U}^\dagger(t) \mathcal{U}(t) \psi(t). \quad (4.14)$$

thus the new Hamilton operator in rotating coordinates reads

$$\mathcal{U}(t) \hat{H}(t) \mathcal{U}^\dagger(t) + i\hbar \dot{\mathcal{U}}(t) \mathcal{U}^\dagger(t). \quad (4.15)$$

4. Alkali atoms in laser fields

Let us first have a look at the last term

$$\begin{aligned} & -i\hbar\dot{\mathcal{U}}(t)\mathcal{U}^\dagger \\ & = -i\hbar\mathbf{1} \otimes \sum_j^n \dot{u}_j(t)\overline{u_j(t)}|j\rangle\langle j|. \end{aligned} \quad (4.16)$$

Now we calculate how $\hat{H}_{\text{BO}}(\mathbf{Y}, t)$ transforms

$$\mathbf{u}(t)\hat{H}_{\text{BO}}(\mathbf{Y}, t)\mathbf{u}^\dagger(t) = \sum_j \epsilon_j(\mathbf{Y})|j\rangle\langle j| + \sum_{k,j=1}^n \left(h_{kj}^L(\mathbf{Y}, t)u_k(t)\overline{u_j(t)} \right) |k\rangle\langle j| \quad (4.17)$$

and sum up

$$\begin{aligned} \mathcal{U}(t) \int d\mathbf{Y} |\mathbf{Y}\rangle\langle \mathbf{Y}| \otimes \hat{H}_{\text{BO}}(\mathbf{Y}, t)\mathcal{U}_2^\dagger(t) - i\hbar\dot{\mathcal{U}}_2(t)\mathcal{U}_2^\dagger \\ = \left[\sum_j \left(\epsilon_j^0(\mathbf{Y})|j\rangle\langle j| + i\hbar\dot{u}_j(t)\overline{u_j(t)}|j\rangle\langle j| \right) \right. \\ \left. + \sum_{k,j=1}^n \left(h_{kj}^L(\mathbf{Y}, t)u_k(t)\overline{u_j(t)} \right) |k\rangle\langle j| \right] \end{aligned} \quad (4.18)$$

So we obtain exactly the same terms in the transformation to a rotating frame as in the non BO case. We can conclude that we can transform time-dependent Hamiltonians of the dipole form into slow and fast rotating terms, which makes a subsequent rotating wave approximation possible. But we also have to transform the remaining terms. The kinetic energy term obviously commutes with $\mathcal{U}(t)$, as long as there is no \mathbf{Y} dependence in the unitary transformation, since it is of the form

$$\sum_{k=1}^N \frac{\hat{\mathbf{p}}_k^2}{2m_k} \otimes \mathbf{1}. \quad (4.19)$$

The terms in the last line of Eq. (4.11) transform to

$$\begin{aligned} \mathcal{U}(t) \left(\sum_{j,p=1}^n \sum_{k=1}^N \left[\frac{i\hbar}{m_k} \tilde{\mathbf{b}}_{pj}^{(k)}(\mathbf{Y}) \cdot \hat{\mathbf{p}}_k + \frac{\hbar^2}{2m_k} \tilde{b}_{pj}^{(k)}(\mathbf{Y}) \right] \otimes |p\rangle\langle j| \right) \mathcal{U}^\dagger(t) \\ = + \sum_{j,l,p=1}^n \sum_{k=1}^N \left[\frac{i\hbar}{m_k} u_p(t)\overline{u_j(t)} \mathbf{b}_{pj}^{(k)} \cdot \hat{\mathbf{p}}_k + \frac{\hbar^2}{2m_k} u_p(t)\overline{u_j(t)} b_{pj}^{(k)} \right] \otimes |p\rangle\langle j|. \end{aligned} \quad (4.20)$$

The sum of Eq. (4.18), Eq. (4.19) and Eq. (4.20) is the full transformed Hamiltonian and we have shown that we can apply the rotating wave approximation as usual, just the coupling terms become time-dependent, but are still of the same order of magnitude, since $|u_j(t)| = 1$. After neglecting fast rotating terms we can apply the methods of the last chapter to bring, e.g. the approximated BO operator into diagonal form, which then can be approximately reduced, such that the \mathbf{Y} dependent eigenvalues serve as effective potentials in the adiabatic case. Now we are ready to apply these results to the case of Rydberg dressing in the vicinity of a nearby trapped ion.

4.3. Dressed Rydberg atom-ion interaction

In this section we make the final step towards the atom-ion spin spin interactions we discuss in the next chapter. We include the light fields for dipole trap and Rydberg dressing and derive the resulting potential, i.e. the dipole trap potential similar to the one we already discussed and an adiabatic interaction potential between atom and ion, which will in the next section be utilized to entangle the atom internal spin states with ion motion. We imagine the following situation: Let each field be tuned close to a single transition in the atom with low coupling strength, such that we can neglect all other transitions and are left with a three level system. The dipole laser couples the states $|g\rangle \leftrightarrow |e\rangle$, we assume this transition to be a dipole allowed, with $|e\rangle = |2P\rangle$. The Rydberg dressing laser is tuned close to the transition $|g\rangle \leftrightarrow |R\rangle$, where $|g\rangle$, $|e\rangle$ and $|R\rangle$ denote ground, excited and Rydberg state. we note that in practice the Rydberg excitation may be realized by a two level transition from the S ground state to some Rydberg state nS via a P state.

But let us first take one step back, and see which steps we have to take to arrive at this three level system. The simulations in the last chapter were all done in the single channel QDT model, which holds just for highly excited states, so we can't hope that it will also deliver an adequate description for the low lying states. Therefore we simply add those in their full description with all electrons, but since the light fields will now couple those low lying states to the Rydberg ones, we also need to substitute the one electron QDT wave functions we projected on, with the full ones. We think of all this to be done after having changed into the diagonal representation of the BO Hamiltonian. We can now add the light fields

$$H_L = \sum_l e\mathbf{r}_l \cdot (\mathbf{E}_{\text{dress}}(\mathbf{r}_a, t) + \mathbf{E}_{\text{dip}}(\mathbf{r}_a, t)), \quad (4.21)$$

where \mathbf{r}_l are the relative nucleus electron coordinates, as in the dipole trap case considered above, $\mathbf{E}_{\text{dip}}(\mathbf{r}_a, t)$ is a tightly focussed laser that creates the atomic trapping potential and $\mathbf{E}_{\text{dress}}(\mathbf{r}_a, t)$, couples the atom off-resonantly to a Rydberg state. We can now perform the three level approximation, thus that the laser Hamiltonian transforms to a three dimensional matrix, where the matrix elements are of the following form

$$\langle j' | H_L | j \rangle = +\mathbf{d}_{j'j}(\mathbf{r}_i, \mathbf{r}_a) \cdot (\mathbf{E}_{\text{dress}}(\mathbf{r}_a, t) + \mathbf{E}_{\text{dip}}(\mathbf{r}_a, t)), \quad (4.22)$$

with $\mathbf{d}_{j'j}(\mathbf{r}_i, \mathbf{r}_a) = \langle j' | \sum_l e\mathbf{r}_l | j \rangle$ and $|j\rangle$ the full wave functions of the given states, for $j \in \{g, e, R\}$. For atom-ion distances $R \gg R^*$ we can safely neglect the position dependence of the low lying energies and states $|g\rangle$ and $|e\rangle$, but the Rydberg state $|R\rangle$ gets shifted. To take this into account we take the energy shift calculated in dipole approximation combined with second order perturbation theory. This yields the Rydberg state energy $\epsilon_R^0 - \alpha_{|R\rangle} |\mathbf{E}_{\text{ion}}(|\mathbf{R}|)|^2/2$ [26]. To simplify the calculations we assume the light fields to be linearly polarized and that $\mathbf{d}_{jj}(\mathbf{r}_i, \mathbf{r}_a) \approx 0$ for $j \in \{g, e, R\}$,

4. Alkali atoms in laser fields

thus that we arrive at the following 3-level approximation of the BO Hamiltonian

$$\hat{H}_{\text{BO}}(\mathbf{r}_i, \mathbf{r}_a, t) = \begin{pmatrix} \epsilon_g & 2\hbar\Omega_d(\mathbf{r}_a) \cos(\omega_d t) & 2\hbar\Omega(\mathbf{r}_i, \mathbf{r}_a) \cos(\omega t) \\ 2\hbar\Omega_d^*(\mathbf{r}_a) \cos(\omega_d t) & \epsilon_e & 0 \\ 2\hbar\Omega^*(\mathbf{r}_i, \mathbf{r}_a) \cos(\omega t) & 0 & \epsilon_R^0 - \frac{C_4^{(R)}}{R^4} \end{pmatrix}, \quad (4.23)$$

where ϵ_g and ϵ_e denote the energy of ground and excited state, respectively, ϵ_R^0 is the energy of the unperturbed Rydberg states, which gets shifted depending on the atom ion distance R by $-C_4^{(R)}/R^4$, where we neglect effects of the trapping fields on the atom. The Rabi frequencies are defined as follows

$$\begin{aligned} \Omega_d(\mathbf{r}_a) &= \frac{1}{\hbar} \mathbf{d}_{ge} \cdot \hat{\mathbf{e}}_{\text{dip}} E_{\text{dip}}^0(\mathbf{r}_a) \\ &\text{and} \\ \Omega(\mathbf{r}_i, \mathbf{r}_a) &= \frac{1}{\hbar} \mathbf{d}_{gR}(\mathbf{r}_i, \mathbf{r}_a) \cdot \hat{\mathbf{e}}_{\text{dress}} E_{\text{dress}}^0, \end{aligned} \quad (4.24)$$

where $\hat{\mathbf{e}}_{\circ}$ denotes the direction of the according polarization, and we assumed the dressing laser to be homogeneous over the atoms trapping region. If we neglect the position dependence of the Rydberg eigenstate, also \mathbf{d}_{gR} gets position independent. Thus we arrive at

$$\hat{H}_{\text{BO}}(\mathbf{r}_i, \mathbf{r}_a, t) \approx \begin{pmatrix} \epsilon_g & 2\hbar\Omega_d(\mathbf{r}_a) \cos(\omega_d t) & 2\hbar\Omega \cos(\omega t) \\ 2\hbar\Omega_d^*(\mathbf{r}_a) \cos(\omega_d t) & \epsilon_e & 0 \\ 2\hbar\Omega^* \cos(\omega t) & 0 & \epsilon_R^0 - \frac{C_4^{(R)}}{R^4} \end{pmatrix}, \quad (4.25)$$

and can transform into a rotating frame via

$$\mathbf{u}(t) = \begin{pmatrix} e^{i\frac{\epsilon_g}{\hbar}t} & 0 & 0 \\ 0 & e^{i(\frac{\epsilon_g}{\hbar} + \omega_d)t} & 0 \\ 0 & 0 & e^{i(\frac{\epsilon_g}{\hbar} + \omega)t} \end{pmatrix}, \quad (4.26)$$

with ω_d and ω the dipole trap and dressing laser frequencies. We now make a rotating wave approximation and thus neglect fast rotating terms, such that we get

$$\tilde{\hat{H}}_{\text{BO}}(\mathbf{r}_i, \mathbf{r}_a, t) \approx H_{3\text{-level}} = \begin{pmatrix} 0 & \hbar\Omega_d(\mathbf{r}_a) & \hbar\Omega \\ \hbar\Omega_d(\mathbf{r}_a) & -\hbar\Delta_d & 0 \\ \hbar\Omega & 0 & -\hbar\Delta_0 - \frac{C_4^{(R)}}{R^4} \end{pmatrix}, \quad (4.27)$$

with $\Delta_d = \omega_d - (\epsilon_e - \epsilon_g)/\hbar$ and $\Delta_0 = \omega - (\epsilon_R^0 - \epsilon_g)/\hbar$ the detunings of dipole trap and Rydberg dressing laser, respectively. Assuming $|\Delta_0| \gg |\Omega|$, $\Delta_0 > 0$, i.e. blue detuning as well as $|\Delta_d| \gg |\Omega_d(\mathbf{r}_a)|$ and $\Delta_d < 0$, the Hamiltonian can be diagonalised to second order in Ω and $\Omega_d(\mathbf{r}_a)$. This yields the adiabatic potential for the eigenstate that stays dominantly in the ground state

$$V_{ad} = \hbar \frac{|\Omega_d(\mathbf{r}_a)|^2}{\Delta_d} + \frac{\hbar^2 |\Omega|^2}{\hbar\Delta_0 + \frac{C_4^{(R)}}{R^4}}. \quad (4.28)$$

4.3. Dressed Rydberg atom-ion interaction

The first term represents the dipole trap, which we assume traps the atom harmonically with trap frequencies $\omega_a^{x,y,z}$. The last term is up to a constant equivalent to

$$V(R) = -\frac{AR_w^4}{R^4 + R_w^4}, \quad (4.29)$$

with the potential depth $A = \hbar\Omega^2/\Delta_0$ and its width $R_w = (C_4^{|R|}/\hbar\Delta_0)^{1/4}$. We notice the similarity of Eq. (4.29) to the case of the atom-atom dressed Rydberg potential, see e.g. [44], but the atom-ion potential retains a R^{-4} character instead of the R^{-6} Van der Waals nature of the atom-atom case. In addition the atom-ion potential is always attractive for the $|nS_{1/2}\rangle$ states. We mention that the potential is also of lower order, scaling as Ω^2/Δ_0 instead of Ω^4/Δ_0^3 , because for the ion-atom case only a single particle needs to be dressed. This relaxes restraints on the required laser power. For red detunings, the potential is also attractive, but an avoided crossing occurs at $R = R_w$, such that resonant Rydberg excitation may result.

We also give the eigenstate to the above potential up to first order in Ω and $\Omega_d(\mathbf{r}_a)$

$$\mathbf{w} = \left(1, \frac{\Omega_d}{\Delta_d}, \frac{\hbar\Omega}{\hbar\Delta_0 + \frac{C_4^{|R|}}{R^4}} \right). \quad (4.30)$$

Now we also take the Paul trapping field into account. We include the potential in dipole approximation combined with second order perturbation theory, so we simply have to substitute the ion electric field by the sum of the trap electric field $\mathbf{E}_{PT}(\mathbf{r}_a, t)$ and the ion one $\mathbf{E}_{ion}(|\mathbf{r}_i - \mathbf{r}_a|)$. Apart from that nothing changes in the above derivation. Therefore the adiabatic potential (4.29) is changed to:

$$\tilde{V}(\mathbf{r}_i, \mathbf{r}_a) = \frac{\hbar\Omega^2}{\Delta_0 + \frac{\alpha_{|R|}}{2\hbar} |\mathbf{E}_{ion}(|\mathbf{r}_i - \mathbf{r}_a|) + \mathbf{E}_{PT}(\mathbf{r}_a, t)|^2}. \quad (4.31)$$

For blue detunings adiabaticity of the potential is not affected, since the Stark shift due to the electric fields always increases the frequency offset $\Delta_0 \gg |\Omega|$. We conclude this chapter with the consideration of a lithium atom with $n = 30$, $\Omega = 2\pi \cdot 10$ MHz, $\Delta_0 = 2\pi \cdot 1$ GHz, for which we have $A/\hbar = 100$ kHz and $R_w = 1 \mu\text{m}$, such that $R_w \gg R^*$ (e.g., assuming a Ytterbium ion). We note that those values lifetime of the dressed Rydberg atom is enhanced by a factor of 10^4 see Eq. (4.30), compared against the pure Rydberg state. This puts coherent experiments on the 100 ms timescale in reach. In Fig. 4.2 we show the resulting potential for the numbers considered. As it is shown, the adiabatic potential of a Rydberg dressed atom discussed above (red dash-dotted and blue dashed lines) has a much longer-ranged character than the corresponding ground state atom-ion interaction (solid black line). We remark that the interaction is to a good approximation linear at distances of 1-2 μm with respect to the atom-ion separation and pronounce that this will be a crucial element for the implementation of quantum gates and the impact of the ionic micromotion on the atom, as we discuss in the next chapter.

4. Alkali atoms in laser fields

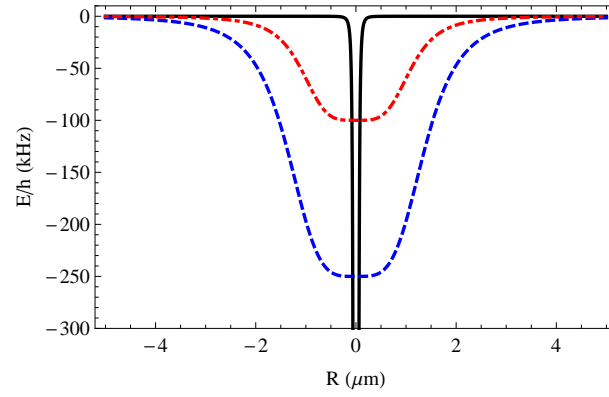


Figure 4.2.: Adiabatic potentials for a ground state atom and an ion (solid black), for a dressed atom with $\Omega = 2\pi 10$ MHz and $\Delta = 2\pi 1$ GHz (red dash-dotted) and $2\pi 0.4$ GHz (blue dashed) assuming coupling to the $|30S_{1/2}\rangle$ state of lithium.

5. Atom-ion spin-spin interactions

In this chapter we study a particular implementation of a trapped ion interacting with a Rydberg dressed atom. In particular, we study the coupling of the two systems at the quantum level, by engineering a spin-spin interaction between an atom and an ion as sketched in chapter 1. This interaction could be used to entangle the atom with the ion. We will study the effect of imperfect atom and ion cooling and the ionic micromotion and demonstrate that the scheme is to a large extent immune to these effects. We begin with the Hamiltonian derived in the last section, but we couple to the Rydberg state now dependent on the atoms internal pseudospin states. With an appropriate choice of parameters we can approximate by restricting to the one dimensional case along the z -direction. Since for the parameters chosen the potential is approximately linear for atom-ion positions close to the trap minima, we are able to take only the dominant linear terms for the interaction potential into account. If we vary the interaction strength in time, we can excite motion in the trapped particles. By amplitude modulating the Rydberg laser, with the ion trap frequency, we can excite ion motion resonantly. Since the dressing is dependent on the atomic pseudospin, we are thus able to entangle the atom's internal states with ion motion. To couple via ion motion to the ion's internal states, we add a bichromatic laser field, which couples just one of the ions spin states to its motion. The resulting hamiltonian closely resembles the one of phase gates in trapped ions. We will show that we can generate entanglement between the atom's and ion's internal states. Afterwards we give our results for the phase gate simulations performed. To complete the discussion we study the effects of micromotion.

5.1. Ion motion mediated spin-spin interactions

We start with the Hamiltonian derived in the previous chapter, but now we couple just one of the atoms pseudospins to the Rydberg state. The atomic pseudospins are encoded in two long lived hyperfine states $|\downarrow\rangle_a$ and $|\uparrow\rangle_a$ as shown in Fig. 1.1(b). We can achieve the state selective coupling by choosing laser polarizations (or by employing frequency differences due to fine or hyperfine structure splittings). As discussed in 3.4, to minimize the influence of the rf trapping field, it is favorable to fix the optical dipole trap minimum along the Paul trap axis. Along this axis the ion field dominates for distances $d \ll \ell_z$ away from the ion and we remind that we also restricted $d \gg R^*$, such that we can assume the bound energies close to the ground state to be constant. Restricting to this range of atom-ion distances, enables us to neglect for now the effect of Paul trap potential on the atom, as justified in 3.4. Restricting the atom and ion

5. Atom-ion spin-spin interactions

positions to the region just discussed, we can write the total Hamiltonian

$$\hat{H} = \left[\frac{\hat{\mathbf{p}}_i^2}{2m_i} + e\Phi_{PT}(\mathbf{r}_i, t) + \frac{\hat{\mathbf{p}}_a^2}{2M} + V_{\text{dip}}(\mathbf{r}_a) \right] \otimes \mathbb{1}_a + V(|\mathbf{r}_i - \mathbf{r}_a + \mathbf{d}|) \otimes |\uparrow\rangle_a \langle \uparrow|, \quad (5.1)$$

where we couple the $|\uparrow\rangle_a$ state of the atom to a Rydberg state with Rabi frequency Ω and detuning Δ_0 , such that the interaction Hamiltonian V is given by Eq. (4.29), the atom and ion coordinates \mathbf{r}_i and \mathbf{r}_a are now chosen relative to the particular trap minima, whereby $\mathbf{d} = (0, 0, d)$ denotes the minimum position of the atom trap relative to the ion trap minimum. We restrict the problem to the z -axis, therefore we neglect all terms that couple the x and y directions to the z direction. The interaction Hamiltonian is then given by $\hat{H}_{ai} = V(\hat{z}_i - \hat{z}_a + d) |\uparrow\rangle_a \langle \uparrow|$ with \hat{z}_i and \hat{z}_a the ion and atom position with respect to their equilibrium position. We now expand this potential around the ion and atom equilibrium positions $\bar{z}_i = 0$ and $\bar{z}_a = 0$: $V \approx V(d) + F_0 z_i - F_0 z_a + \dots$, with

$$F_0 = \left. \frac{dV}{dz_i} \right|_{z=\bar{z}} = - \left. \frac{dV}{dz_a} \right|_{z=\bar{z}}, \quad (5.2)$$

where we used $\bar{z} \equiv (\bar{z}_i, \bar{z}_a)$ as a short hand notation for the two equilibrium positions. The force between the atom and ion reaches its highest value of $F_0 = 1.065A/R_w$ for $d = 0.88R_w$, whereas the second order terms vanishes at this point. We want to rewrite the atom and ion trapping terms in means of the harmonic oscillator creation and annihilation operators defined as

$$\hat{a} = \sqrt{\frac{m\omega}{2\hbar}} \left(\hat{z} + \frac{i}{m\omega} \hat{p} \right) \quad \text{and} \quad \hat{a}^\dagger = \sqrt{\frac{m\omega}{2\hbar}} \left(\hat{z} - \frac{i}{m\omega} \hat{p} \right), \quad (5.3)$$

for a one dimensional harmonic oscillator Hamiltonian of the form

$$\hat{H}_{\text{HO}} = \frac{\hat{p}^2}{2m} + \frac{m\omega^2}{2} \hat{z}^2 = \hbar\omega \left(\hat{a}^\dagger \hat{a} + \frac{1}{2} \right). \quad (5.4)$$

In the following we denote with \hat{b}^\dagger and \hat{b} the creation and annihilation operators of the atom, whereas with \hat{a}^\dagger and \hat{a} we denote the ion ones. Thus we can write the full Hamiltonian as $\hat{H} = \hat{H}_{\text{trap}} + \hat{H}_{ai}$ with

$$\begin{aligned} \hat{H}_{\text{trap}} &= \hbar\omega_i \hat{a}^\dagger \hat{a} + \hbar\omega_a \hat{b}^\dagger \hat{b}, \\ \hat{H}_{ai} &\approx \left[V(d) + F_0 \ell_i (\hat{a}^\dagger + \hat{a}) - F_0 \ell_a (\hat{b}^\dagger + \hat{b}) \right] \otimes |\uparrow\rangle_a \langle \uparrow|. \end{aligned} \quad (5.5)$$

Here, $\ell_j = \sqrt{\hbar/(2m_j\omega_j)}$ for $j = i, a$, and $|\uparrow\rangle_a \langle \uparrow| = (\hat{\sigma}_z^a + \mathbb{1})/2$, where $\hat{\sigma}_z^a$ denotes the Pauli matrix for the atom and $\mathbb{1}$ is the identity matrix. In order to induce large ion motion we modulate the force between the atom and ion close to the ionic trap frequency. Therefore, we introduce time-dependence in $A \rightarrow A(t) = A_0(1 - \cos \omega_v t)/2$, by amplitude modulating the Rydberg laser, e.g. using an acousto-optical modulator [39]. As

5.1. Ion motion mediated spin-spin interactions

long as $\omega_v \ll \Delta_0$, the minimal detuning of the laser, no resonant Rydberg excitation can occur and we can treat the modulation of the dressed potential quasi-statically. In order to obtain the slowly changing dynamics we go into an interaction picture with respect to $\hat{H}_0 = \hat{H}_{trap} + V_{static}(d) |\uparrow\rangle_a \langle\uparrow| / 2$, with $V_{static}(d)$ denoting the static part of $V(z)$. This is done by choosing the inverse propagator $\mathcal{U}(t) = e^{iH_0 t/\hbar}$ of this Hamiltonian as a time-dependent transformation. The time-dependent Schrödinger equation transforms as Eq. (4.14) and we have to analyze the following transformed Hamiltonian for the rotating states

$$\tilde{H} = \mathcal{U}(t)\hat{H}\mathcal{U}^\dagger(t) + i\hbar\dot{\mathcal{U}}(t)U^\dagger(t). \quad (5.6)$$

We first note that \hat{H}_0 commutes with its own propagator and

$$\begin{aligned} i\hbar\dot{\mathcal{U}}(t)U^\dagger(t) &= i\hbar\left(\frac{i}{\hbar}\hat{H}_0\right)e^{i\hat{H}_0 t/\hbar}e^{-i\hat{H}_0 t/\hbar} \\ &= -\hat{H}_0, \end{aligned} \quad (5.7)$$

Thus we obtain that the terms $i\hbar\dot{\mathcal{U}}(t)U^\dagger(t)$ and $\mathcal{U}(t)\hat{H}_0\mathcal{U}^\dagger(t) = H_0$ exactly cancel and it remains to solve

$$\mathcal{U}(t) \left(\left[V_{dyn} + F\ell_i(\hat{a}^\dagger + \hat{a}) - F\ell_a(\hat{b}^\dagger + \hat{b}) \right] \otimes |\uparrow\rangle_a \langle\uparrow| \right) \mathcal{U}^\dagger(t), \quad (5.8)$$

with $F = F_0(1 - \cos(\omega_v t))/2$ and $V_{dyn} = -V_{static} \cos(\omega_v t)/2$. Therefore we need to know how the normal creation and annihilation operators $a^\dagger, \hat{a}, \hat{b}^\dagger$ and \hat{b} transform. We observe that we have just to consider the following problems

$$e^{it\omega_i \hat{a}^\dagger \hat{a}} \hat{a}^\dagger e^{-it\omega_i \hat{a}^\dagger \hat{a}} \quad \text{and} \quad e^{it\omega_i \hat{a}^\dagger \hat{a}} \hat{a} e^{-it\omega_i \hat{a}^\dagger \hat{a}}. \quad (5.9)$$

We exemplarily discuss the case $e^{it\omega_i \hat{a}^\dagger \hat{a}} \hat{a}^\dagger e^{-it\omega_i \hat{a}^\dagger \hat{a}} = \hat{a}^\dagger(t)$. For $t = 0$ we know that the operator will be equal to \hat{a}^\dagger . For all later times we want to obtain the operator by integrating the problem

$$\begin{aligned} \partial_t \hat{a}^\dagger(t) &= \partial_t e^{it\omega_i \hat{a}^\dagger \hat{a}} \hat{a}^\dagger e^{-it\omega_i \hat{a}^\dagger \hat{a}} \\ &= e^{it\omega_i \hat{a}^\dagger \hat{a}} (i\omega_i \hat{a}^\dagger \hat{a}) \hat{a}^\dagger e^{-it\omega_i \hat{a}^\dagger \hat{a}} + e^{it\omega_i \hat{a}^\dagger \hat{a}} \hat{a}^\dagger (-i\omega_i \hat{a}^\dagger \hat{a}) e^{-it\omega_i \hat{a}^\dagger \hat{a}} \\ &= i\omega_i e^{-it\omega_i \hat{a}^\dagger \hat{a}} \hat{a}^\dagger e^{it\omega_i \hat{a}^\dagger \hat{a}} \\ &= i\omega_i \hat{a}^\dagger(t), \end{aligned} \quad (5.10)$$

where we used $[\hat{a}^\dagger \hat{a}, \hat{a}^\dagger] = \hat{a}^\dagger$. Therefore we can conclude that $\hat{a}^\dagger(t) = \hat{a}^\dagger e^{i\omega_i t}$, equivalently we obtain $\hat{a}(t) = \hat{a} e^{-i\omega_i t}$. We can now calculate the still missing term of the

5. Atom-ion spin-spin interactions

total Hamiltonian

$$\begin{aligned}
\mathcal{U}(t) & \left[V_{dyn} + F\ell_i(\hat{a}^\dagger + \hat{a}) - F\ell_a(\hat{b}^\dagger + \hat{b}) \right] \otimes |\uparrow\rangle_a \langle \uparrow| \mathcal{U}^\dagger(t) \\
& = \left[V_{dyn} + F\ell_i(\hat{a}^\dagger e^{i\omega_i t} + \hat{a} e^{-i\omega_i t}) - F\ell_a(\hat{b}^\dagger e^{i\omega_a t} + \hat{b} e^{-i\omega_a t}) \right] \otimes |\uparrow\rangle_a \langle \uparrow| \\
& = \frac{1}{2} \left[-\frac{1}{2} V_{static} (e^{i\omega_v t} + e^{-i\omega_v t}) \right. \\
& \quad + F_0 \ell_i \left[\hat{a}^\dagger \left(e^{i\omega_i t} + \frac{1}{2} \left(e^{i(\omega_i - \omega_v)t} + e^{i(\omega_i + \omega_v)t} \right) \right) \right. \\
& \quad \quad \quad \left. + \hat{a} \left(e^{-i\omega_i t} + \frac{1}{2} \left(e^{-i(\omega_i - \omega_v)t} + e^{-i(\omega_i + \omega_v)t} \right) \right) \right] \\
& \quad \left. - F_0 \ell_a \left[\hat{b}^\dagger \left(e^{i\omega_a t} + \frac{1}{2} \left(e^{i(\omega_a - \omega_v)t} + e^{i(\omega_a + \omega_v)t} \right) \right) \right. \right. \\
& \quad \quad \left. \left. + \hat{b} \left(e^{-i\omega_a t} + \frac{1}{2} \left(e^{-i(\omega_a - \omega_v)t} + e^{-i(\omega_a + \omega_v)t} \right) \right) \right] \right] \otimes |\uparrow\rangle_a \langle \uparrow|
\end{aligned} \tag{5.11}$$

Now, by defining $\delta = \omega_v - \omega_i$ and assuming $\hbar|\omega_v - \omega_a| \ll F_0\ell_a, F_0\ell_i$ we can make a rotating wave approximation by neglecting terms rotating faster than δ to obtain:

$$\hat{H}_I = \frac{F_0\ell_i}{4} \left(\hat{a}^\dagger e^{i\delta t} + \hat{a} e^{-i\delta t} \right) |\uparrow\rangle_a \langle \uparrow|. \tag{5.12}$$

Here, we also assumed $\hbar\omega_v \gg V(d)/2$ such that fast oscillating position-independent Stark shifts in the atom average out.

The Hamiltonian (5.12) entangles the motion of the ion with the internal state of the atom. In particular, for $\delta = 0$, and starting from the state $|\psi_{in}\rangle = |0\rangle_{mi}(|\downarrow\rangle_a + |\uparrow\rangle_a)$, where $|0\rangle_{mi}$ denotes the ground state of ion motion, the Hamiltonian generates cat-like states of the form $|\psi_{out}\rangle = |0\rangle_{mi}|\downarrow\rangle_a + |\beta\rangle_{mi}|\uparrow\rangle_a$ after a time t with $|\beta\rangle_{mi}$ denoting a coherent state of amplitude $\beta = F_0\ell_i t / (4\hbar)$.

We seek to map this atom spin-ion motion entanglement onto the internal states of the ion. This can be realized by adding an ion spin-motion Hamiltonian of the following form

$$\hat{H}_{S-M} = \frac{\eta\hbar\Omega_{S-M}}{2} \left(\hat{a}^\dagger e^{i\delta t} + \hat{a} e^{-i\delta t} \right) |\uparrow\rangle_i \langle \uparrow| \tag{5.13}$$

5.1. Ion motion mediated spin-spin interactions

To see how this will work we calculate the total Hamiltonian

$$\begin{aligned}
& \hat{H}_I + \hat{H}_{S-M} \\
&= \frac{F_0 \ell_i}{4} \left(\hat{a}^\dagger e^{i\delta t} + \hat{a} e^{-i\delta t} \right) |\uparrow\rangle_a \langle \uparrow| \\
&+ \frac{\eta \hbar \Omega_{S-M}}{2} \left(\hat{a}^\dagger e^{i\delta t} + \hat{a} e^{-i\delta t} \right) |\uparrow\rangle_i \langle \uparrow| \\
&= \left(\hat{a}^\dagger e^{i\delta t} + \hat{a} e^{-i\delta t} \right) \\
&\quad \left[\left(\frac{F_0 \ell_i}{4} + \frac{\eta \hbar \Omega_{S-M}}{2} \right) |\uparrow_i \uparrow_a\rangle \langle \uparrow_i \uparrow_a| \right. \\
&\quad \left. + \left(\frac{F_0 \ell_i}{4} \right) |\downarrow_i \uparrow_a\rangle \langle \downarrow_i \uparrow_a| + \left(\frac{\eta \hbar \Omega_{S-M}}{2} \right) |\uparrow_i \downarrow_a\rangle \langle \uparrow_i \downarrow_a| \right]
\end{aligned} \tag{5.14}$$

If we set $\eta \hbar \Omega_{S-M}/2 = -F_0 \ell_i/4$ no motion is excited in the ion when the spin of both atom and ion are down. When both particles are in the spin up state, also no motion is excited since the two forces cancel. Only when the particles have opposite spins is the ion motion excited and thereby the energy changed. This results in an interaction that is similar to the one usually encountered in Mølmer-Sørensen gates or phase gates in ions [43, 51].

To see what happens if time evolves we will now give a short derivation of the propagator for Hamiltonians of the form. We follow [42, 59] and define the phase Hamiltonian

$$\hat{H}_{Ph}(t) = \left(\hat{a}^\dagger \gamma^*(t) + \hat{a} \gamma(t) \right) \tag{5.15}$$

Therefore we need the following relation for the operators $D(\alpha) = (\hat{a}^\dagger \alpha^* + \hat{a} \alpha)$

$$D(\alpha)D(\beta) = D(\alpha + \beta)e^{i\text{Im}(\alpha\beta^*)}, \tag{5.16}$$

which follows from the BCH formula. The propagator takes the following form

$$\mathcal{U}(t) = \lim_{n \rightarrow \infty} \prod_{k=1}^n \exp \left(-\frac{i}{\hbar} \hat{H}_{Ph}(k\Delta t) \Delta t \right) = D(\alpha(t))e^{i\Phi(t)}, \tag{5.17}$$

with $\Delta t = t/n$, $\alpha(t) = \int_0^t \gamma(t') dt'$ and $\Phi(t) = \text{Im} \left(\int_0^t \gamma(t) \int_0^{t'} \gamma(t'') dt'' dt' \right)$.

For our case with $\gamma(t) = W \exp(i\delta t)$ this yields:

$$\alpha(t) = i \frac{W}{\delta} \left(1 - e^{i\delta t} \right) \quad \text{and} \quad \Phi(t) = \left(\frac{W}{\delta} \right)^2 (\delta t - \sin(\delta t)). \tag{5.18}$$

After a time $\tau = 2\pi/\delta$ this accumulates in an effective interaction that is locally equivalent to $\hat{H}_{zz} = J \hat{\sigma}_z^i \hat{\sigma}_z^a / 2$ with $J = F_0^2 \ell_i^2 / (32 \hbar \delta)$ and the ionic motion returns to the initial orbit. Setting $J\tau/\hbar = \pi/4$ corresponds to a geometric phase quantum gate [43, 66].

5. Atom-ion spin-spin interactions

We now want to derive the spin motion Hamiltonian H_{S-M} . Therefore we want to couple just one of the ions internal qubit states $|\uparrow\rangle_i$ weakly to an excited state $|e\rangle$ with a bichromatic linearly polarized laser field. The Hamiltonian reads

$$\hat{H}_i = \omega_i \hat{a} \hat{a}^\dagger + \mathbb{1} \otimes \left[\begin{aligned} & \left(\begin{array}{cc} \epsilon_\uparrow & 0 \\ 0 & \epsilon_e \end{array} \right) + \left(\begin{array}{cc} 0 & \hbar\Omega_1 \\ \hbar\Omega_1^* & 0 \end{array} \right) \left(e^{-i(k_1 z - \omega_1 t)} + e^{i(k_1 z - \omega_1 t)} \right) \\ & + \left(\begin{array}{cc} 0 & \hbar\Omega_2 \\ \hbar\Omega_2^* & 0 \end{array} \right) \left(e^{-i(k_2 z - \omega_2 t)} + e^{i(k_2 z - \omega_2 t)} \right) \end{aligned} \right]. \quad (5.19)$$

We assume counter propagating beams and detunings $\Delta_1 = (\epsilon_e - \epsilon_\uparrow)/\hbar - \omega_1$ and $\Delta_2 = (\epsilon_e - \epsilon_\uparrow)/\hbar - \omega_2$, both positive which means red detuning and $\Delta_1 < \Delta_2$. We want to solve the problem for each position z along the trap axis, by changing to a rotating frame with respect to ω_1 which is less detuned. The internal hamiltonian for fixed position is of the form

$$\left[\begin{aligned} & \left(\begin{array}{cc} \epsilon_\uparrow & 0 \\ 0 & \epsilon_e \end{array} \right) + \left(\begin{array}{cc} 0 & \hbar\Omega_1 \\ \hbar\Omega_1^* & 0 \end{array} \right) (C_1 e^{i\omega_1 t} + C_1^* e^{-i\omega_1 t}) \\ & + \left(\begin{array}{cc} 0 & \hbar\Omega_2 \\ \hbar\Omega_2^* & 0 \end{array} \right) (C_2 e^{i\omega_2 t} + C_2^* e^{-i\omega_2 t}) \end{aligned} \right], \quad (5.20)$$

where we encoded the z dependence of the waves in the complex coefficients

$$C_1 = e^{-ik_1 z t} \quad \text{and} \quad C_2 = e^{-ik_2 z t}. \quad (5.21)$$

We pass to a rotating frame via the unitary transformation

$$\mathcal{U}(t) = \begin{pmatrix} e^{i\epsilon_\uparrow t/\hbar} & 0 \\ 0 & e^{i(\epsilon_e/\hbar - \Delta_1)t} \end{pmatrix} \quad (5.22)$$

and neglect terms oscillating faster than $e^{i\Delta_2 t}$. This yields

$$\begin{pmatrix} 0 & \hbar C_1 \Omega_1 \\ \hbar C_1^* \Omega_1^* & \Delta_1 \end{pmatrix} + \begin{pmatrix} 0 & \hbar C_2 \Omega_2 e^{i\Delta_2 t} \\ \hbar C_2^* \Omega_2^* e^{-i\Delta_2 t} & 0 \end{pmatrix}. \quad (5.23)$$

Now we change to a diagonal representation of the first matrix. The resulting operator has a far off resonant coupling for $|\Omega_1^0|, |\Omega_2^0| \ll \Delta_1$, therefore we restrict just to the first entry which corresponds to the self coupling of the weakly dressed $|\uparrow\rangle_i$ state. We denote this weakly dressed state with $|\tilde{\uparrow}\rangle_i$. Up to second order in the Rabi frequencies we get a term of the following form

$$\left[(e^{i\Delta_2 t} \hbar C_1 \Omega_1 C_2 \Omega_2 + e^{-i\Delta_2 t} \hbar C_1^* \Omega_1^* C_2^* \Omega_2^*) C - \hbar \frac{\Omega_1 \Omega_1^*}{\Delta_1} \right] \otimes |\tilde{\uparrow}\rangle_i \langle \tilde{\uparrow}|, \quad (5.24)$$

with C a z -independent constant depending on Δ_1 and the Rabi frequencies. Resubstituting C_1 and C_2 and for counter propagating beams we arrive at

$$\hat{H}_i = \omega_i \hat{a} \hat{a}^\dagger + \mathbb{1} \otimes \left[\left(\frac{\hbar\Omega_{S-M}}{2} e^{i(\Delta_2 - \delta k z)t} + \frac{\hbar\Omega_{S-M}^*}{2} e^{-i(\Delta_2 - \delta k z)t} \right) - \hbar \frac{\Omega_1 \Omega_1^*}{\Delta_1} \right] \otimes |\tilde{\uparrow}\rangle_i \langle \tilde{\uparrow}|, \quad (5.25)$$

5.1. Ion motion mediated spin-spin interactions

with $\delta k = k_1 - k_2$ and $\Omega_{S-M} = 2\Omega_1\Omega_2C$. We change to the interaction frame where also the constant term $\propto \frac{\Omega_1\Omega_1^*}{\Delta_1}$ is rotated away. We assume the spin motion Hamiltonian to be in the Lamb-Dicke regime $\eta = \delta k \ell_i \ll 1$, δk , neglecting fast rotating terms we arrive at a Hamiltonian of the desired form

$$\hat{H}_{S-M} = \frac{\eta\hbar\Omega_{S-M}}{2} \left(\hat{a}^\dagger e^{i\delta t} + \hat{a} e^{-i\delta t} \right) |\uparrow\rangle_i \langle\uparrow|. \quad (5.26)$$

5.1.1. Simulation

To verify the above derivation of the atom-ion gate Hamiltonian $\hat{H}_I + \hat{H}_{S-M}$, we simulate the dynamics of the Hamiltonian

$$\begin{aligned} \hat{H}_g = \hat{H}_{trap} + \frac{V^{(3)}(\hat{z}_i, \hat{z}_a)}{2} (1 + \cos \omega_v t) |\uparrow\rangle_a \langle\uparrow| \\ + \eta\hbar\Omega_{S-M} \cos(\omega_v t) \left(\hat{a}^\dagger + \hat{a} \right) |\uparrow\rangle_i \langle\uparrow| \end{aligned} \quad (5.27)$$

where $V^{(3)}(\hat{z}_i, \hat{z}_a)$ denotes the Taylor expansion around the equilibrium positions up to third order of $V(\hat{z}_i, \hat{z}_a)$ and the last term denotes \hat{H}_{S-M} in the non-rotating frame. We note that in this Hamiltonian terms up to third order in \hat{z}_i and \hat{z}_a and also terms rotating faster than δ for the \hat{H}_I part are included, but we neglected the effect of the rf trapping field as well as couplings to the x - and y -directions.

As a particular example, we consider a ${}^7\text{Li}$ atom interacting with a ${}^{171}\text{Yb}^+$ ion. We set the trap frequency of the ion to $\omega_i = 2\pi$ 250 kHz and the trap frequency of the atom to $\omega_a = 2\pi$ 205 kHz. Using $n = 30$, $\Omega = 2\pi$ 10.02 MHz, $\Delta_0 = 2\pi$ 0.4 GHz, we have $A_0/h = 250$ kHz and $R_w = 1.4$ μm . Further, for the ion laser driving field we use $\eta\Omega_{S-M} = 2\pi$ 1.045 kHz and $\delta = 2\pi$ 1.040 kHz, and we set the distance between the atom and ion trap to $d = 0.88 R_w = 1.23$ μm to optimize the coupling. From the simulations in chapter 3 we know that for those distances we are still in a regime where the dipole approximation combined with second order perturbation theory, on which our derivations are based, holds. For the simulation we projected \hat{H}_g on the seven lowest harmonic oscillator states of atom and ion respectively, which turns the operator into a time-dependent matrix. Therefore the Schrödinger equation becomes a finite dimensional linear differential equation for the time-dependent coefficient functions of the base states projected on. This problem can be solved by standard numerical methods for a given input state.

In our simulations we took the product states $|\psi_i^{\pm\pm}\rangle = (|\uparrow\rangle_a \pm |\downarrow\rangle_a)(|\uparrow\rangle_i \pm |\downarrow\rangle_i)/2$, which can be prepared by simple radio-frequency pulses, and assume the motional ground states for the atomic and ionic oscillators. After a time $\tau_g = 2\pi/\delta = 962.5$ μs the ion is back in its initial orbit. Applying an additional local unitary ($\pi/2$ -pulse) $\hat{U} = \exp(-i\pi(\hat{\sigma}_y^a + \hat{\sigma}_y^i)/4)$ the internal states of atom and ion are found to be in an entangled state. As an example we consider the input state $|\psi_i^{++}\rangle$ and denote the time evolved state with $|\psi^{++}(t)\rangle$. In Fig. 5.1 we show the population of the internal states of $\hat{U}|\psi^{++}(t)\rangle$. The motion of the ion returns to its initial orbit after $\tau_g = 2\pi/\delta = 962.5$ μs and the electronic state of the atom-ion system is found to be

5. Atom-ion spin-spin interactions

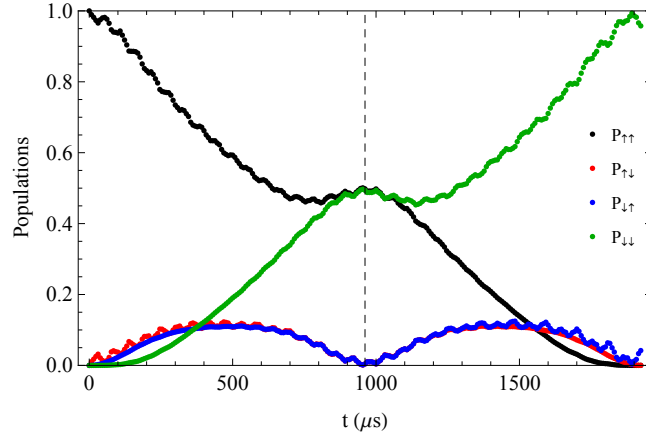


Figure 5.1.: Dynamics of the populations $P_{\uparrow\uparrow}, \dots$ during the gate for the input state $|\psi_i\rangle = (|\uparrow\rangle_a + |\downarrow\rangle_a)(|\uparrow\rangle_i + |\downarrow\rangle_i)/2$ and after performing an additional $\pi/2$ -pulse (see text). The dashed line indicates the time at which the gate is finished. The small oscillations are due to the term $V(d)|\uparrow\rangle_a\langle\uparrow|/2$ that was neglected in the rotating wave approximation in deriving Eq. (5.12). For the present parameters we have that $V(d)/(2\hbar\omega_v) = 0.31$, but notwithstanding the fidelity of the gate is not seriously affected.

locally equivalent to the entangled state $|\Phi^+\rangle = (|\uparrow\rangle_a |\uparrow\rangle_i + i |\downarrow\rangle_a |\downarrow\rangle_i)/\sqrt{2}$. after performing the local unitary ($\pi/2$ -pulse) $\hat{U} = \exp(-i\pi(\hat{\sigma}_y^a + \hat{\sigma}_y^i)/4)$ to the state after the gate, leading to a fidelity of $F = 0.997$. The fidelity is simply defined as the modulus square of the scalar product between the time evolved state $|\psi_{out}\rangle$ and the goal state $|0_i, 0_a\rangle \otimes |\Phi^+\rangle$. Similarly, the input states $|\psi_i^{+-}\rangle$, $|\psi_i^{-+}\rangle$ and $|\psi_i^{--}\rangle$ map to the entangled states $(|\uparrow\rangle_a |\downarrow\rangle_i \pm i |\downarrow\rangle_a |\uparrow\rangle_i)/\sqrt{2}$ and $(|\uparrow\rangle_a |\uparrow\rangle_i - i |\downarrow\rangle_a |\downarrow\rangle_i)/\sqrt{2}$, respectively following the gate and the unitary \tilde{U} , all with fidelities $F \geq 0.992$. We attribute the deviation from unit fidelity to interactions beyond linear and rotating terms neglected in the rotating wave approximation, but we expect that further parameter tuning, for example, via optimal control, can improve the fidelity further.

5.1.2. Spin-spin interactions for particles in thermal states of motion

For the Hamiltonian $\hat{H}_I + \hat{H}_{S-M}$ we have solved the dynamics analytically. After a time $2\pi/\delta$ the propagator is equal to $e^{i\Phi(t)}\mathbb{1}$ thus in this approximation the gate works for all motional input states equally. We infer, that we need not to be ground state cooled as in e.g. Mølmer Sørensen gates in trapped ions [51]. Therefore we did the simulations also with a thermal state of the form

$$\hat{\rho}_{th} = \sum_{n_i, n_a} P_{n_i}(\bar{n}_i) P_{n_a}(\bar{n}_a) |n_i, n_a\rangle \langle n_i, n_a| \otimes |\psi^{++}\rangle \langle \psi^{++}| \quad (5.28)$$

5.1. Ion motion mediated spin-spin interactions

with $P_n(\bar{n}) = \frac{1}{1+\bar{n}} \left(\frac{\bar{n}}{\bar{n}+1} \right)^n$ and \bar{n} the average phonon number.

When we start with both the atom and the ion in a thermal motional state with average phonon number $\bar{n}_i = \bar{n}_a = 0.25$, the fidelity of the resulting Bell state is found to be $F = 0.992$, demonstrating that the gate indeed works for non-ground state cooled particles too. We note that in this case the fidelity is defined as: $F = \text{Tr}\{\hat{\rho}_g \hat{\rho}_{out}\}$, where $\hat{\rho}_g$ represents the goal state (e.g., $\hat{\rho}_g = \sum_{n_i, n_a} P_{n_i}(\bar{n}_i) P_{n_a}(\bar{n}_a) |n_i, n_a\rangle \langle n_i, n_a| \otimes |\Phi^+\rangle \langle \Phi^+|$) and $\hat{\rho}_{out}$ the output state after the gate and unitary \hat{U} . We attribute the fidelity loss to the higher order terms in \hat{z}_i and \hat{z}_a , as the linear approximation in the atom-ion interaction works less well for higher lying Fock states. For the simulation, we limited the summation range in Eq. (5.28) to $n_a, n_i = \{0, \dots, 3\}$ in a Hilbert space that spans 9 phonons for both the atom and ion and such that $\text{Tr}(\hat{\rho}_{th}) = 0.997$.

We note, that in comparison to ionic quantum gates that are essentially described by the same equations to first order, we need the Lamb-Dicke regime for both the ion-laser and the atom-ion interaction, namely $\eta \ll 1$ and $F_0 \ell_a \ll \hbar \omega_a$, $F_0 \ell_i \ll \hbar \omega_i$.

5.1.3. The role of micromotion

We announced to also investigate the role of micromotion. Therefore we consider now, that the atom is trapped in the transverse direction of the ion. We again restrict the discussion just to one dimension. The Hamilton operator thus reads

$$\begin{aligned} \hat{H}_{tot} &= \frac{p_i^2}{2m_i} + e\Phi_{PT}((x_i, 0, 0), t) + \frac{p_a^2}{2M} + \frac{m_a}{2} \omega_a^2 x_a^2 \\ &\quad + \frac{\tilde{V}(\hat{x}_i, \hat{x}_a)}{2} (1 + \cos \omega_v t) \otimes |\uparrow\rangle_a \langle \uparrow| + \eta \hbar \Omega_{S-M} \cos(\omega_v t) (\hat{a}^\dagger + \hat{a}) |\uparrow\rangle_i \langle \uparrow| \\ &\approx \frac{p_i^2}{2m_i} + m_i \Omega_{rf}^2 q x_i^2 \cos(\Omega_{rf} t) / 4 + \frac{p_a^2}{2M} + \frac{m_a}{2} \omega_a^2 x_a^2 \\ &\quad + \frac{\tilde{V}(\hat{x}_i, \hat{x}_a)}{2} (1 + \cos \omega_v t) \otimes |\uparrow\rangle_a \langle \uparrow| + \eta \hbar \Omega_{S-M} \cos(\omega_v t) (\hat{a}^\dagger + \hat{a}) |\uparrow\rangle_i \langle \uparrow|, \end{aligned} \tag{5.29}$$

where we neglect the static trapping field, which is typically a factor 10-100 smaller than the time-dependent field in a Paul trap. We note that \tilde{V} denotes the adiabatic potential including also the trapping field. We now change to a harmonic oscillator base for atom \hat{b}^\dagger, \hat{b} and ion \hat{a}^\dagger, \hat{a} , where we set $\omega_i = \Omega_{rf} q / 2^{3/2}$ [13] for the ion, while for the atom we choose the base according to its transverse trapping frequency ω_a . The position operator for the ion is thus represented by $\hat{x}_i = \ell_i (\hat{a}^\dagger + \hat{a})$. We simplify further by substituting \tilde{V} by its Taylor expansion around the equilibrium positions up to third order $\tilde{V}^{(3)}(\hat{x}_i, \hat{x}_a)$. Thus we arrive at

$$\begin{aligned} \hat{H}_{tot} &\approx \hat{H}_{trap} + \frac{m_i \omega_i^2}{2} \hat{x}_i^2 \left(\frac{\Omega_{rf}^2}{2\omega_i^2} q \cos(\Omega_{rf} t) - 1 \right) \\ &\quad + \frac{\tilde{V}^{(3)}(\hat{x}_i, \hat{x}_a)}{2} (1 + \cos \omega_v t) \otimes |\uparrow\rangle_a \langle \uparrow| + \eta \hbar \Omega_{S-M} \cos(\omega_v t) (\hat{a}^\dagger + \hat{a}) |\uparrow\rangle_i \langle \uparrow|. \end{aligned} \tag{5.30}$$

5. Atom-ion spin-spin interactions

We note that $\tilde{V}^{(3)}(\hat{x}_i, \hat{x}_a)$ is time-dependent, because of the oscillating electric field of the Paul trap. Therefore also the coupling strength $F_0 = \partial_{x_i} \tilde{V}(0, 0)$ will become time-dependent. To choose F_0 and Ω_{S-M} , such that the first order terms cancel, we want to obtain the mean value of F_0 over one period T_{rf} in the trapping frequency Ω_{rf} . Therefore let us first calculate $\partial_{x_i} \tilde{V}(0, 0)$

$$\partial_{x_i} \tilde{V}(\hat{x}_i, \hat{x}_a) = -\frac{\hbar\alpha_{|R|}\Omega^2}{2(\Delta_0 + \frac{\alpha_{|R|}}{2\hbar}|\mathbf{E}|^2)^2} \partial_{x_i} |\mathbf{E}|^2, \quad (5.31)$$

with the total electric field $\mathbf{E} = \mathbf{E}_{ion} + \mathbf{E}_s + \mathbf{E}_{rf}$. Thus the time average is given by

$$\left\langle \frac{\partial}{\partial x_i} \tilde{V}(0, 0) \right\rangle_{T_{rf}} = -\left\langle \frac{\hbar\alpha_{|R|}\Omega^2}{2(\Delta_0 + \frac{\alpha_{|R|}}{2\hbar}|\mathbf{E}|^2)^2} \partial_{x_i} |\mathbf{E}|^2 \right\rangle_{T_{rf}}.$$

For the sake of simplicity, we computed the time average as

$$\left\langle \frac{\partial}{\partial x_i} \tilde{V}(0, 0) \right\rangle_{T_{rf}} = -\frac{\hbar\alpha_{|R|}\Omega^2}{2(\Delta_0 + \frac{\alpha_{|R|}}{2\hbar} \langle |\mathbf{E}|^2 \rangle_{T_{rf}})^2} \langle \partial_{x_i} |\mathbf{E}|^2 \rangle_{T_{rf}}. \quad (5.32)$$

We again consider $^{171}\text{Yb}^+$ and ^7Li coupled to $n = 30$ and use the parameters $\omega_a = 2\pi \cdot 200$ kHz, $\Omega_{rf} = 2\pi \cdot 2.5$ MHz, $q = 0.28$ and $\eta\Omega_{S-M} = 2\pi \cdot 1.06$ kHz and the (approximate) ground states of motion. The secular frequency of the ion can be approximated by $\omega_i^{(\perp)} \approx \frac{\Omega_{rf}}{2} \sqrt{a + q^2/2}$ for small q and a . We set $a = 0$, since we neglected the static trapping field, and get $\omega_i^{(\perp)} \approx 2\pi \cdot 250$ kHz. However, a more accurate calculation based on continued fractions for solving the Mathieu equations [42] yields: $\omega_i^{(\perp)} = 2\pi \cdot 254.089$ kHz such that $\delta^{(\perp)} = \omega_v - \omega_i^{(\perp)} = 2\pi \cdot 1.064$ kHz, corresponding to a gate time of $\tau_g = 940 \mu\text{s}$. This in turn gives $J\tau_g/\hbar = \pi/4$, corresponding to the desired phase gate.

For the Rydberg laser, we set $\Omega = 2\pi \cdot 13.1$ MHz and $\Delta_0 = 2\pi \cdot 0.8$ GHz. To limit the induced motion in the atom, we switch on the Rydberg dressing in $50 \mu\text{s}$. In Fig. 5.2 we show the dynamics of the position expectation values for the atom and the ion for each of the possible spin states, demonstrating that the micromotion does not distort the motion of the particles during the gate significantly. As in the case without micromotion, the motion returns to its input state after the gate is finished, that is, in about $2\pi/\delta^{(\perp)} = 940 \mu\text{s}$ without additional energy exchange between the atom and ion, demonstrating the resilience of the scheme to micromotion. This calculation was performed by Antonio Negretti at Hamburg University as our methods did not quite reach convergence [65].

The presented quantum gate closely resembles that of common ion gates, e.g. [39]. As with those gates, we can improve the fidelity by making sure the approximations made to obtain the gate dynamics - neglecting fast rotating terms and assuming the Lamb-Dicke regime - are well justified. This means for the atom that tight confinement

5.1. Ion motion mediated spin-spin interactions

needs to be reached. Furthermore, to reach a gate time that is much faster than the photon scattering rate $\Gamma_{ph} \sim (4\Delta_0^2/\Omega^2) \times \Gamma_{Ryd}$, strong laser fields are useful. In the present example, the lifetime of the bare Rydberg state lies in the 10-20 μs regime [4], leading to lifetimes of ~ 100 ms [3] for the dressed case.

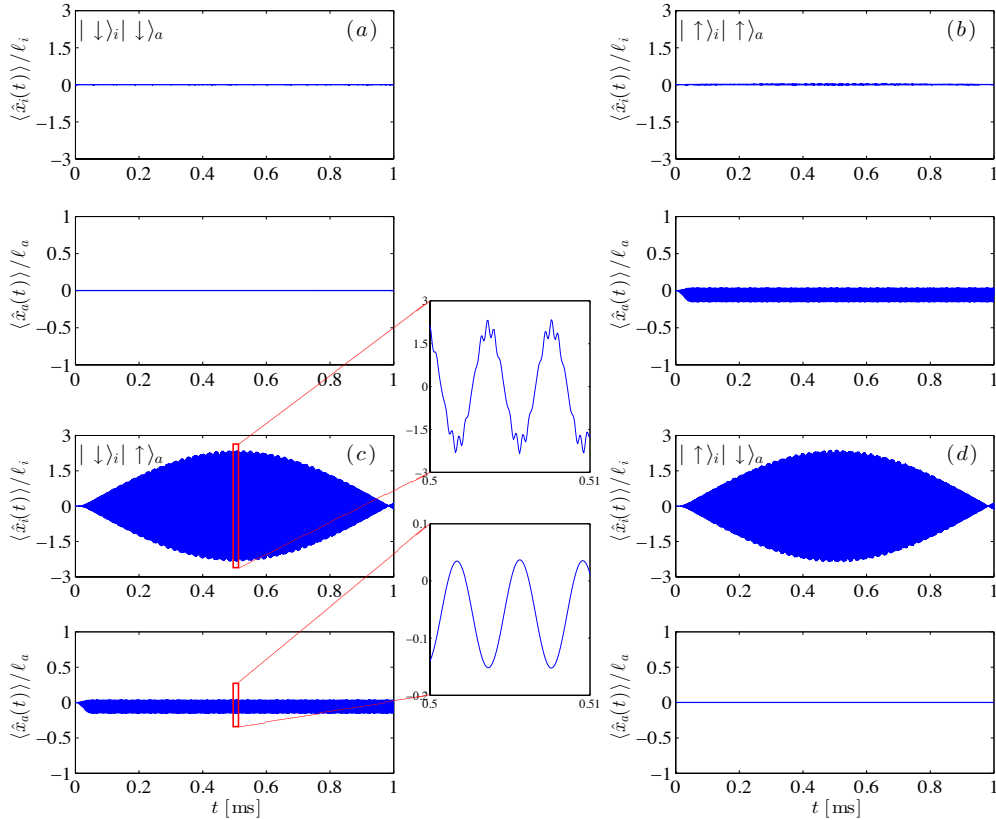


Figure 5.2.: Expectation values $\langle \hat{x}_i \rangle$ and $\langle \hat{x}_a \rangle$ during the gate for each of the four possible spin input states. The insets also show zoom ins of the ion and atom motion, clearly showing the micromotion. Some residual atomic motion occurs for the states $|\uparrow\rangle_a$, where the atom gets pulled closer to the ion.

6. Outlook

In the present thesis we examined the interaction of an atom weakly coupled to a Rydberg state with an ion trapped in a Paul trap. The large polarizability and the huge spatial extent of the Rydberg wave functions made a detailed analysis of the Rydberg ion interaction and the influence of the Paul trap necessary. Our simulations could verify that for the atom in a state of the $n = 30$ manifold and atom-ion distances $R \sim 1 \mu\text{m}$ a perturbational treatment within the dipole approximation delivers still an excellent description. In the perturbational approach and for those distances, the large polarizability of the Rydberg states allows for strong interactions even for weak Rydberg admixing. We demonstrated that the interaction can be used to generate entanglement of the internal states of the atom with the motional and also the internal states of the ion over distances in the μm range. The gate we considered could be shown to closely resemble standard ion phase gates and the simulations have shown, that the gate considered has similar benefits, as no need for ground state cooling, full dynamical control and near immunity to micromotion.

The proposed interaction scheme allows for various generalizations. One could weakly admix Rydberg states with negative polarizability to obtain repulsive potentials, as the repulsive potential would prevent hard core collisions in the atom-ion system, which cause heating in the Paul trap.

Dressing with higher angular momentum states may bring interesting potential shapes such as charge dipole $1/R^2$ and charge quadrupole $1/R^3$ within experimental reach. Additional light fields could open even a wider class of potential shapes such as anisotropic potentials.

Increasing the number of particles forms another direction. Scenarios like two Rydberg atoms and an ion could be studied to yield the effect of the ion potential on the Rydberg blockade radii. Strongly interacting atom-ion systems may also be created, in which ion crystals couple to Rydberg dressed clouds of atoms. Here, it may also be of interest to look at resonant Rydberg excitation or even photo-ionization of atoms, such that ion-electron interactions may be studied. Such many-body interacting systems pose increasingly demanding hurdles for theoretical predictions. The few-body results presented in the present work may however form the starting point for such an endeavour.

Finally, recent experiments [17, 52, 62] bring also experiments with Rydberg ions to the scene. These experiments demonstrate the feasibility of Rydberg excitations in

6. *Outlook*

the presence of the ion trapping field. The similarities between those experiments and our proposal makes our approach of confining Rydberg dressed atom inside a Paul trap indeed very promising.

A. Level scheme of ${}^6\text{Li}$

The Rydberg eigenenergies of ${}^6\text{Li}$ can be obtained by Tab. A.1 together with

$$\delta_{n,l,j} = \delta_{l,j}^0 + \delta_{l,j}^1 (n - \delta_{l,j}^0)^{-2} \quad (\text{A.1})$$

and

$$\epsilon = \frac{-C}{(n - \delta_{n,l,j})^2}, \quad (\text{A.2})$$

with $C = \frac{1}{2}6.5796839207 \times 10^6$ GHz [50]. We give the energies for $n \in \{20, \dots, 40\}$ in Tab A.2

Table A.1.: Quantum defects ${}^6\text{Li}$ [23]

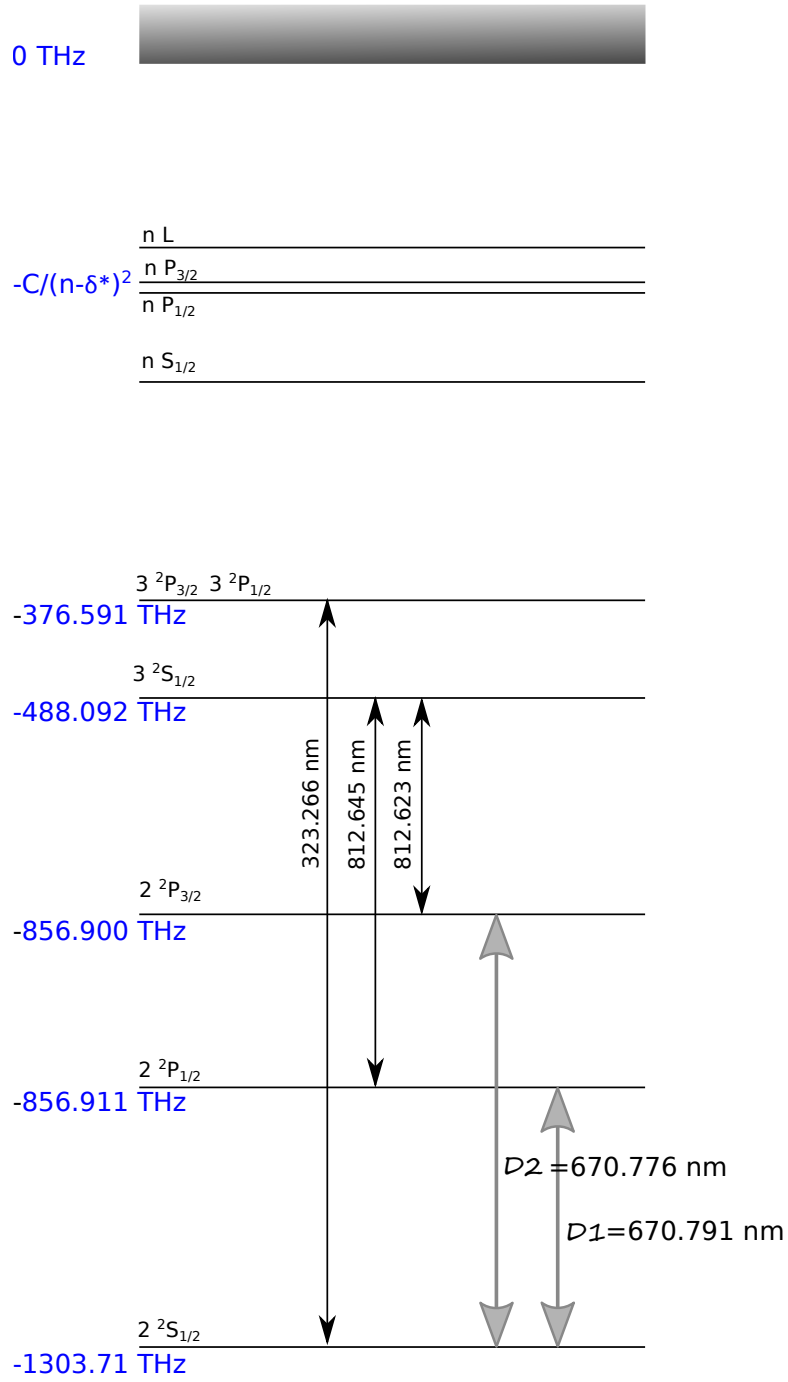
State	δ^0	δ^1
$nS_{1/2}$	0.3995101(10)	0.0290(5)
$nP_{1/2}$	0.0471835(20)	-0.024(1)
$nP_{3/2}$	0.0471720(20)	-0.024(1)

A. Level scheme of ${}^6\text{Li}$

Table A.2.: Rydberg state energies in GHz

n	nS	$nP_{1/2}$	$nP_{3/2}$	$nL \geq 2$
20	-8563.34	-8263.70	-8263.69	-8224.70
21	-7752.15	-7493.72	-7493.72	-7460.05
22	-7051.00	-6826.56	-6826.55	-6797.28
23	-6440.84	-6244.68	-6244.67	-6219.06
24	-5906.58	-5734.14	-5734.14	-5711.60
25	-5436.15	-5283.75	-5283.75	-5263.81
26	-5019.75	-4884.41	-4884.41	-4866.69
27	-4649.43	-4528.69	-4528.69	-4512.87
28	-4318.62	-4210.46	-4210.46	-4196.28
29	-4021.91	-3924.64	-3924.63	-3911.87
30	-3754.75	-3666.96	-3666.95	-3655.42
31	-3513.36	-3433.84	-3433.84	-3423.39
32	-3294.52	-3222.27	-3222.27	-3212.77
33	-3095.50	-3029.67	-3029.67	-3021.01
34	-2913.99	-2853.84	-2853.84	-2845.92
35	-2747.99	-2692.88	-2692.87	-2685.62
36	-2595.78	-2545.16	-2545.16	-2538.49
37	-2455.87	-2409.27	-2409.27	-2403.13
38	-2326.98	-2283.98	-2283.98	-2278.31
39	-2207.98	-2168.22	-2168.22	-2162.97
40	-2097.87	-2061.04	-2061.04	-2056.18

Figure A.1.: Level scheme of ⁶Lithium [40, 50, 72]



Bibliography

- [1] ABRAMOWITZ, M., AND STEGUN, I. A.
Handbook of mathematical functions.
New York: Dover, 1972, p. 784.
- [2] BAER, M., VIBOK, A., HALSZ, G. J., AND KOURI, D. J.
The electronic non-adiabatic coupling terms: On the connection between molecular physics and field theory.
Advances in Quantum Chemistry 44 (2003), 103.
- [3] BALEWSKI, J. B., KRUPP, A. T., GAJ, A., HOFFERBERTH, S., LÖW, R., AND PFAU, T.
Rydberg dressing: understanding of collective manybody effects and implications for experiments.
New J. Phys. 16 (2014), 063012.
- [4] BETEROV, I. I., RYABTSEV, I. I., TRETYAKOV, D. B., AND ENTIN, V. M.
Quasiclassical calculations of blackbody-radiation-induced depopulation rates and effective lifetimes of Rydberg ns, np, and nd alkali-metal atoms with $n < 81$.
Phys. Rev. A 79 (2009), 052504.
- [5] BISSBORT, U., COCKS, D., NEGRETTI, A., IDZIASZEK, Z., CALARCO, T., SCHMIDT-KALER, F., HOFSTETTER, W., AND GERRITSMAN, R.
Emulating solid-state physics with a hybrid system of ultracold ions and atoms.
Phys. Rev. Lett. 111 (2013), 080501.
- [6] BROWN, J., AND CARRINGTON, A.
Rotational Spectroscopy of Diatomic Molecules.
Cambridge University Press, 2003.
- [7] CETINA, M., GRIER, A. T., AND VULETIĆ, V.
Fundamental limit to atom-ion sympathetic cooling in paul traps.
Phys. Rev. Lett. 109 (2012), 253201.
- [8] CHEN, K., SULLIVAN, S. T., AND HUDSON, E. R.
Neutral gas sympathetic cooling of an ion in a paul trap.
Phys. Rev. Lett. 112 (2014), 143009.
- [9] CHILD, M. S.
Theory of Molecular Rydberg States.

BIBLIOGRAPHY

- Cambridge University Press, 2011.
- [10] CINTI, F., JAIN, P., BONINSEGNI, M., MICHELI, A., ZOLLER, P., AND PUPILLO, G.
Supersolid droplet crystal in a dipoleblockaded gas.
Phys. Rev. Lett. *105* (2010), 135301.
 - [11] CINTI, F., MACRI, T., LECHNER, W., PUPILLO, G., AND POHL, T.
Defect-induced supersolidity with soft-core bosons.
Nat. Commun. *5* (2014), 3235.
 - [12] COOK, R. J.
Atomic motion in resonant radiation: An application of ehrenfest's theorem.
Phys. Rev. A *20* (1979), 224.
 - [13] COOK, R. J., SHANKLAND, D. G., AND WELLS, A. L.
Quantum theory of particle motion in a rapidly oscillating field.
Phys. Rev. A *31* (1985), 564.
 - [14] DEIGLMAYR, J., GÖRITZ, A., BEST, T., WEIDEMÜLLER, M., AND WESTER, R.
Reactive collisions of trapped anions with ultracold atoms.
Phys. Rev. A *86* (2012), 043438.
 - [15] DOERK, H., IDZIASZEK, Z., AND CALARCO, T.
Atom-ion quantum gate.
Phys. Rev. A *81* (2010), 012708.
 - [16] EWALD, N. V.
Quest for an ultracold hybrid atom-ion experiment.
Master's thesis, Johannes Gutenberg Universität Mainz, Germany, May 2015.
 - [17] FELDKER, T., BACHOR, P., STAPPEL, M., KOLBE, D., GERRITSMAN, R., WALZ, J., AND SCHMIDT-KALER, F.
Rydberg excitation of a single trapped ion.
Phys. Rev. Lett. *115* (2015), 173001.
 - [18] FRIEDRICH, H.
Theoretical atomic physics.
Springer, 2006.
 - [19] GALLAGHER, T. F.
Rydberg Atoms.
Cambridge University Press, 1994.
 - [20] GERRITSMAN, R., NEGRETTI, A., DOERK, H., IDZIASZEK, Z., CALARCO, T., AND SCHMIDT-KALER, F.
Bosonic josephson junction controlled by a single trapped ion.
Phys. Rev. Lett. *109* (2012), 080402.

BIBLIOGRAPHY

- [21] GOOLD, J., DOERK, H., IDZIASZEK, Z., CALARCO, T., AND BUSCH, T.
Ion-induced density bubble in a strongly correlated one-dimensional gas.
Phys. Rev. A 81 (2010), 041601(R).
- [22] GOSWAMI, A.
Quantum Mechanics, Second Edition.
Wm. C. Brown Publishers, 1997.
- [23] GOY, P., LIANG, J., GROSS, M., AND HAROCHE, S.
Quantum defects and specific-isotopic-shift measurements in ns and np highly excited states of lithium: Exchange effects between Rydberg and core electrons.
Phys. Rev. A 34 (1986), 2889.
- [24] GRIER, A. T., CETINA, M., ORUČEVIĆ, F., AND VULETIĆ, V.
Observation of cold collisions between trapped ions and trapped atoms.
Phys. Rev. Lett. 102 (2009), 223201.
- [25] GUSTAFSON, S. J., AND SIGAL, I. M.
Mathematical Concepts of Quantum Mechanics, Second Edition.
Springer, 2011.
- [26] HAHN, Y.
Polarizability of Rydberg atoms and the dominant long-range interaction.
Phys. Rev. A 62 (2000), 042703.
- [27] HÄRTER, A., AND DENSCHLAG, J. H.
Cold atom-ion experiments in hybrid traps.
Contemporary Physics 55 (2014), 33–45.
- [28] HÄRTER, A., KRÜKOW, A., BRUNNER, A., SCHNITZLER, W., SCHMID, S., AND HECKER DENSCHLAG, J.
Single ion as a three-body reaction center in an ultracold atomic gas.
Phys. Rev. Lett. 109 (2012), 123201.
- [29] HENKEL, N., CINTI, F., JAIN, P., PUPILLO, G., AND POHL, T.
Supersolid vortex crystals in rydberg-dressed Bose–einstein condensates.
Phys. Rev. Lett. 108 (2012), 265301.
- [30] HENKEL, N., NATH, R., AND POHL, T.
Three-dimensional roton excitations and supersolid formation in Rydberg-excited Bose–Einstein condensates.
Phys. Rev. Lett. 104 (2010), 195302.
- [31] HUBER, T., LAMBRECHT, A., SCHMIDT, J., KARPA, L., AND SCHAETZ, T.
A far-off-resonance optical trap for a ba⁺ ion.
Nature Communications 5 (2014).

BIBLIOGRAPHY

- [32] IDZIASZEK, Z., CALARCO, T., JULIENNE, P. S., AND SIMONI, A.
Quantum theory of atom-ion collisions.
Phys. Rev. A 79 (2009), 010702(R).
- [33] IDZIASZEK, Z., CALARCO, T., AND ZOLLER, P.
Controlled collisions of a single atom and an ion guided by movable trapping potentials.
Phys. Rev. A 76 (2007), 033409.
- [34] JOACHAIN, C. J., KYLSTRA, N. J., AND POTVLIEGE, R. M.
Atoms in Intense Laser Fields.
Cambridge University Press, 2012.
- [35] JOGER, J., NEGRETTI, A., AND GERRITSMAN, R.
Quantum dynamics of an atomic double-well system interacting with a trapped ion.
Phys. Rev. A 89 (2014), 063621.
- [36] JOHNSON, W. R., AND CHENG, K. T.
Quantum defects for highly stripped ions.
J. Phys. B: Atom. Molec. Phys. 12 (1979), 863.
- [37] KAMENSKI, A. A., AND OVSIANNIKOV, V. D.
Formal approach to deriving analytically asymptotic formulas for static polarizabilities of atoms and ions in rydberg states.
J. Phys. B: At. Mol. Opt. Phys. 47 (2014), 095002.
- [38] KATO, T.
Perturbation Theory of Linear Operators.
Springer, 1980.
- [39] KIRCHMAIR, G., BENHELM, J., ZÁHRINGER, F., GERRITSMAN, R., ROOS, C. F., AND BLATT, R.
Deterministic entanglement of ions in thermal states of motion.
New J. Phys. 11 (2009), 023002.
- [40] KRAMIDA, A., YU. RALCHENKO, READER, J., AND AND NIST ASD TEAM.
NIST Atomic Spectra Database (ver. 5.3), [Online]. Available: <http://physics.nist.gov/asd> [2016, March 31]. National Institute of Standards and Technology, Gaithersburg, MD., 2015.
- [41] KRYCH, M., AND IDZIASZEK, Z.
Description of ion motion in a paul trap immersed in a cold atomic gas.
Phys. Rev. A 91 (2015), 023430.
- [42] LEIBFRIED, D., BLATT, R., MONROE, C., AND WINELAND, D.
Quantum dynamics of single trapped ions.
Rev. Mod. Phys. 75 (2003), 281.

- [43] LEIBFRIED, D., DEMARCO, B., MEYER, V., LUCAS, D., BARRETT, M., BRITTON, J., ITANO, W. M., JELENKOVIĆ, B., LANGER, C., ROSEN BAND, T., AND WINELAND, D. J.
Experimental demonstration of a robust, high-fidelity geometric two ion-qubit phase gate.
Nature 422 (2003), 412–415.
- [44] MACRI, T., AND POHL, T.
Rydberg dressing of atoms in optical lattices.
Phys. Rev. A 89 (2014), 011402.
- [45] MARINESCU, M., SADEGHPOUR, H. R., AND DALGARNO, A.
Dispersion coefficients for alkali-metal dimers.
Phys. Rev. A 49 (1994), 982.
- [46] MATTIOLI, M., DALMONTE, M., LECHNER, W., AND PUPILLO, G.
Cluster luttinger liquids of rydberg-dressed atoms in optical lattices.
Phys. Rev. Lett. 111 (2013), 165302.
- [47] MAUCHER, F., HENKEL, N., SAFFMAN, M., KROLIKOWSKI, W., SKUPIN, S., AND POHL, T.
Rydberg-induced solitons: three-dimensional self-trapping of matter waves.
Phys. Rev. Lett. 106 (2011), 170401.
- [48] MIFFRE, A., JACQUEY, M., BÜCHNER, M., TRÉNEC, G., AND VIGUÉ, J.
Atom interferometry measurement of the electric polarizability of lithium.
Eur. Phys. J. D 38 (2005), 353.
- [49] MÖBIUS, S., GENKIN, M., EISFELD, A., WÜSTER, S., AND ROST, J. M.
Supersolid vortex crystals in rydberg-dressed Bose–einstein condensates.
Phys. Rev. A 87 (2013), 051602.
- [50] MOHR, P. J., NEWELL, D. B., AND TAYLOR, B. N.
Codata recommended values of the fundamental physical constants: 2014.
arXiv:1507.07956 (2014).
- [51] MØLMER, K., AND SØRENSEN, A.
Multiparticle entanglement of hot trapped ions.
Phys. Rev. Lett. 82 (1999), 1835.
- [52] MÜLLER, M., LIANG, L.-M., LESANOVSKY, I., AND ZOLLER, P.
Trapped Rydberg ions: From spin chains to fast quantum gates.
New J. Phys. 10 (2008), 093009.
- [53] NGUYEN, L. H., KALEV, A., BARRETT, M., AND ENGLERT, B.-G.
Micromotion in trapped atom-ion systems.
Phys. Rev. A 85 (2012), 052718.

BIBLIOGRAPHY

- [54] PORRAS, D., AND CIRAC, J. I.
Effective quantum spin systems with trapped ions.
Phys. Rev. Lett. *92* (2004), 207901.
- [55] PUPILLO, G., MICHELI, A., BONINSEGNI, M., LESANOVSKY, I., AND ZOLLER, P.
Strongly correlated gases of Rydberg dressed atoms: quantum and classical dynamics.
Phys. Rev. Lett. *104* (2010), 223002.
- [56] RATSCHBACHER, L., SIAS, C., CARCAGNI, L., SILVER, J. M., ZIPKES, C., AND KÖHL, M.
Dynamics and decoherence of a single spin-qubit in a tunable environment.
arXiv:1301.5452 (2013).
- [57] RATSCHBACHER, L., ZIPKES, C., SIAS, C., AND KÖHL, M.
Controlling chemical reactions of a single particle.
Nat. Phys. *8* (2012), 649–652.
- [58] REED, M., AND SIMON, B.
Methods of Modern Mathematical Physics IV: Analysis of Operators.
Academic Press, 1978.
- [59] ROOS, C.
Ion trap quantum gates with amplitude-modulated laser beams.
arXiv:0710.1204v1 [quant-ph] (2007).
- [60] SAKURAI, J. J.
Modern Quantum Mechanics, revised edition ed.
Addison-Wesley, 1994.
- [61] SCHMID, S., HÄRTER, A., AND HECKER DENSCHLAG, J.
Dynamics of a trapped ion in a Bose-Einstein condensate.
Phys. Rev. Lett. *105* (2010), 133202.
- [62] SCHMIDT-KALER, F., FELDKER, T., KOLBE, D., WALZ, J., MÜLLER, M., ZOLLER, P., LI, W., AND LESANOVSKY, I.
Rydberg excitation of trapped cold ions: a detailed case study.
New J. Phys. *13* (2011), 075014.
- [63] SCHNEIDER, C., ENDERLEIN, M., HUBER, T., AND SCHAETZ, T.
Optical trapping of an ion.
Nature Photonics *4* (2010), 772.
- [64] SEATON, M. J.
Quantum defects theory.
Rep. Prog. Phys. *46* (1983), 167.

BIBLIOGRAPHY

- [65] SECKER, T., GERRITSMAN, R., GLAETZLE, A., AND NEGRETTI, A.
Controlled long-range interactions between rydberg atoms and ions.
arXiv:1602.04606 (2016).
- [66] SØRENSEN, A., AND MØLMER, K.
Quantum computation with ions in thermal motion.
Phys. Rev. Lett. 82 (1999), 1971.
- [67] TESCHL, G.
Mathematical Methods in Quantum Mechanics With Applications to Schrödinger Operators.
American Mathematical Society, 2009.
- [68] THIRRING, W.
Lehrbuch der Mathematischen Physik Band 3: Quantenmechanik von Atomen und Molekülen.
Springer Verlag Wien New York, 1994.
- [69] TOMZA, M., KOCH, C. P., AND MOSZYNSKI, R.
Cold interactions between an yb+ ion and a li atom: Prospects for sympathetic cooling, radiative association, and feshbach resonances.
arXiv:1409.1192 (2015).
- [70] VAN DITZHUIJZEN, C.
Dipole-dipole interactions between Rydberg atoms.
PhD thesis, Universiteit van Amsterdam, 2009.
- [71] WECKESSER, P., HÖLTKEMEIER, B., LÓPEZ-CARRERA, H., AND WEIDEMÜLLER, M.
Buffer-gas cooling of ions in a multipole radio frequency trap beyond the critical mass ratio.
arXiv:1505.06909 (2015).
- [72] ZAIDEL, A. N., PROKOFEV, V. K., RAISKII, S. M. AND SLAVNYI, V. A., AND SCHREIDER, E. Y.
Tables of Spectral Lines, 3rd Edition.
IFI/Plenum, New York, 782 pp., 1970.
- [73] ZIPKES, C., PALTZER, S., RATSCHBACHER, L., SIAS, C., AND KÖHL, M.
Cold heteronuclear atom-ions collisions.
Phys. Rev. Lett. 105 (2010), 133201.
- [74] ZIPKES, C., PALTZER, S., SIAS, C., AND KÖHL, M.
A trapped ion inside a Bose-Einstein condensate.
Nature 464 (2010), 388.

Danksagung

Hier möchte ich allen herzlich danken, die mich bei meiner Diplomarbeit begleitet und unterstützt haben.

Zuallererst gilt mein Dank Dr. René Gerritsma für die herausragende Betreuung. Er hatte stets ein offenes Ohr für meine Probleme und Anliegen und stand mir mit Rat und Tat zur Seite. Mein besonderer Dank gilt auch Antonio Negretti und Alexander Glätzle für die hervorragende Zusammenarbeit an der Publikation zur vorliegenden Arbeit. Wertvolle Ratschläge kamen außerdem von Krzysztof Jachymski, Thomas Feldker und Ferdinand Schmidt-Kaler.

Weiter will ich Henning Fürst einen speziellen Dank aussprechen, der mich erst auf die Gruppe von René Gerritsma aufmerksam gemacht hat und stets für Diskussionen offen stand.

Als nächstes möchte ich mich beim Rest der Gruppe - Jannis, Norman und Matthias - ganz herzlich bedanken, deren freundliche und hilfsbereite Art das Arbeiten für mich hier im letzten Jahr so angenehm gestaltet hat.

Außerdem danke ich der kompletten Arbeitsgruppe für die netten Gespräche und die tolle Atmosphäre.

Schließlich danke ich meinen Freunden und meiner Familie, die meine Studienzeit so angenehm gestaltet haben. Insbesondere danke ich meiner Mutter, die mir das Studium ermöglicht und auf deren volle Unterstützung ich immer bauen konnte.

Eidstattliche Erklärung

Ich versichere, dass ich meine Diplomarbeit selbstständig verfasst und keine anderen als die angegebenen Quellen und Hilfsmittel verwendet habe. Alle Stellen, die wörtlich oder sinngemäß aus anderen Veröffentlichungen entnommen wurden, sind im Text als solche gekennzeichnet.

Mainz, den 31.3.2016

Thomas Secker